Properties of nanoclusters and the electron tunneling effects from a combined exact diagonalization - *ab initio* approach

Roman Zahorbeński

Ph. D. Thesis
under the supervision of
Prof. dr hab. Józef Spałek

Jagiellonian University
Marian Smoluchowski Institute of Physics
Condensed Matter Theory Department

Kraków, October 2004

Własności nanoklastrów i efekty tunelowania elektronów opisane metodą ścisłej diagonalizacji połączonej z podejściem *ab initio*

Roman Zahorbeński

Rozprawa doktorska

Promotor:
Prof. dr hab. Józef Spałek

Zakład Teorii Materii Skondensowanej
Instytut Fizyki im. Mariana Smoluchowskiego
Uniwersytet Jagielloński

Kraków, październik 2004

Contents

Abstract iii

Acknowledgments v

Published papers vi

1 Introduction 1
- 1.1 Experimental properties of nanowires . . . 3
- 1.2 Theoretical modelling of nanowires . . . 5
- 1.3 Aim and scope of the Thesis . . . 10

2 The EDABI approach 11
- 2.1 Second quantization formulation . . . 11
- 2.2 Single-particle basis choice . . . 13
- 2.3 Variational parameters . . . 15
- 2.4 Exact diagonalization technique . . . 16
- 2.5 Recapitulation . . . 18

3 Numerical analysis 20
- 3.1 The role of intersite terms . . . 20
- 3.2 The renormalization ansatz . . . 21
- 3.3 The single-particle parameters . . . 29
- 3.4 The requirement lists . . . 32

4 Cluster properties 34
- 4.1 The dissociation patterns . . . 35
- 4.2 The metastable configurations . . . 39
- 4.3 The harmonic oscillations . . . 41
- 4.4 The density profiles . . . 42
- 4.5 The *Wannier* basis . . . 43
- 4.6 The excited states . . . 46
- 4.7 The absolute stability . . . 50
- 4.8 The computational limitations . . . 54

5 Electron tunneling 57
- 5.1 The analytical approach . . . 57
- 5.2 The complementary descriptions . . . 59
- 5.3 The transport analysis . . . 60

6 A brief summary 62

Appendices **63**

A Quantum characteristics **63**
A.1 Relation to MCI method 63
A.2 Particle density profile 65
A.3 *Landauer-Büttiker* transport 67
A.4 Renormalized wave-equation 69

B Applied algorithms **71**
B.1 The *Wannier* basis determination 71
B.2 The 3- and 4-site contributions 73
B.3 The modified *Lanczos* algorithm 74

C *Ab-initio* calculations **77**
C.1 The 3-center integral 77
C.2 The *Euler* integral 82
C.3 The microscopic parameters 83
C.4 The transport amplitude 84

Bibliography **90**

Abstract

In this Thesis we implement the method of *exact diagonalization* combined with an *ab initio* approach (EDABI) to studies of simple H_N nanoclusters. In this method all configurations of the interacting particles are taken into account and treated rigorously with the use of the *modified Lanczos* algorithm. Additionally, the single-particle wave functions are allowed to relax in the correlated many-particle state. We calculate the ground-state energies, the *Hubbard* subband structures of excited states, as well as the electron-density profiles beyond the *Hartree-Fock* approximation. To achieve this we introduce a novel type of approximation to estimate 3- and 4-site integrals describing the interparticle *Coulomb* interactions in the *Slater*-orbital representation. The renormalized *Wannier* functions and the microscopic parameters of the studied systems are determined as well. All the properties are analyzed as a function of interatomic distance. In the final part of the Thesis we calculate the quantum tunneling conductivity of those systems.

Streszczenie

W obecnej rozprawie doktorskiej metoda ścisłej diagonalizacji połączona z podejściem *ab initio* (EDABI) została zastosowana do badania prostych nanoklastrów typu H_N. W metodzie tej uwzględniane są wszystkie konfiguracje oddziaływujących cząstek, na bazie których operuje w sposób ścisły zmodyfikowany algorytm *Lanczosa*. Dodatkowo, jednocząstkowe funkcje falowe w stanie wielocząstkowym mają możliwość rozprężania się i kurczenia. Obliczenia obejmują energie stanu podstawowego, widma podpasm *Hubbarda* złożone ze stanów wzbudzonych, jak również profile gęstości elektronowej wychodzące ponad przybliżenie *Hartree-Focka*. Aby to osiągnąć wprowadzamy nowy rodzaj przybliżenia umożliwiający szacowanie 3- i 4-węzłowych całek opisujących międzycząstkowe oddziaływania *Coulombowskie* w reprezentacji orbitali *Slatera*. Również określane są zrenormalizowane funkcje *Wanniera* oraz mikroskopowe parametry badanych układów. Wszystkie analizowane przez nas cechy badane są w zależności od odległości międzyatomowej. W końcowej części rozprawy badane są efekty tunelowania elektronów we wspomnianych układach.

Acknowledgments

I would like to express my sincerest thanks and gratitude to my research advisor Prof. Józef Spałek. His passion for Condensed Matter Physics, nanotechnology, and *ab initio* approach was a source of inspiration and motivation for this work.

This Thesis was not performed in isolation. It was the combination of many discussions, interactions, and help with people at Condensed Matter Theory Department. I would like to make a special mention to a few of these people, although, any attempt to make a conclusive acknowledgement is inadequate and, by its very nature, incomplete. I would like to thank to Prof. Krzysztof Rościszewski for his relevant remarks, and to my colleagues: E. M. Görlich, R. Podsiadły, M. Maśka, and A. Rycerz for the insightful comments and fruitful discussions.

The part of work presented here was supported by the State Committee for Scientific Research (KBN), Grant No. 2P03B 05023, as well as by Senior Fellowship of the Foundation for Science (FNP) awarded to Prof. J. Spałek.

Published papers

1. E. M. Görlich, J. Kurzyk, A. Rycerz, R. Zahorbeński, R. Podsiadły, W. Wójcik, and J. Spałek, "Electronic states of nanoscopic chains and rings from first principles: EDABI method", ed. A. S. Alexandrov *et al*, Kluwer Academic Publisher, Netherlands 2004, pp. 355–375.

2. J. Spałek, E. M. Görlich, A. Rycerz, R. Zahorbeński, and R. Podsiadły, "Properties of correlated nanoscopic systems from the combined exact diagonalization - *ab initio* method", in: *Concepts in Electron Correlation*, ed. A. C. Hewson, V. Zlatic, Kluwer Academic Publisher, Dordrecht 2003, pp. 257–268.

3. E. M. Görlich, R. Zahorbeński, and J. Spałek, "Correlated States for Atoms and Atomic Clusters: a combined exact diagonalization - *ab initio* approach", Acta Phys. Polon. B **34**/2, pp. 645–649, 2003.

4. J. Spałek, A. Rycerz, E. M. Görlich, and R. Zahorbeński, "Electron correlations at nanoscale", in: *Highlights in Condensed Matter Physics*, ed. A. Avella *et al*, American Institute of Physics, Melville, New York 2003, pp. 291–303.

1 Introduction

In the recent years much attention has been devoted to molecular-scale systems ranging from vast organic molecules through multi-atom nanowires to single molecules [1]. The stability of those systems, their electronic structure, and their electronic-transport properties have been a major focus of research in the condensed matter physics. Also, because of the progress in nanotechnology, lithographic techniques, mechanically controllable break-junctions (MCBJ), and scanning tunneling microscopy (STM), it is now possible to make various submicron devices, with the help of which accurate measurements can be carried out [2]. Such devices are typically made of two separated electrodes (the source and the drain) bridged by a single molecule or a quantum wire. Relative position of the two electrodes can be precisely controlled with piezoelectric transducers and the electronic conductance can be monitored as a function of either the applied bias voltage or the electrode separation distance.

Electrodes are the key factor in the study of nanojunction-transport properties such as the current-voltage characteristics or the charge distribution. In STM, the tip is driven into contact with the metal surface and the conductance is measured during subsequent retraction. In the alternative method of the mechanically controllable break-junctions (MCBJ), a macroscopic notched wire is broken, and the contact is re-established between the fractured surfaces of the wire by piezoelectric control. What is more important, it has been found that the same conductance quantization (CQ) features appear for both microscopic, as well as macroscopic contacts [3]. This is probably due to the formation of nanoscopic threads between the macroscopic contacts that are brought close enough. The above indicates a universal quantum nature of the conductance at microscopic level.

Obviously, the current flow through a nanojunction depends on quantum nature of the molecular bridge, electronic properties of the electrodes near the *Fermi* energy level, and on the strength of the molecule-electrode interaction. It has been observed that the conductance of quantum nanowires exhibits quantization steps in units of the conductance quantum $G_0 = 2e^2/h$ ($G_0^{-1} \approx$

12.9 kΩ). Wide range of experiments with gold nanochains have been carried out recently [3, 4, 5], most of them dealing with the multiwalled, helical, or stretched configurations of gold atoms with diameters of the order of 10 Å. The experimental results comprise typically one to four equally spaced abrupt steps located with a period of about G_0, what is consistent with the *Landauer-Büttiker* theory of electronic transport in mesoscopic systems.

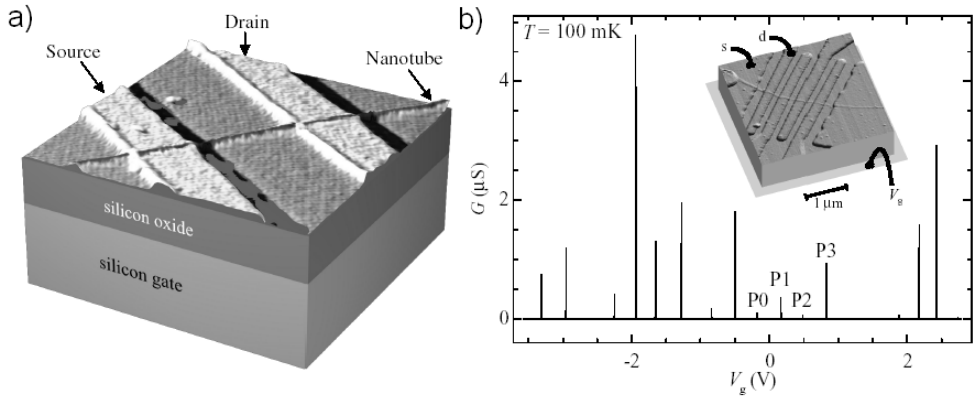

Figure 1: (a) Typical device geometry for electrical transport measurement. (b) Conductance G of a nanotube rope vs. gate voltage V_g. ([6, 7])

The single-wall carbon nanotubes (SWNT), though with diameters of the order of ten times larger than the gold nanowires, can exhibit similar transport phenomena, which have been observed already in mesoscopic metallic conductors. Namely, for the nanotubes having high contact resistance with the electrical leads (Fig. 1a), the low-temperature transport is dominated by the *Coulomb* blockade effect [6]. The effect occurs at low temperature when the energy required to inject a single electron into the nanotube is larger than the thermal energy (due to small capacitance of the nanotube). It is considered that for a typical $\sim 1\mu m$ long tube, the *Coulomb* blockade would set in below the temperature $\sim 50K$. The ground state spin configuration of nanotubes was revealed by *Cobden et al* [7], the unusual even-odd effect was seen that cannot be understood within the constant interaction model (Fig. 1b). The contradiction is in the peak $P0 - P3$ heights which are predicted to be equal, the peaks $P0$ and $P2$ represent the nanotube with even number

of electrons injected, and the peaks $P1$ and $P3$ with the odd number. As can be easily seen from the figure, the odd peaks are significantly larger. *Tans et al* [8] have found that the spin degeneracy can be lifted at zero magnetic field and all the electrons enter the nanotube with the same spin, what cannot be explained by using independent-particle models or simple shell-filling schemes. These experimental observations, as suggested by the authors, point to significant electron-electron correlations, which seem to be a common factor of the transport properties in many nanoscopic systems.

Mechanical and electrical properties of nanostructures have drawn much attention recently because the miniaturization requirement has been forcing the engineers to design smaller and smaller components. Simultaneously with this process, the properties of such components are substantially different from those of the mesoscopic systems, as the quantum nature of this truly microscopic matter starts to play a predominant role. *This is the rationale behind the theoretical analysis of the few-atom complexes in this Thesis.*

1.1 Experimental properties of nanowires

The experiments with stretched gold wires present very interesting conductance characteristics. The interest in such nanowires becomes clear when we recognize that during the last stage of nanowire elongation the conductance takes place in the system of one atom in cross-section. This suggests that the wire, while stretched, forms a chain of single atoms. The longest bridges can have as much as $20 - 25$ Å in length and are found to break at the multiples of approximately 3.6 Å, which would correspond to a stretched Au-Au bond distance [9]. Once pulled out, the atomic chains remain very stable, some for as long as one hour, and are able to sustain enormous current densities of up to 8×10^{14} A/m^2. This makes them suitable candidates as conductors in the research of atomic electronic circuits.

The conductance of the atomic nanowires is always obtained by drawing the histograms assembling a few hundred experimental curves, causing thus a controversy if the step-like behavior is caused by the conductance quantization or by discrete contact-size changes during the nanowire elongation

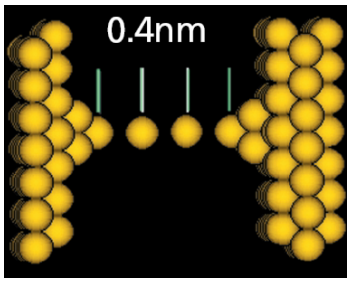

Figure 2: The model of a single strand of gold atoms. The atoms in the strand are spaced at approximately 4 Å. The size of Au atoms is of the order of $1-2$ Å. ([5])

process, due to discrete atomic size. Recent MCBJ, as well as STM experiments show, that at room temperature, the conductance quantization is more prominent than in the low-temperature studies. The explanation given by *Muller et al* [10] is that at $T > 0$ the tunneling through nanowire involves larger number of atomic configurations due to the higher kinetic energy of the carriers. There is also a difficulty with detecting the subsequent conductance peaks beyond that at G_0 at 4.2 K, whereas up to $3-4$ peaks are observed at room temperature. Moreover, some of the experimental data exhibit the indifference to the temperature or the conductance peaks are not located exactly at integer values of G_0. Also, there is almost no discussion of the possible origin of these observations [4]. As we can see, the measurements of properties of such nanoscopic systems leave much room to interpretation because of the indirect, statistical nature of the experiments.

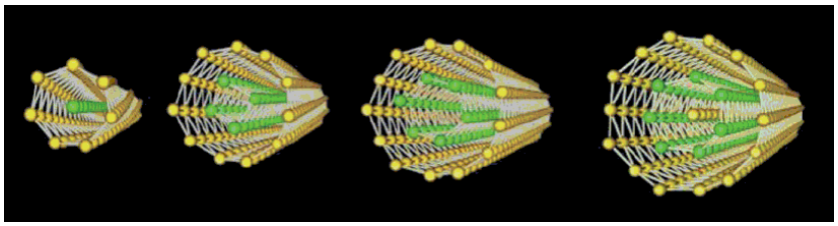

Figure 3: Helical multi-shell structures of gold nanowires. The helix of each shell composes a tube with triangular close-packed network of gold atom. ([5])

The multiwalled nanowires of diameter of less than ten atoms, on the other side, possess different electrical and mechanical properties. For example, it has been found that under certain conditions, the ability of the nanowires to conduct electricity declines to the point that they resemble insulators. The conductance of such atomic-scale gold wires depends on their length, lateral dimensions, the state of atomic order (disorder), and the elongation mechanism of the wires. Although the nanowires shorter than 50 Å show linear and ohmic characteristics, the nature of the resistance changes as the wire becomes longer and narrower, going through a stage, in which the wire properties look very much like those of a semiconductor. The very long wires, up to $150 - 200$ Å, appear to be insulating. The current through such wires varies in a stepwise manner as the STM tip is pulled from the substrate, what is attributed to the formation of new layers (atomic shells) and corresponding reduction in the diameter of the wires [11]. The quasi-metallic character of the short-chain conductivity can be understood by noting that electrons tunnel then through a finite-size barrier. By the same token, the sufficiently long wires become effectively localized due to the *Coulomb* repulsion between the carriers, which prevent the extra electrons from tunneling through. The same result was obtained theoretically by *Lieb* and *Wu* [12] for the infinite *Hubbard* chain of hydrogen atoms.

1.2 Theoretical modelling of nanowires

The experimental work discussed above has been paralleled by theoretical effort, which can be divided into two categories. The first group includes models that take into account the confinement of electrons in reduced dimensions, but ignore the atomic structure of the system. These attempts include self-consistent electronic-structure calculations, mainly within the jellium framework [13, 14]. The stabilized jellium method is found to be very useful in the investigations of alkali-metal clusters. Lately, it has been used to model the metallic leads (electrodes) attached to a chain of Na atoms [14]. The electronic properties of the system have been obtained with the use of the density-functional theory (DFT) within the local-density approximation

(LDA) and assuming the limit of zero external bias. The approach predicts conductance oscillations as a function of the number of atoms in the chain, as well as the lead opening angle α (Fig. 4), but still does not provide a satisfactory picture of the conductance quantization at the nanoscopic level. The models utilizing the effective-mass approximation in quantum dots also belong to this group.

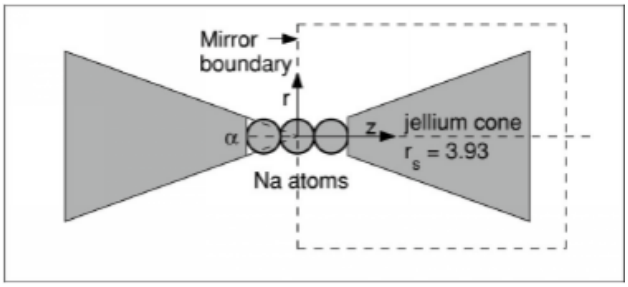

Figure 4: Sketch of a nanochain of Na atoms between the metallic leads, which are described by the jellium model. The cone angle α (the opening angle) can be varied continuously. ([14])

The second group of models includes semiclassical or *ab initio* calculations, in which the atomic structure of nanowires is taken into account. These methods have been successful in showing the mechanisms of the elongation force and the conductance, and they are predominantly based on the S-matrix, *Hartree-Fock*, or *ab initio* quantum mechanical formalism. The S-matrix formalism addresses the problem of the conductance through such systems by formulating the *Schrödinger* equation as a scattering problem. However, according to the conductance theory, the elements of the S-matrix can be expressed in terms of the *Green*'s function of nanoconductor [15] which, in practice, is sometimes easier to compute. Thus lately, the authors prefer the *Green*'s function instead of the S-matrix formalism. The *Hartree-Fock* formalism utilizes the variational principle of the many-body theory, and employed originally a single *Slater* determinant wave function to estimate the ground state of the system. The multiconfigurational interaction (MCI) method, extensively used in quantum chemistry, systematically extends the *Hartree-Fock* approach by employing many *Slater* determinant representa-

tion of the N-particle wave function. Theoretically, the MCI method can provide us with the exact solution of the many-body problem within the space spanned by the single-particle basis if the basis is complete and all possible electron configurations have been accounted for. In practice, the MCI method is computationally intractable for any but the smallest systems, due to the vast number of states in the single-particle basis as well as the electron configurations. Many applications of the MCI method also make the mean-field approximation of interparticle interactions in the Hamiltonian and thus suffer a partial loss of the correlation energy.

The *exact diagonalization* combined with an *ab initio* approach (EDABI), we employ in the Thesis, has much in common with the MCI method. In fact, it can be proved they are equivalent (Appendix A.1). Yet, the EDABI approach has numerous advantages over the standard version known from the quantum-chemical calculations. Namely, the approach applies exact diagonalization technique for the Hamiltonian matrix in the *Fock* space, and thus lets us obtain the ground state of the system within fixed (but otherwise arbitrary) single-particle basis, not just the upper approximation as in the variational methods. As can be easily seen, the approach takes account of all possible electron configurations, what is equivalent to the method known in quantum chemistry as the *full-CI* (FCI) method. Furthermore, the EDABI approach, as opposed to the CI or MCI-SCF methods, does not suffer from size-extensivity or size-consistency problems [16] and thus does not require any specific choice of electron configurations as in the *complete-active-space* (CAS) technique [17] developed in quantum chemistry. Although the methods differ in a way the ground state of the system is obtained, all of them work with the reduced single-particle basis, and the reduction is considered a major source of their approximation. Also, the approach can be compared to the *Møller-Plesset* (MP) or *coupled-cluster* (CC) methods, which do not suffer from the problems either, and yet they have a serious weakness as well. Namely, they do not provide upper bounds to the true energies of the system. A whole range of the numerical methods used in modern quantum chemistry or chemical physics can be found in the book [18] or in the overview [19]. We discuss their implementation details to emphasize the essential assump-

tions and drawbacks, and hence the reasons why we have chosen the EDABI approach.

Most of the mentioned methods rely on the concept of *configuration state function* (CSF). The CSFs are simply *Slater* determinants of the single-particle wave functions of the system in the effective Hamiltonian approximation. These, on the other hand, are obtained either from the self-consistent approach or the LCAO approximation. The latter methods deal with the two fundamentally different kinds of parameters that need to be determined - the CI (many-particle wave-function composition) coefficients and the LCAO (single-particle wave-function composition) coefficients. In general, the methods differ in the manner they determine them. We characterize them briefly next.

In the *multiconfigurational interaction self-consistent field* (MCI-SCF) method the CI, as well as the LCAO, coefficients are variationally treated to minimize the energy of the system. The only constraint is that both the many-particle and single-particle wave functions have to be normalized. Simultaneous optimization of the LCAO and CI coefficients performed within MCI-SCF calculations is quite a formidable task. Although the system-energy variational expression depends quadratically on the CI coefficients, its dependence on the LCAO coefficients is of the fourth order. It is a well known fact that minimization of the functions of several non-linear parameters is a difficult task that can suffer from poor convergence and locate local rather than global minima. In the MCI-SCF method the energy is only weakly dependent on the orbitals that are weakly occupied, in contrast to the strongly occupied. Therefore, one is faced with the minimization of the function of many variables that depends strongly on several of the variables and weakly on many others. As we can see, the stationary states are extremely difficult to obtain.

The *configuration interaction* (CI) method differs from the MCI-SCF method in the manner the LCAO coefficients are obtained. The latter uses either a single CSF or a small number of CSFs to determine them. The CI coefficients are subsequently determined in the same variational manner with the LCAO coefficients set fixed. In this process, the optimizations of orbitals

and CSF amplitudes are carried out in separate steps, what usually leads to a better treatment of electron correlations for the number of CSFs included in the CI calculations can be far in excess of the number considered typical in the MCI-SCF calculations.

The *Møller-Plesset* (MP) method, also referred to as the *many-body perturbation theory* (MBPT), utilizes the single-configuration SCF process (usually the UHF implementation) to determine a set of LCAO coefficients, and hence a set of single-particle orbitals. The orbitals are subsequently used to define the unperturbed Hamiltonian of the system and then the regular perturbation theory is used to finetune the energy as well as the wave function of the system. As has been already said, the MP method, despite all of the advantages, provides the energies which are not upper bounds to the true energies of the system, and therefore it may not be able to treat cases where two or more CSFs have equal or nearly equal amplitudes because it obtains the amplitudes of all but the dominant CSF from the perturbation theory formulas that assume the perturbation is small [20].

The *coupled-cluster* (CC) method expresses the CI part of the wave function in a somewhat different manner. Although it starts much like the MP method, the single-particle orbitals are used to construct the ground many-particle state and the so-called cluster operator is introduced to generate the excitations. Parameters for the specific excitations play here a similar role as the CI coefficients in the CI or MCI-SCF methods. In general, the CC equations are quartic functions of these parameters and thus cause the problems similar to those of the MCI-SCF method. Thus, the CC working equations are often obtained by neglecting all of the terms that are non-linear in them. The CC method, as presented here, suffers from the same drawbacks as the MP method. Moreover, solution of the non-linear CC equations may be difficult and slowly convergent.

As we can see, each of the methods has its own field of applicability and leads to a different degree of approximation. Having described the most important aspects of the above methods a list of required properties for an acceptable method may be compiled. An early attempt to compile such a list was published by *Pople et al* [21]. Half a decade later another list was

published by *Bartlett* [22]. The EDABI approach is checked against such lists in the following Chapters.

1.3 Aim and scope of the Thesis

The aim of the Thesis is to provide a systematic study of nanoscale cluster systems with the use of the EDABI approach. We present the comparative results for various systems composed of hydrogen-like atoms. The microscopic parameters, ground state energies, charge distributions, as well as the patterns of the excited states are examined and compared against different space-arrangements of atoms.

In our approach, we study hydrogen clusters containing up to $N = 6$ atoms. The starting parametrized Hamiltonian in the second-quantization formulation is characterized in Chapter 2. The 3- and 4-site interactions required to determine the Hamiltonian parameters are estimated using an *ansatz* discussed in detail in Appendix B.2. The exact diagonalization method of the Hamiltonian is based on the modified *Lanczos* algorithm and has been detailed in Appendix B.3, whereas the relevant physical quantities and the comparison with the MCI method are provided in Appendix A. The starting atomic wave functions, used to compose the *Wannier* functions, have their *Bohr* radius $a \equiv 1/\alpha$ adjusted to minimize the interacting-system energy. In this manner, the renormalized *Wannier* functions are obtained. This Thesis is complementary to the other two [23, 24] that are devoted respectively to the study of the linear chains and fermionic ladders [23], and to the determination of the renormalized structure of atoms, molecules, and ions, as well as to calculation of the crystal-field levels from first principles [24].

2 The EDABI approach

The approach we extensively utilize in this Thesis is called the *Exact Diagonalization* combined with an *Ab Initio* approach (EDABI) [25, 26, 23]. Main features of this approach are: the second quantization formulation, the finite single-particle basis selection to define the field operators and, in turn, the parametrized Hamiltonian, which involves the introduction of the variational parameters characterizing the single-particle basis and the exact diagonalization technique combined with the basis optimization. In this Chapter we summarize the methodology of the approach in the systematic study of nanoscale cluster systems.

2.1 Second quantization formulation

The wave mechanics (*Schrödinger*, 1926), also known as the first quantization scheme, describes the wave aspect of the single-particle quantum states. It is supplemented with the probabilistic interpretation due to *Born* (1926), which introduces the particle aspect in an *ad hoc* to the description of those quantum states. The second quantization formulation (*Fock*, 1932, 1957), on the other hand, is often the only choice when the particle number is variable or the interparticle correlations start to play a predominant role. It is particularly useful in describing multiparticle quantum states in interacting systems. Although both formulations are known to be equivalent, at least for nonrelativistic systems, the latter seems to be better suited for dealing with nanoscopic systems, in which the electrons can form a collective, highly correlated state.

In general, the spin-independent Hamiltonian of many-particle system in the first quantization formulation can be written down as follows

$$H = \sum_i H_1(\mathbf{r}_i) + \frac{1}{2}\sum_{i\neq j} H_2(\mathbf{r}_i - \mathbf{r}_j), \tag{1}$$

where H_1 and H_2 represent respectively the single- and the two-particle parts of the Hamiltonian. On the other hand, the second quantization formulation works with the field operators $\widehat{\Psi}^+(\mathbf{r})$ and $\widehat{\Psi}(\mathbf{r})$, creating (anihilating) parti-

cles in the states at given point $\mathbf{r}$ in the *Fock* space. The Hamiltonian can be expressed then as follows

$$\begin{aligned} \widehat{H} &= \int d^3r \hat{\Psi}^+ (\mathbf{r}) H_1 (\mathbf{r}) \hat{\Psi} (\mathbf{r}) \\ &+ \frac{1}{2} \int d^3r d^3r' \hat{\Psi}^+ (\mathbf{r}) \hat{\Psi}^+ (\mathbf{r}') H_2 (\mathbf{r} - \mathbf{r}') \hat{\Psi} (\mathbf{r}') \hat{\Psi} (\mathbf{r}) . \end{aligned} \tag{2}$$

The field operator (containing, as a rule, an infinite number of functions) has the following form

$$\hat{\Psi} (\mathbf{r}) \equiv \sum_{i\sigma} w_i (\mathbf{r}) \chi_\sigma \cdot a_{i\sigma}, \tag{3}$$

where $a_{i\sigma}$ is the anihilation operator of the particle in the single-particle state $\{w_i (\mathbf{r}) \chi_\sigma\}$. In this notation $\sigma = \pm 1$ labels the spin quantum number and the index "i" comprises all other quantum numbers for the single-particle state $|i\sigma\rangle$. There are no further requirements on the basis apart from its completeness and orthonormality. However, in practical calculations we select here the *Wannier* basis comprising orthogonalized atomic states; the label "i" characterizes then the site located at $\mathbf{R}_i$, on which a particular function $w_i (\mathbf{r})$ is centered (i.e. we select the *position* representation). Thus, by combining Eq. (2) and Eq. (3), we obtain the well known expression for the many-particle Hamiltonian in the particle creation- (anihilation-) operator language, namely

$$\widehat{H} = \sum_{ij\sigma} t_{ij} \cdot a^+_{i\sigma} a_{j\sigma} + \frac{1}{2} \sum_{\sigma\sigma'} \sum_{ijkl} V_{ijkl} \cdot a^+_{i\sigma} a^+_{j\sigma'} a_{l\sigma'} a_{k\sigma}, \tag{4}$$

where

$$t_{ij} = \int d^3r w^*_i (\mathbf{r}) H_1 (\mathbf{r}) w_j (\mathbf{r}) , \tag{5}$$

and

$$V_{ijkl} = \int d^3r d^3r' w^*_i (\mathbf{r}) w^*_j (\mathbf{r}') H_2 (\mathbf{r} - \mathbf{r}') w_k (\mathbf{r}) w_l (\mathbf{r}') . \tag{6}$$

The first term in Eq. (4) contains the so-called hopping integral $\{t_{ij}\}$ and the second term – the electron-electron interaction parameters $\{V_{ijkl}\}$. The

parameters $\{V_{ijkl}\}$ comprise one-site ($i = j = k = l$), two-site ($i = j = k \neq l$, etc.), three-site ($i = j \neq k \neq l$, etc.), and four-site ($i \neq j \neq k \neq l$) terms.

One should note that some terms of the Hamiltonian (4) may be neglected in more specialized models, e.g. for the *Hubbard* model. In the *Hubbard* model we take into account only the on-site energy $\epsilon_i \equiv t_{ii}$, the nearest-neighbour hopping integrals $t_{\langle ij \rangle}$ (or the limited range of the hopping integrals), and the intraatomic part of the interaction among particles $U_i \equiv V_{iiii}$. In such situation, the Hamiltonian is written in the compact form

$$\widehat{H} = \sum_i \epsilon_i n_i + \sum_{\langle ij \rangle \sigma} t_{\langle ij \rangle} a^+_{i\sigma} a_{j\sigma} + \sum_i U_i n_{i\uparrow} n_{i\downarrow}, \tag{7}$$

where $n_i = \sum_\sigma n_{i\sigma}$. Dropping some terms is often a necessity, as their total number increases to the fourth power of the number of single-particle wave functions taken into account in the field operator. The limitation to a finite basis set constituting the field operator results in a *model Hamiltonian*. However, we should realize that the invariance with respect to the unitary transformations of the single-particle basis is then broken, and thus an extraordinary care should be taken with the single-particle basis choice. Another issue concerning the universality of the *Hubbard* model when applied to correlated systems is that the results can become unstable or even unphysical when we consider consecutive interaction terms in addition to the U_i interaction. This is because some of the terms in the Hamiltonian balance out each other and additional terms need to be taken into account simultaneously. Such additional terms change the universality class of the solution also, e.g. the type of symmetry breaking. It is important to note that the basis choice is the single factor which determines what type of dynamical processes are included and determines relevant physics of a model.

2.2 Single-particle basis choice

The line of approach we take requires usually the explicit knowledge of the single-particle basis before we actually solve the parametrized Hamiltonian. Namely, the basis wave functions are used to determine the Hamiltonian

parameters (5 and 6), as well as the type of dynamical processes we include in the second quantized form. Obviously, one of the possible ways of dealing with the problem is to postulate the form of such basis.[1]

A widely accepted method is to take a linear combination of atomic orbitals (LCAO) as the single-particle basis choice. The legitimacy of the method can be easily justified if we realize that the single-particle wave functions of electron in a solid are predominantly influenced by the atoms they are bound to and they reduce to the atomic wave functions in the limit of a large interatomic separation. Fortunately, such a basis often gives satisfactory results, even without any subsequent basis optimization. The only requirement with respect to the basis, known as the *Wannier* basis for its locality in space, is the orthonormality, achieved with the algorithm detailed in Appendix B.1. Once we have taken Eq. (B1) and the algorithm of determining the LCAO coefficients (cf. Appendix B.1), we can express the Hamiltonian parameters (5 and 6) through the atomic wave functions directly, namely

$$t_{ij} = \sum_{i'j'} t'_{i'j'} \cdot \beta^*_{ii'} \beta_{jj'}, \tag{8}$$

and

$$V_{ijkl} = \sum_{i'j'k'l'} V'_{i'j'k'l'} \cdot \beta^*_{ii'} \beta^*_{jj'} \beta_{ll'} \beta_{kk'}, \tag{9}$$

where $t'_{i'j'}$ and $V'_{i'j'k'l'}$ represent the integrals (5 and 6) with the atomic instead of the *Wannier* functions taken, and $\beta_{ii'}$ are the coefficients expressing the superposition of atomic wave functions composing the *Wannier* function.

The algorithm uniquely defines the *Wannier* basis and in this manner one avoids the variational optimization of the LCAO coefficients, and hence we avoid the problems the MCI method suffers from. Strictly speaking, the LCAO coefficient matrix β is ambiguous for it can be left-multiplied by a unitary matrix and still satisfies the orthonormality condition (B4). The algorithm we apply arbitrarily assumes that $\beta = \beta^+$, what provides best results in the case when the invariance with respect to the unitary transformations

[1] This is not always the case, since a renormalized (self-adjusted) wave equation can be formulated through an *Euler* variational procedure combined with the EDABI method (cf. [24]).

of the basis is broken. The choice is understandable from the physical point of view, since the contributions of any two atomic wave functions to the each other's *Wannier* functions are then of the same amplitude ($|\beta_{ij}| = |\beta_{ji}|$).

2.3 Variational parameters

The atomic wave functions should be readjusted if the atoms form a solid. Thus, the *Wannier* basis constructed from the wave functions of individual atoms does not reflect the actual situation. The solution to the problem is to introduce variational parameters accounting for a variable wave-function size. The parameters allow the electrons to readjust to the resultant many-particle state. In effect, we obtain a better ground state. Strictly speaking, the single-particle wave function could be expanded in any complete basis in the quantum-mechanical sense. However, the selection of a finite subbasis makes it incomplete. Therefore, to minimize the error we adjust the selected wave functions in such a way that they correspond to the absolute minimum of the ground state energy.

In this Thesis we start with the adjustable $1s$ wave functions of hydrogen-like atoms. The Hamiltonian for a single electron in the *atomic units* takes the form

$$H = -\nabla^2 - Z \cdot \frac{2}{|\mathbf{r}|}, \tag{10}$$

where the eigenvalues of H are expressed in *Rydbergs* (Ry), $\mathbf{r}$ - in units of the $1s$ *Bohr* radius (a_0), and Z represents the nuclear charge. The adjustable $1s$-like wave function centered at $i \equiv \mathbf{R}_i$ has then the shape

$$\Phi_i(\mathbf{r};\alpha) = \sqrt{\frac{\alpha^3}{\pi}} \cdot e^{-\alpha|\mathbf{r}-\mathbf{R}_i|}, \tag{11}$$

where α is the variational parameter. The above function is used to determine the primed parameters $t'_{i'j'}$ and $V'_{i'j'k'l'}$; their explicit expressions have been provided in Appendix C.3. The 1- and 2-site interaction parameters in the representation of the atomic wave functions (11) are: the single-site *Hubbard* term $U'_i \equiv V'_{iiii}$, the two-site *Coulomb* term $K'_{ij} \equiv V'_{ijij}$, the *Heisenberg*

exchange integral $J'_{ij} \equiv V'_{ijji}$, and the *correlated hopping* term $V'_{ij} \equiv V'_{jiii}$. Unfortunately, even such simple functions do not allow us to determine all of the parameters explicitly in an analytical form. As it has already been mentioned, the 3- and 4-site interaction parameters cannot be determined analytically and we are forced to propose an approximation scheme explained in detail in Appendix B.2.

The EDABI approach differs from the MCI-class methods in a way variational parameters are used. Our approach utilizes significantly reduced number of the variational parameters and often ensures perfect convergence of the minimization procedure and replaces the variational determination of the coefficients with the quickly convergent algorithm.

2.4 Exact diagonalization technique

The Hamiltonian (4) of the many-particle system needs to be diagonalized once we have determined the microscopic parameters. We use the modified *Lanczos* algorithm as the diagonalization method. The modified form of the *Lanczos* algorithm emphasizes the fact that the algorithm is essentially a minimization procedure and is advantageous with respect to the variational methods by making use of specific (quadratic) dependence of the mean system-energy on the CI coefficients of many-particle state. Namely, the calculated ground state energy E_G fulfills the condition

$$E_G \leq \langle \Phi_N | \widehat{H} | \Phi_N \rangle, \tag{12}$$

where $|\Phi_N\rangle$ represents the N-particle ground state. Decomposing the N-particle state into the series of the CI coefficients according to Eq. (A5) (cf. Appendix A.1), we obtain explicitly that

$$E_G \leq \frac{1}{N!} \sum_{i_1 \ldots i_N} \sum_{j_1 \ldots j_N} C^*_{i_1 \ldots i_N} C_{j_1 \ldots j_N} \cdot \langle 0 | a_{i_1} \ldots a_{i_N} \widehat{H} a^+_{j_1} \ldots a^+_{j_N} | 0 \rangle. \tag{13}$$

The modified *Lanczos* algorithm provides an efficient prescription to iteratively improve the CI coefficients, to finetune the energy in each step of the algorithm iteration (cf. Appendix B.3).

Unfortunately, the *Lanczos* algorithm suffers substantial problems in the case of large systems. Its computational complexity increases expotentially with the number of sites in the system, what makes it unacceptable for the systems with more than about 16 sites. Yet, there is a candidate that addresses the problem and is able to provide with the results for much larger systems than the *Lanczos* algorithm can be applied to. This alternative class of methods of the Hamiltonian diagonalization are the methods known as *quantum Monte Carlo* (QMC). The auxiliary-field QMC (AFMC) method is of particular interest in the field for being free of the fixed-node approximation, which addresses the issue of non-fermionic ground-state solutions plaguing the former methods of the kind. Furthermore, the multi-determinantal AFMC method lets us to calculate the excited states as well as profits from the increased efficiency of the ground state determination. The reason is in the decreased error (Fig. 5) in total energy $E(\beta)$ with respect to the result of the FCI method E_{FCI} for any inverse temperature β. This allows us to reach even larger systems for the method can work for higher temperature.

Although the QMC-class methods allow us to study relatively large systems, with up to 100 sites, they often suffer from the sign-related problems and the computational effort can depend on the system studied. The *Lanczos* method, on the other hand, makes no assumptions about the considered system and the computational time depends on the number of terms in the Hamiltonian, not on the parameter values. Hence, the *Lanczos* algorithm provides us with the reliable, stable, and predictable method of determining eigenstates and eigenenergies of the Hamiltonian. The method is actually the fastest and most accurate, in the case the clusters are small enough. *This is the rationale behind choosing the Lanczos algorithm as the diagonalization technique.* The AFMC method can be a reasonable substitute for the *Lanczos* algorithm when we consider larger clusters.

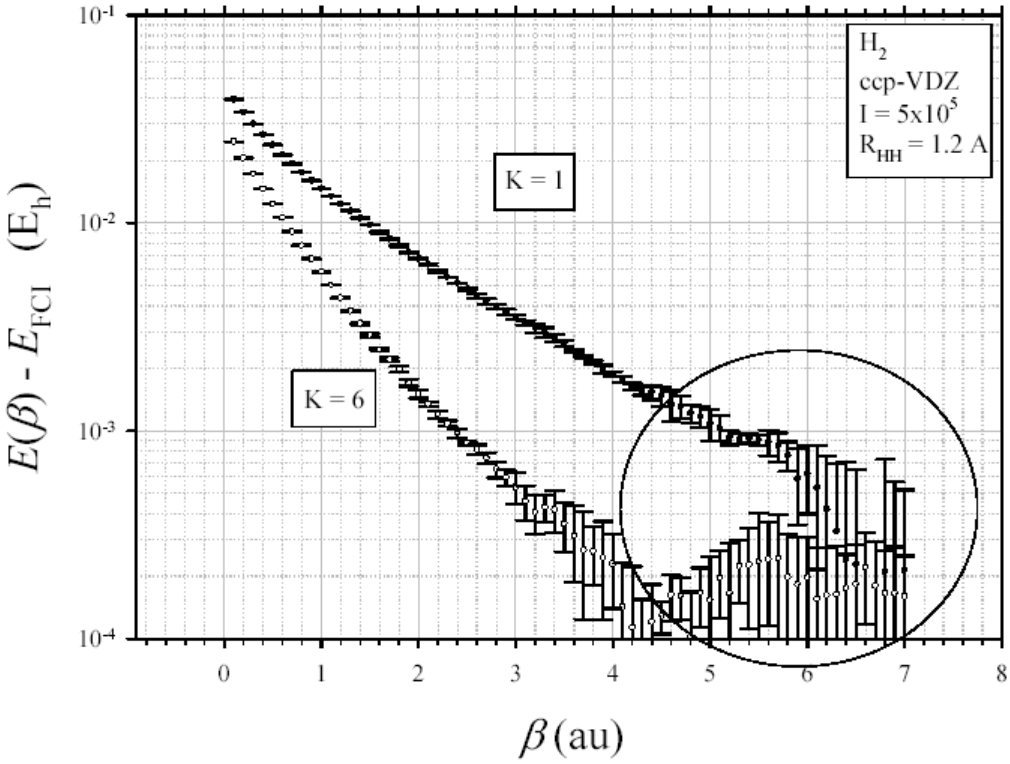

Figure 5: The AFMC error in total energy in a H_2 molecule and the relative statistical error bars. Two calculations are shown, with $K = 1$ and $K = 6$, where K is the number of determinants (CSFs) taken into account. The ellipse indicates the region where the standard error dominates. ([27])

2.5 Recapitulation

All the above features of the EDABI approach are combined into a single scheme of calculating the properties of small atomic clusters. In general, the scheme can be illustrated on the following diagram (Fig. 6).

Initially, we assume the form of the single-particle basis as linear combination of the adjustable $1s$ wave functions of hydrogenic-like atoms. Next, we iteratively build the field operators, determine the ground state of the Hamiltonian expressed through the field operators, and simultaneously adjust the variational parameters to minimize the ground-state energy of the system for given interatomic distance. Finally, we obtain the renormalized

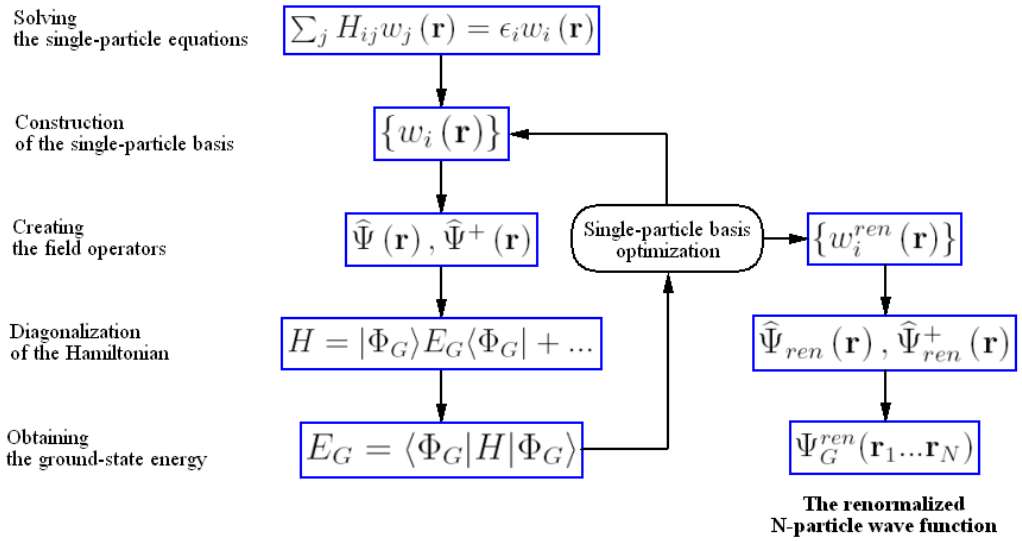

Figure 6: Flowchart diagram of the EDABI approach. The renormalized *Wannier* functions, field operators, as well as N-particle wave function are obtained as a final result, in addition to the ground state energy as a function of interatomic distances in the cluster.

single-particle basis, and hence the N-particle wave function of the system, as will be discussed in the following. Both ground state and the excited states of the nanocluster will be analyzed in detail.

3 Numerical analysis

Exact solutions of interacting (correlated) electronic systems, incorporating an *ab initio* framework in a consistent manner, should be very valuable, even for model systems. This is because we can obtain the system properties as a function of the lattice parameter, not only as a function of the interaction parameters, as is usually the case. Actually, the microscopic parameters are also calculated as a function of interatomic distance for given cluster geometry. We apply the EDABI approach, detailed in the previous Chapter, to small atomic clusters, with up to 6 hydrogen-like atoms, for different 3D configurations. As a result, we obtain not only the electronic properties, but also the local electron-lattice interaction parameters, the dimerization amplitude, the zero-point energies, and much more, all as a function of the lattice parameter. Moreover, it has been found that some of the characteristics are of the solid-state character even for such small systems. The model aspect of the study is reflected only in taking the hydrogenic-like 1s orbitals (11) when constructing the orthonormalized single-particle wave functions. Therefore, the present results may be regarded as a reference point to realistic calculations for nanoscopic systems composed of more complex atoms. In this Chapter we present a few crucial aspects of the EDABI approach that have essential influence on the method stability and the consistency of its results.

3.1 The role of intersite terms

Hydrogen molecule is the simplest system we test our methodology of approach on. What is even more important, in the case of hydrogen molecule we do not encounter the difficulties with the 3- and 4-site terms in the interaction part, as well as there are no other sites contributing with their potentials to the hopping and different from the pair involved. All the terms in the Hamiltonian (4) for the hydrogen molecule are determined analytically (cf. Appendix C.3). We identify the most important of them by starting from the *Hubbard* Hamiltonian (7) and incorporating the additional intersite terms next. As we can see from Fig. 7a, the two-site *Coulomb* term has a crucial influence on the results, the remaining terms practically do not change the

character of the results for E_G.

It seems that taking into account all the 1- and 2-site terms is completely sufficient to obtain precise results. However, we shall see, it is far from it when the number of sites $N \gg 2$. As we can see from Fig. 7b, the reason is in the increasing percentage (with the number of sites N) of the number of the 3- and 4-site terms over the 1- and 2-site terms. Such percentage can be easily obtained from simple combinatoric calculations namely, the portion of one- and two-site interactions is

$$P_{12} \equiv \frac{N_{12}}{N^4} = \frac{1}{N^4}\left[N + 7N(N-1)\right], \tag{14}$$

whereas the corresponding number of three- and four-site terms is

$$P_{34} \equiv \frac{N_{34}}{N^4} = \frac{1}{N^4}\left[6N(N-1)(N-2) + N(N-1)(N-2)(N-3)\right]. \tag{15}$$

Hence, although the energy values of the 3- and 4-site terms are small, their total contribution cannot be completely neglected, since their number dominates even in the case of systems composed of $N = 4$ atoms.

3.2 The renormalization ansatz for 3- and 4-site parameters

The H_3 system is the simplest many-particle system with the number of sites $N > 2$. Unfortunately, in this system the 3-site interaction terms appear.

The 3-site (and, in general, 4-site) terms cannot be calculated efficiently with numerical methods. In Fig. 8a, we present the results of three alternative approximation schemes that can be applied here. The first approximation scheme relies on simply neglecting the 3-site terms in the representation of atomic wave functions, i.e. we take $V'_{\xi'_{|3}} = 0$ and use Eq. (B12) to evaluate the interaction terms V_ξ in the *Wannier* representation (cf. Appendix B.2 for notation and details). In the second scheme, we additionally set the 3-site terms in the *Wannier* representation to zero, i.e. $V_{\xi_{|3}} = 0$. As can be easily seen, both schemes produce the results having no global minimum for the ground state energy with respect to the variational parameter α (cf.

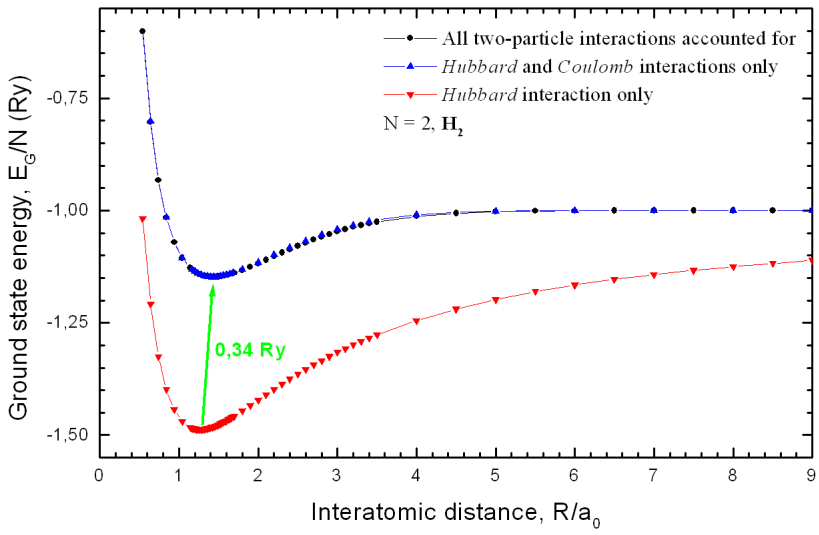

(a)

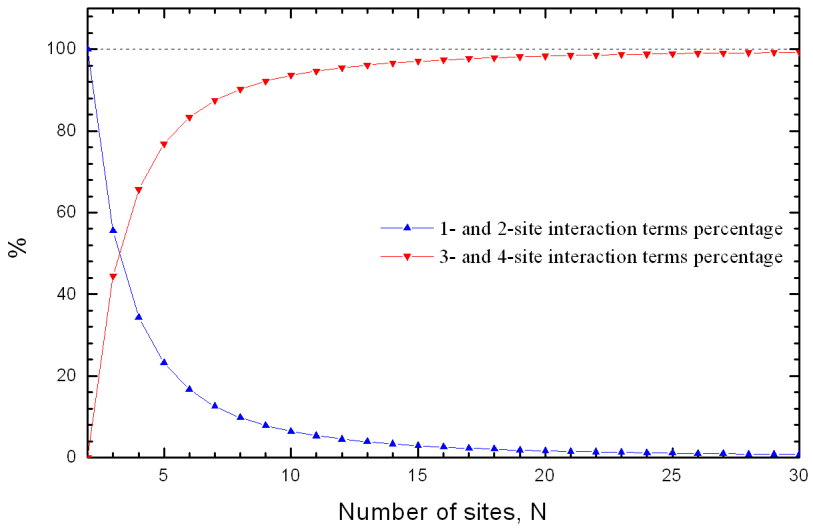

(b)

Figure 7: (a) Total ground state energy (per atom, including both the electron and the lattice contributions) for H_2 molecule. The consecutive two-particle interaction terms are accounted for. (b) Relative number of different interaction terms contributing to E_G versus number of sites in the H_N ring.

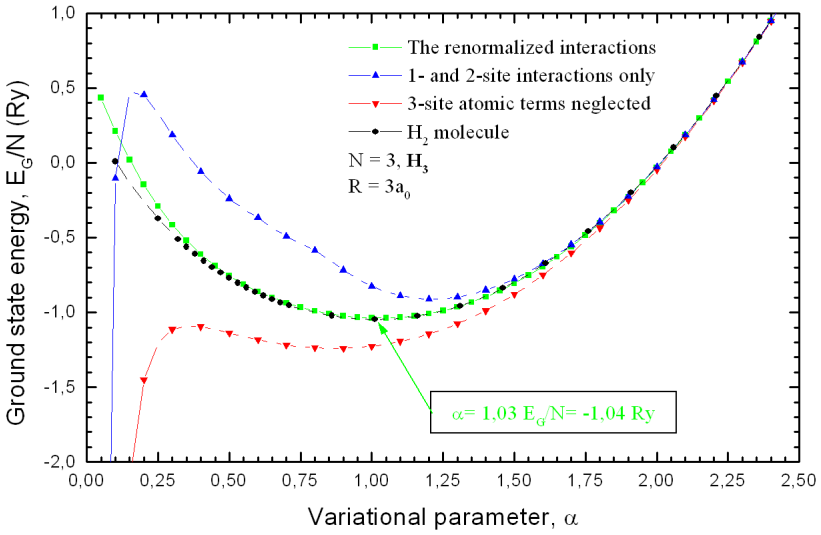

(a)

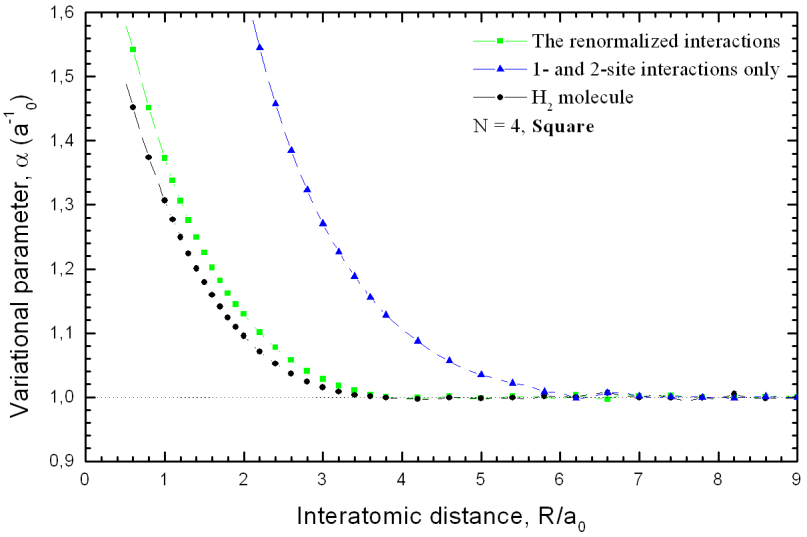

(b)

Figure 8: (a) Total ground state energy for the H_3 system. We compare different approximations of the 3-site terms, as explained in the main text. (b) The optimized variational parameter α for the square configuration of four atoms and comparison with the result for H_2 molecule.

Chapter 2.3). The only scheme providing stable results relies on an *ansatz* explained in detail in Appendix B.2 and amounting for renormalizing of 1- and 2-site interaction terms by the 3-site terms in the atomic representation. This scheme also works for the systems with the number of sites $N > 3$, where additionally the 4-site interaction terms appear.

We have developed the above mentioned scheme assuming that the 3- and 4-site terms in the *Wannier* representation vanish (in our strongly localized basis). The similar pattern remains even when the renormalization *ansatz* is applied. Furthermore, the optimized value of the variational parameter α (cf. Fig. 8b) indicates contraction of the orbital size $a \equiv 1/\alpha$ with the decreasing interatomic distance, making the *ansatz* work even better because of the further localization of the basis. One should note the EDABI approach disqualifies some of the approximation schemes with the use of global minimum requirement, what would not be possible without orbital readjustment.

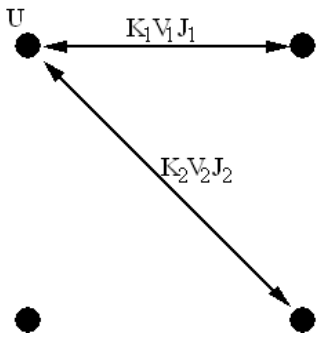

Figure 9: The planar (square) configuration of the system composed of four atoms. The corresponding 1- and 2-site interaction terms are marked.

In Fig. 10ab, we plot the values of microscopic parameters (cf. also Table 1) obtained with the renormalization *ansatz* explained above. The only parameters significantly contributing to the Hamiltonian, especially when the atomic spacing is small, are the intrasite *Hubbard U* and the intersite *Coulomb K* terms (cf. Fig. 9). The remaining 2-site interactions, namely the *correlated hopping V* and the *Heisenberg* exchange *J* terms, are at least two orders of magnitude smaller. This is the rationale behind the assumption that the 3- and 4-site interactions in the *Wannier* representation can be neglected.

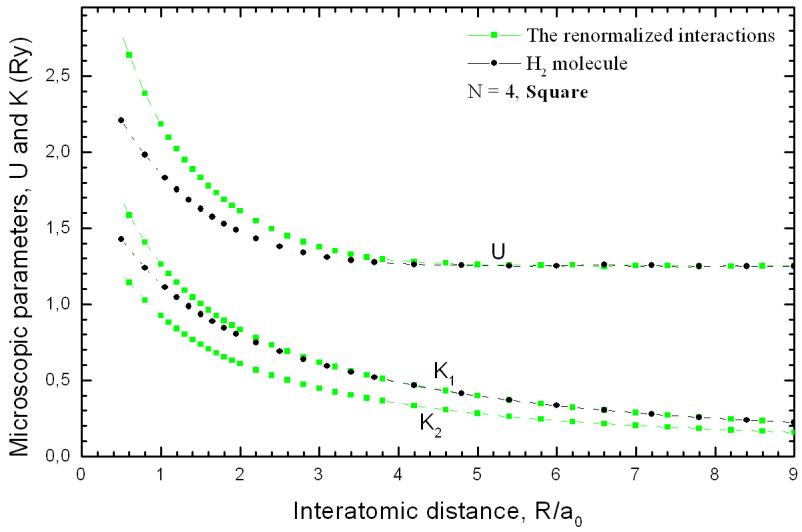

(a)

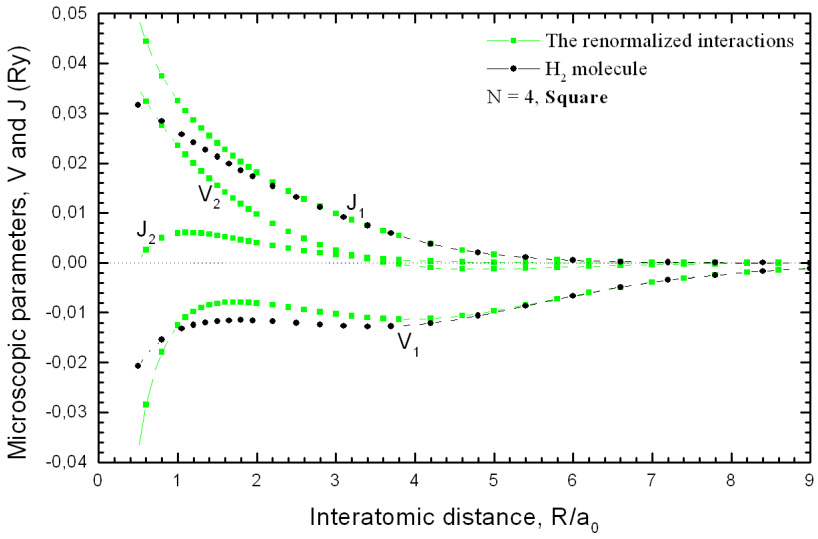

(b)

Figure 10: Microscopic parameters vs. R in the *Wannier* representation for the square configuration of the $N = 4$ atom cluster. (a) *Hubbard* (U) and intersite *Coulomb* interaction (K) parameters. (b) *Correlated hopping* (V) and *Heisenberg*-exchange interaction (J) parameters.

Table 1: Microscopic interaction parameters vs. interatomic distance R for the square configuration of four atoms. The star marks the distance R with the lowest energy.

R/a_0	U (Ry)	K_1 (Ry)	K_2 (Ry)	V_1 (mRy)	V_2 (mRy)	J_1 (mRy)	J_2 (mRy)
0,5	2,78	1,68	1,20	-37,30	35,02	49,04	0,49
1,0	2,18	1,26	0,92	-12,54	23,56	32,54	5,93
1,5	1,83	1,00	0,74	-8,15	15,52	24,03	5,49
1,8	1,69	0,89	0,65	-7,88	11,83	20,28	4,63
1,9*	1,65	0,86	0,63	-7,96	10,75	19,17	4,33
2,0	1,61	0,83	0,61	-8,1	9,73	18,12	4,03
2,5	1,47	0,71	0,52	-9,13	5,53	13,57	2,66
3,0	1,38	0,62	0,45	-10,29	2,53	9,91	1,61
3,5	1,32	0,55	0,39	-11,12	0,50	6,93	0,89
4,0	1,28	0,49	0,35	-11,31	-0,69	4,58	0,45
5,0	1,26	0,40	0,28	-9,64	-1,25	1,66	0,08

Moreover, in Fig. 10b we illustrate our earlier statement that some of the microscopic parameters could balance each other out in the Hamiltonian. The *correlated hopping* interaction, for example, presents completely different characteristics depending on which pair of the sites is taken (cf. Fig. 9). Furthermore, the parameters V_1 and V_2 contribute to the Hamiltonian with different signs reducing their contribution in the final result. Thus, ignoring any one of them could provide unsatisfactory results.

The interaction terms in the representation of atomic wave functions (cf. Table 2), on the other side, present a qualitatively different picture, as illustrated in Fig. 11ab. All of them are positively defined and their values are of the same order for a smaller interatomic distance. The renormalization *ansatz* allows us to recover the 3- and 4-site parameters in the atomic representation (cf. Table 3). One should note that their magnitudes are comparable to the 1- and 2-site parameters and this is the reason why the renormalization *ansatz* of the 1- and 2-site parameters provides such an essential improvement of the results.

One remark at the end of this Chapter is in place. Namely, most au-

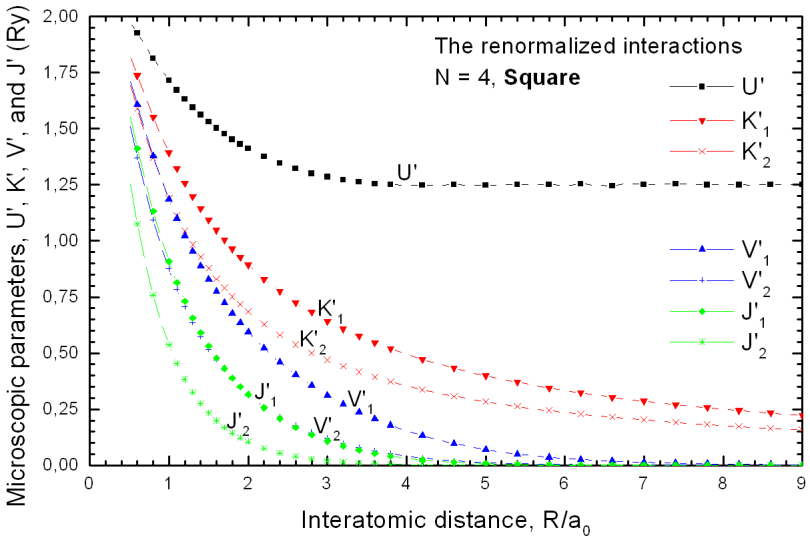

(a)

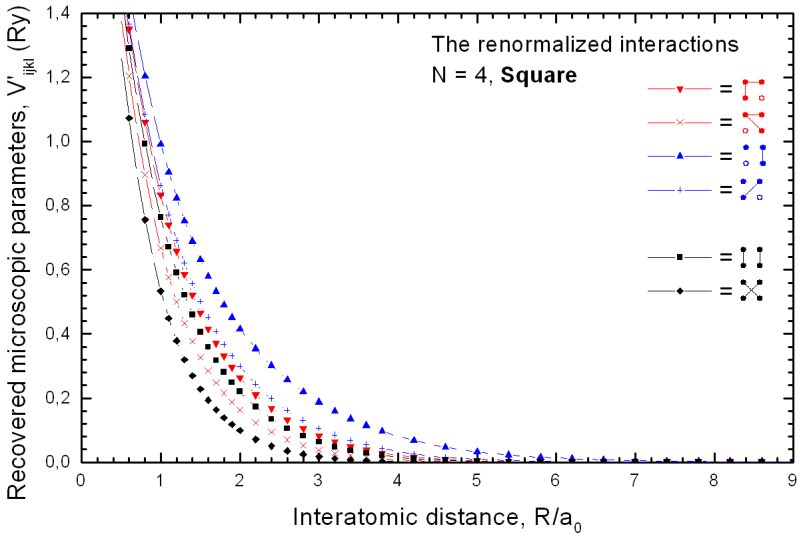

(b)

Figure 11: Microscopic parameters vs. R in the atomic representation for the square configuration of the $N = 4$ atom cluster. (a) 1- and 2-site interaction parameters. (b) The values of 3- and 4-site interaction parameters using the renormalization *ansatz*. The inset specifies various types of 3- and 4-site parameters.

Table 2: One- and two-site microscopic parameters vs. R in the atomic representation for the square configuration of four atoms. The star marks the distance R with the lowest energy.

R/a_0	U' (Ry)	K'_1 (Ry)	K'_2 (Ry)	V'_1 (Ry)	V'_2 (Ry)	J'_1 (Ry)	J'_2 (Ry)
0,5	1,98	1,83	1,71	1,73	1,53	1,57	1,27
1,0	1,72	1,39	1,19	1,18	0,88	0,91	0,54
1,5	1,53	1,09	0,88	0,83	0,52	0,53	0,23
1,8	1,45	0,96	0,75	0,68	0,38	0,39	0,14
1,9*	1,43	0,93	0,72	0,63	0,35	0,35	0,12
2,0	1,41	0,89	0,69	0,59	0,32	0,32	0,10
2,5	1,33	0,75	0,56	0,43	0,20	0,19	0,05
3,0	1,29	0,64	0,47	0,31	0,12	0,11	0,02
3,5	1,26	0,56	0,40	0,22	0,07	0,06	0,01
4,0	1,25	0,50	0,35	0,15	0,04	0,03	0,00
5,0	1,25	0,40	0,28	0,07	0,01	0,01	0,00

thors [19, 20, 18] suggest using the *Gaussian* reference functions to describe approximately the *Slater* orbitals (11). At present, STO-3G, 4-31G, and 6-31G are the bases used most frequently in the calculations of properties of nanoscopic systems [19]. The reason for using the *Gaussian* bases is they can provide us with the 3- and 4-site interaction parameters in an analytic form. On the other hand, linear combinations of the *Gaussian* functions do not approximate the *Slater* functions accurately, there are four such combinations in the definition of interaction parameters (6), and the number of parameters increases sharply ($\sim N^4$) with the number of atoms in the system. This can result in an error, the impact of which might be substantial for larger systems.

Therefore, we have chosen yet another approach to approximate the integrals itself and not their building blocks. An *ansatz* we utilize makes an approximation that applies to the complete set of interaction parameters and not to the particular parameters, and thus does not cause the accumulation of the error.

Table 3: Three- and four-site microscopic parameters vs. R in the atomic representation for the square configuration of four atoms. The star marks the distance R with the lowest energy.

R/a_0	V'_{1142} (Ry)	V'_{1132} (Ry)	V'_{1213} (Ry)	V'_{1412} (Ry)	V'_{4312} (Ry)	V'_{1432} (Ry)
0,5	1,52	1,39	1,61	1,53	1,47	1,27
1,0	0,83	0,67	0,99	0,86	0,76	0,53
1,5	0,47	0,33	0,63	0,50	0,41	0,23
1,8	0,33	0,22	0,49	0,37	0,28	0,14
1,9*	0,30	0,19	0,45	0,33	0,25	0,12
2,0	0,26	0,16	0,42	0,30	0,22	0,10
2,5	0,15	0,08	0,28	0,18	0,12	0,04
3,0	0,08	0,04	0,19	0,11	0,06	0,02
3,5	0,04	0,02	0,12	0,06	0,03	0,01
4,0	0,02	0,01	0,08	0,03	0,02	0,00
5,0	0,00	0,00	0,03	0,01	0,00	0,00

3.3 The single-particle parameters

Apart from the two-particle interactions, the single-particle part (namely, the atomic t_{ii} and the hopping t_{ij} parameters) provides a major contribution to the system energy. The single-particle microscopic parameters (cf. Table 4) are drawn in Fig. 12a. One should note the ground state energy reflects the dependence on R of the microscopic atomic energy.

For the number of sites $N > 2$ we encounter one additional feature, there appear the sites contributing with their potentials to the hopping and different from the pair involved. The contribution originates from the form of $H_1(\mathbf{r})$ in Eq. (5). Namely, the hopping term is influenced, in general, by all nuclear potentials in the system, since we have that

$$H_1(\mathbf{r}) = -\nabla^2 - Z \cdot \sum_k \frac{2}{|\mathbf{r} - \mathbf{R}_k|}, \tag{16}$$

where $\mathbf{R}_k$ is the atomic position. This circumstance introduces the 3-center integrals to the hopping parameters (cf. Appendix C.1). The integrals contain non-analytical functions, but they can be calculated with reasonable

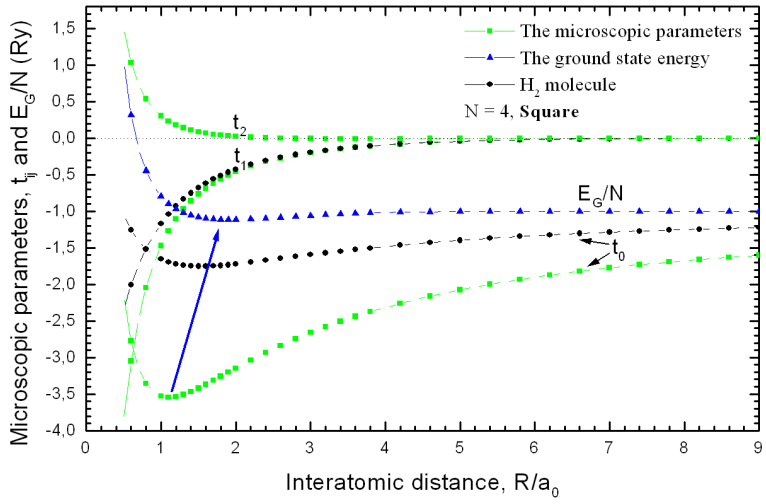

(a)

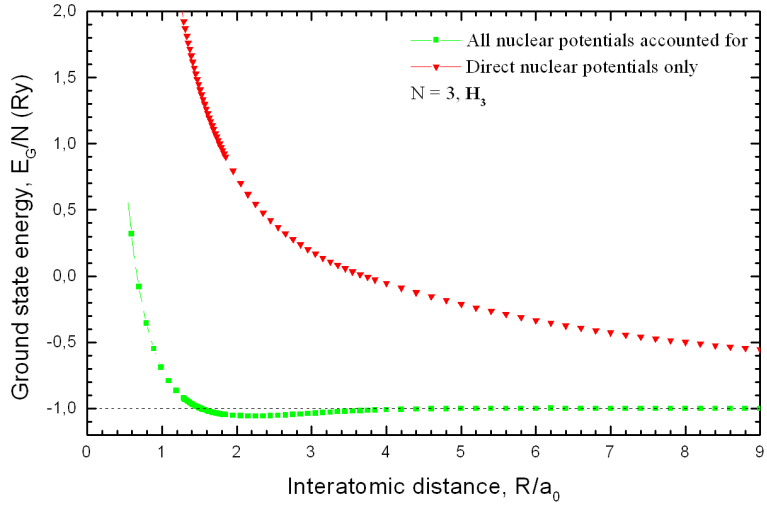

(b)

Figure 12: (a) Single-particle hopping parameters in the *Wannier* representation for the square configuration of four atoms. The atomic energy t_0, the hopping parameters t_1 and t_2, and relation to the ground state energy E_G. (b) Ground state energy for the H_3 system. The influence of the sites contributing with their potentials to the hopping and different from the pair involved is shown (lower curve).

Table 4: The ground state energy, the atomic energy, as well as the hopping parameters for the square configuration of four atoms. The star marks the distance R with the lowest energy.

R/a_0	t_0 (Ry)	t_1 (Ry)	t_2 (Ry)	α (a_0^{-1})	$E_{el.}$ (Ry)	E_G (Ry)
0,5	-2,15	-3,87	1,51	1,585	-4,3834	1,0308
1,0	-3,53	-1,47	0,30	1,373	-3,5042	-0,7971
1,5	-3,42	-0,77	0,09	1,225	-2,8861	-1,0814
1,8	-3,26	-0,56	0,04	1,162	-2,6167	-1,1127
1,9*	-3,20	-0,50	0,03	1,145	-2,5394	-1,1147
2,0	-3,15	-0,46	0,02	1,130	-2,4676	-1,1140
2,5	-2,88	-0,30	0,00	1,067	-2,1738	-1,0909
3,0	-2,66	-0,20	-0,01	1,028	-1,9617	-1,0593
3,5	-2,47	-0,14	-0,01	1,007	-1,8068	-1,0333
4,0	-2,32	-0,09	-0,01	1,000	-1,6932	-1,0165
5,0	-2,07	-0,04	-0,00	1,000	-1,5446	-1,0032

precision within a reasonable time (cf. Appendix C.2). In Fig. 12b we show the importance of taking into account all the nuclear potentials, regardless of the computational effort. The results are stable only when all the potentials are included. More importantly, taking into account only the potentials $V(\mathbf{r}-\mathbf{R}_i)$ and $V(\mathbf{r}-\mathbf{R}_j)$ as contributing to t_{ij}, breaks the size-consistency of the result.

As could be expected, the single-particle parameters, calculated in this manner, are predominant factors, their magnitudes can have values larger than the largest interaction parameters by factor of two for small R. Moreover, the atomic energy changes dramatically when the number of neighbouring atoms in the system (the coordination number) increases (cf. Fig. 12a). The above seems to be a steady pattern when approaching the solid-state limit. One should underline that the atomic part involves *Wannier* functions and this contributes to its strong R dependence.

3.4 The requirement lists

Requirement lists for an acceptable method of dealing with nanoscale cluster systems are widely known in quantum chemistry. One of the first such lists, published by *Pople et al* [21], contains four points:

1. A method should provide well-defined results for the energies of electronic states for any arrangement of fixed nuclei, leading to a set of continuous potential energy surfaces.
2. A method should be such that the amount of computation does not increase too rapidly with the size of the system.
3. A method should be size-consistent.
4. A method should yield upper bounds to the exact solutions, i.e. be variational.

Another such list, published by *Bartlett* [22], states that:

1. A method should be size-extensive.
2. A method should be generally applicable to a wide class of problems within one framework, i.e. not dependent on specific choices of configurations.
3. A method should be invariant to unitary transformations among degenerate orbitals.
4. A method should be efficient and cost-effective.
5. A method should be applicable to excited states and open shells.
6. A method should be able to dissociate a molecule correctly into its fragments.

The second, the third, and the fifth items on the *Bartlett*'s list can together be considered as a more explicit statement of the *Pople*'s first requirement. New

on this list is the realization that even though a method yields continuous potential energy surfaces it may also yield unphysical results if it fails to describe dissociations properly. Furthermore, the upper bound requirement has been dropped for it has been found that the requirement is of little importance without a lower bound. The upper bound, in this case, gives no real information about the accuracy of calculation and hence, in practice, is of little use. Implications of the requirement lists are widely discussed in the PhD Thesis of van Dam [20].

The EDABI approach as a whole, supplemented with the referred stabilization techniques, can also be checked against such lists. The results we present in this and the following Chapters are also supposed to prove its consistency with the above requirements. We could already note that our approach satisfies the *Pople*'s first and fourth requirements for tiny atomic displacements always yield tiny changes in the Hamiltonian and what follows they yield tiny changes in the ground state energy also. Furthermore, the approach provides exact results, which in particular are the upper bounds, though it is not variational by nature (it mixes exact diagonalization with variational determination of the microscopic parameters). The more explicit *Bartlett*'s requirements (the second, third, and fifth) are also satisfied, what can be easily seen from the fact that the EDABI approach provides exact solutions within the space spanned by the single-particle basis, which do not depend on the particular basis choice.

Unfortunately, the present implementation of the EDABI approach requires significant amounts of computation for large systems. Thus, it violates the *Pople*'s second and the *Bartlett*'s fourth requirements, and we shall see these are the only obstacles we face with the approach. Yet, the rapid growth of computer power and the development of *ab initio* methods give hope the problem could be overcome in the future. Additional feature is the explicit solution of the renormalized wave equation, which would make the EDABI approach self-contained.

4 Cluster properties of different size

In this Chapter we compare the results obtained with the help of the EDABI approach for several nanosystems in the configurations shown in Fig. 13. The studied clusters represent regular geometric figures and all of them are controlled by a single interatomic-distance parameter.

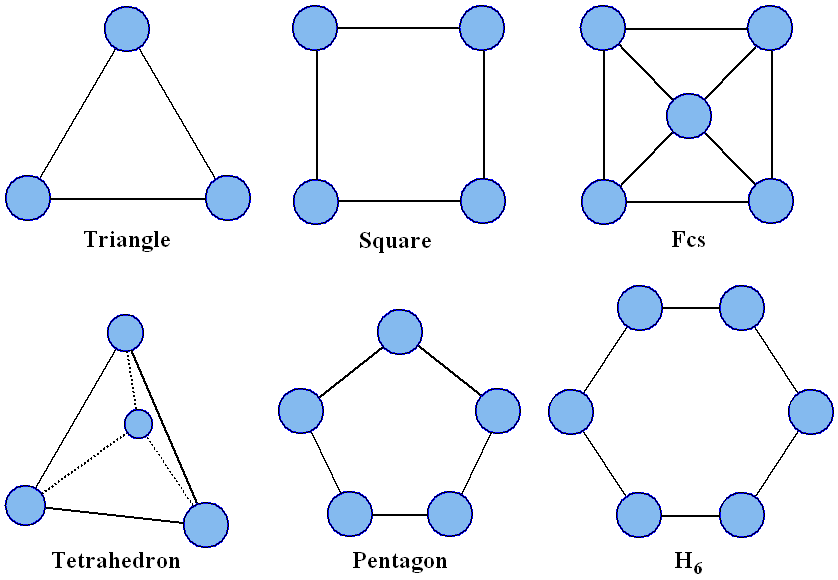

Figure 13: Configurations of the studied nanosystems. Labels identifying the particular systems in the subsequent figures are also provided.

We discuss the energetic stability at temperature of 0 K, the dimerization amplitude, as well as the excited-state profiles of the above nanosystems. Furthermore, we analyze the impact of small distortions applied to the system regular geometry by smoothly changing atomic positions, that provides us with the zero-point energies and the phonon frequencies. The present discussion is meant to provide a systematic analysis of the nanosystems composed of 3 to 6 atoms in the above configurations. In the following Chapters we present those properties and compare them with those of H_2 molecule.

4.1 The dissociation patterns

Ground state energy is one of the most important characteristics when considering the system stability. Our results, presented in Fig. 15ab, indicate that all of the configurations are stable with respect to dissociation into the individual atoms ($E_G/N < -1$ Ry). Yet, all of them also have the ground state energy at the optimal interatomic distance far larger than the H_2 molecule. That could be an explanation why there are no such complexes in nature, they just simply separate into hydrogen molecules.

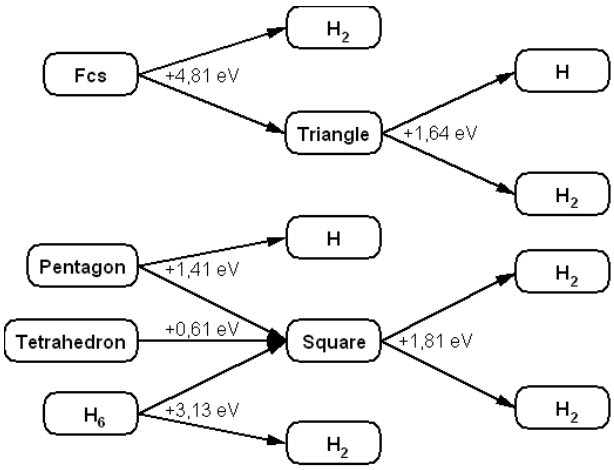

Figure 14: Dissociation diagrams of the studied complexes into H_2 molecules. The energy-gain in the process is also shown.

However, an external pressure or a background potential can influence this behavior and make H_2 molecules combine into more complex structures. Such dimerization could take place in the solid hydrogen when the *hcp* structure is formed under high pressure at low temperature. The diagram (Fig. 14) shows possible patterns of dissociation of the studied complexes, they finally always dissociate into H_2 molecules, and yet some of them can have the intermediate *Triangle* or *Square* configuration, for they appear to have appropriate separation energies, making them the most likely objects when the system is under the pressure. In Table 5 we list the corresponding numerical values for the studied clusters. The configurations are arranged in

the descending order of the separation energy per atom, $E_{sep.}/N$. The optimized orbital size $a \equiv 1/\alpha$ and the optimal interatomic distance R/a_0 are also shown.

Table 5: The optimal interatomic distance, the orbital size, and the separation energy for several nanosystems.

Configuration	R/a_0	a (a_0)	$E_{sep.}$ (eV)	$E_{sep.}/N$ (eV)
H_2	1.45	0.84	4.02	2.01
Square	1.9	0.88	6.24	1.56
Tetrahedron	2.1	0.89	5.63	1.41
H_6	2.0	0.89	7.14	1.19
Pentagon	1.8	0.91	4.83	0.97
Triangle	2.2	0.93	2.38	0.79
Fcs	3.4	0.95	1.59	0.32

One should note that all the configurations are unstable and hence the results cannot be compared to the experimental values, and yet the relevance of the obtained separation energies can be demonstrated by considering the H_2 molecule where the experimental value for the heat of formation 436 kJ/mol indicates the error of about 10%. One should also note that the *Tetrahedron* configuration is less stable energetically, though it is composed of the same number of atoms as the *Square* configuration. The *Fcs* configuration, on the other hand, shows the lowest separation energy from the studied configurations and the optimal interatomic distance almost twice as that for the others. Obviously, that situation can be explained by the presence of the central atom. However, in Fig. 16a we point out that the variational parameter α readjusts in the *Fcs* configuration more rapidly than for the others. This circumstance hints to the possibility that more than just one variational parameter are required to minimize the ground state energy further.

Furthermore, in Fig. 15ab we also characterize the size-consistency, as well as the size-extensivity, of the EDABI approach, what satisfies both the *Pople*'s [21] as well as the *Bartlett*'s [22] requirements for an acceptable method to be used in quantum chemistry.

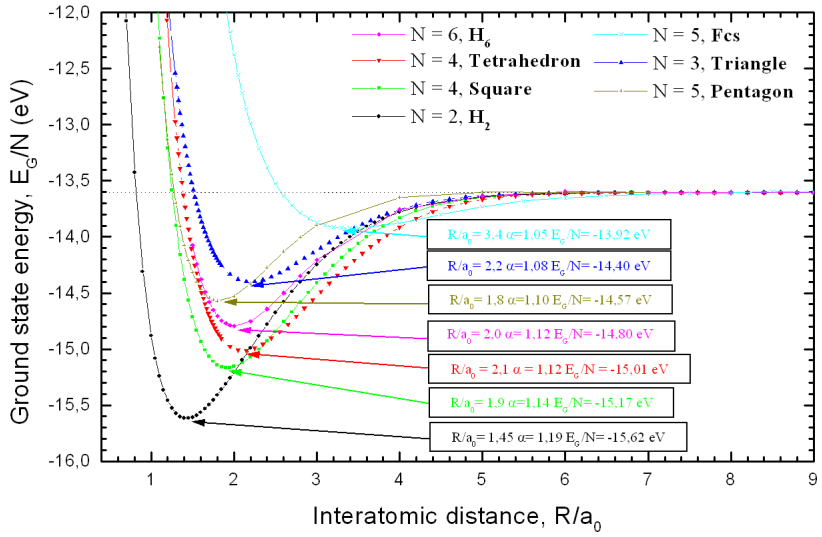

(a)

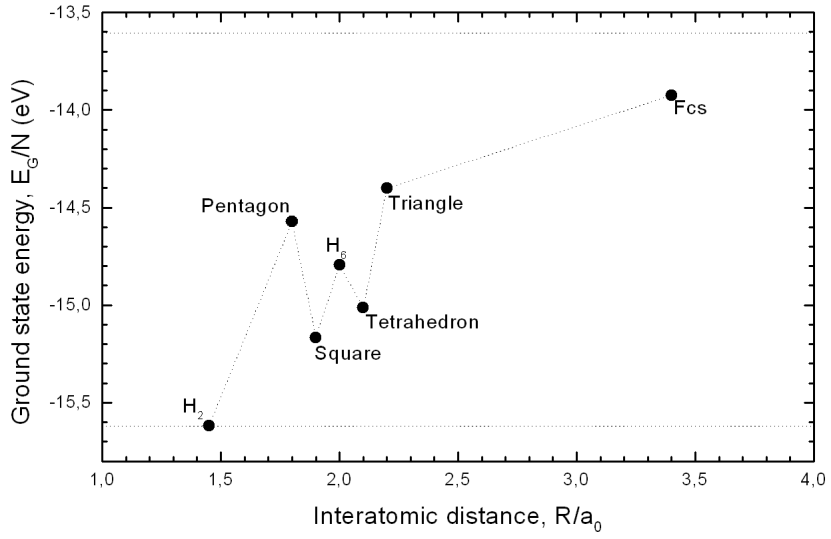

(b)

Figure 15: (a) R dependences of the total ground state energy (per atom, including both the electron and the lattice contributions) for several nanosystems. (b) The stability points for each of the nanosystems studied.

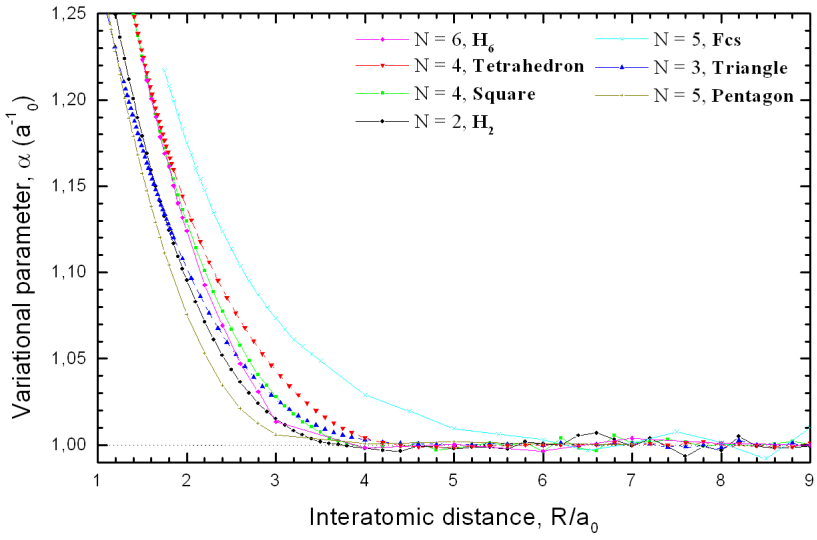

(a)

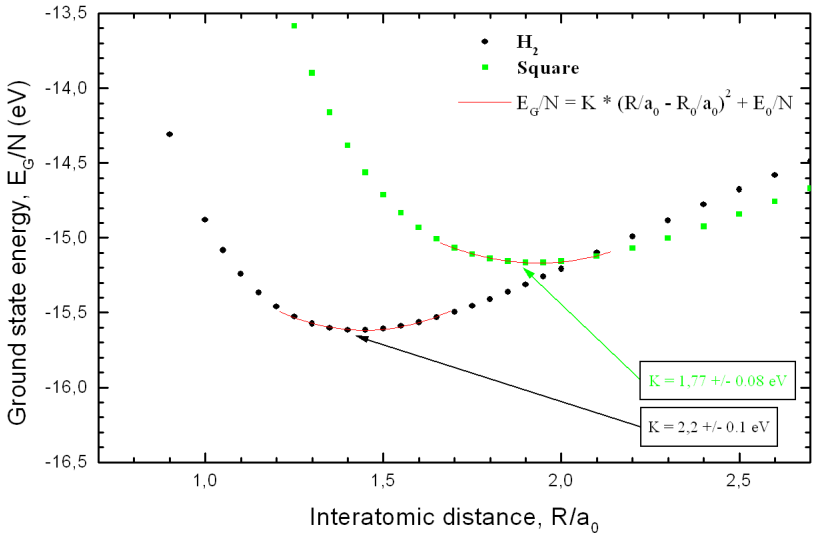

(b)

Figure 16: (a) Optimal value of the variational parameter for several nanosystems. (b) Total ground state energy approximated with parabolic function used to calculate the zero-point energies and the phonon frequencies.

4.2 The metastable configurations

It was suggested in the previous Chapter that the *Triangle* and the *Square* configurations can play the role of intermediate steps in the dissociation processes of more complex structures. Such intermediate configurations dissociate finally into H_2 molecules. The dissociation patterns, where the intermediate configurations are taken into consideration, (cf. Fig. 14) were obtained by simply analyzing the separation energies and the optimal interatomic distances of the studied nanosystems (cf. Table 5). We still need to determine if the configurations are metastable in order to see the system sustainability for a reasonable time interval. The Figure below presents the dissociation of the chosen configurations.

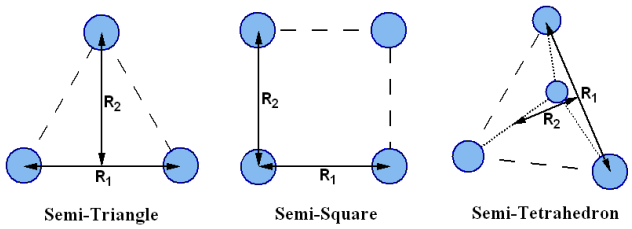

Figure 17: The irregular *Triangle*, *Square*, and *Tetrahedron* configurations dissociating. The interatomic distance parameters R_1 and R_2 are also marked.

Obviously, all the configurations in the dissociation limit $R_2 \to \infty$ have the separation energies per atom $E_{sep.}/N$ identical with that of the H_2 molecule. However, the studied systems behave differently as the parameter R_2 decreases. The parameter R_1 is always chosen to minimize the ground state energy of the system.

In Fig. 18ab we can see the effect of deformation applied to the regular configurations. The obtained ground-state energy dependency in the case of the *Triangle* configuration has no global minimum, and yet there is an interesting local minimum in the direct closeness to the regularity point. The local minimum depth is about 50 meV. This result indicates that the regular *Triangle* configuration can be sustained within relatively long period of time, i.e. it is metastable. The *Square* and the *Tetrahedron* configurations,

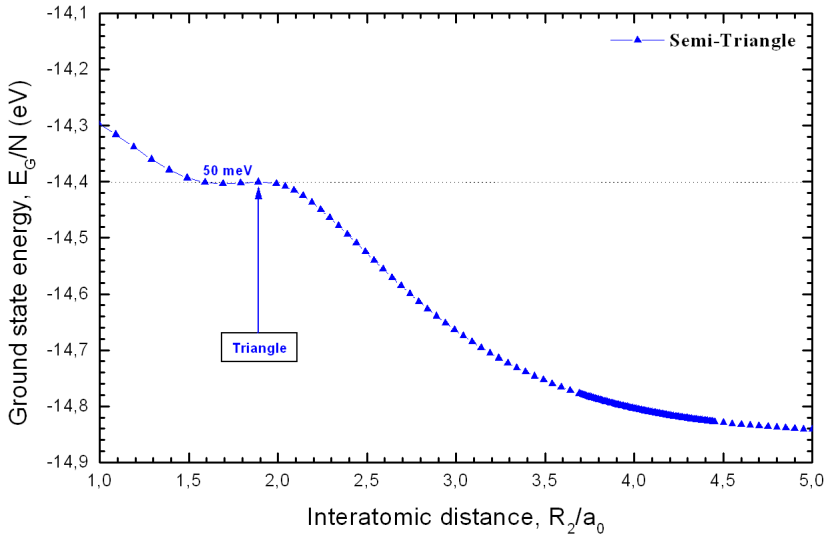

(a)

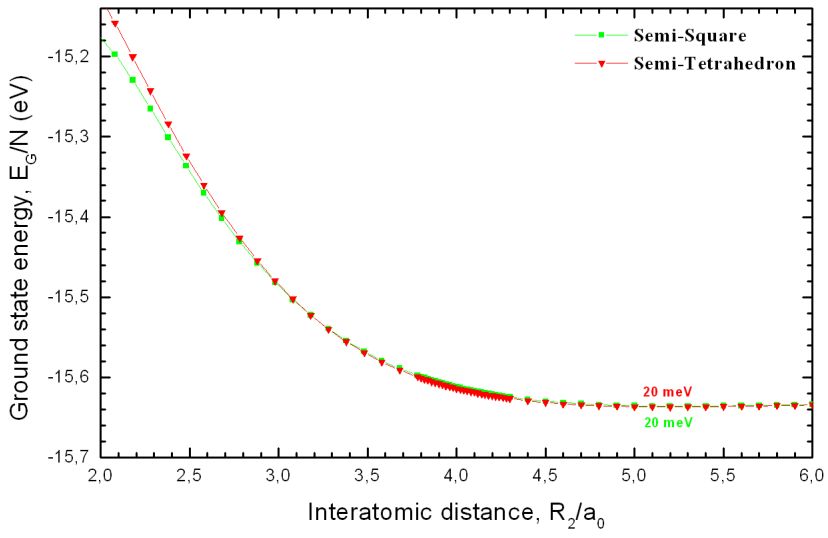

(b)

Figure 18: (a) Dissociation of the third atom in the *Triangle* configuration. The regular figure coincides with local maximum in the energy. (b) Dissociation of the atomic pair in the *Square* and the *Tetrahedron* configurations. There is a slight global minimum in the energy.

on the other hand, have global minima situated below even the energy of the H_2 molecule, what suggests some kind of long-range interaction between the H_2 molecules ($R_1/a_0 \sim 1.43$ and $R_2/a_0 \sim 5.2$). However, the obtained minima do not mean that the studied configurations can be sustained infinitely, their depth is so small that we can claim they are surpassed with the zero-point energies (discussed in the following Chapter) or they originate from the approximations of the EDABI approach.

4.3 The harmonic oscillations

Dynamical properties of the studied nanosystems can be derived from the ground state energy dependence on the interatomic distance (Fig. 16b). We approximate it with parabolic function and determine the second order coefficient K. The approximation allows us to obtain the phonon (breathing-mode) frequency in the system by applying the harmonic oscillator theory. The results are obtained for the H_2 molecule and the *Square* configuration.

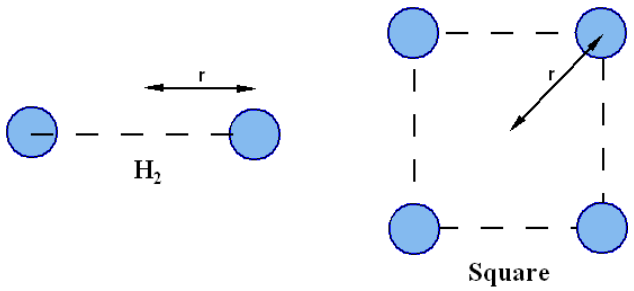

Figure 19: The H_2 molecule and the *Square* configuration oscillating around the center of mass. The oscillation variable **r** is also marked.

The oscillation (phonon) frequency of the breathing-mode can be easily obtained from the following equation

$$\ddot{\mathbf{r}} + \omega^2 \cdot (\mathbf{r} - \mathbf{r}_0) = 0, \tag{17}$$

where **r** represents distance from the center of mass in the system and ω is the breathing-mode frequency, and thus

$$\omega = \frac{S}{a_0}\sqrt{\frac{e}{m_H} \cdot 2K}. \tag{18}$$

Here, m_H represents hydrogen atom mass, S is the structural factor, which yields 2 for the H_2 molecule and $\sqrt{2}$ for the *Square* configuration, and K is the elastic constant. Thus, the zero-point energy can be obtained through the relation

$$E_{z.p.} = \frac{\hbar\omega}{2}. \tag{19}$$

The phonon breathing-mode frequencies, as well as the zero-point energies, are shown in the following table.

Table 6: The phonon breathing-mode frequency and the zero-point energy of the chosen configurations.

Configuration	ν (THz)	$E_{z.p.}$ (meV)
H_2	123 ± 3	255 ± 6
Square	78 ± 2	162 ± 4

One should note, the above results could be obtained only because of the fact that the EDABI approach allows us to analyze the system evolution as a function of interatomic distance. The zero-point energies we obtain with good precision (about 3%) and their relevance can be seen by considering the H_2 molecule where the experimental value 25.9 kJ/mol indicates the error of about 5%.

4.4 The density profiles

Electron density profiles, considered in this Chapter, are another properties of the studied systems that provide real-space characteristic. The ability to determine it is an important feature of the EDABI approach, and is of significant interest. The electron density is often taken to determine molecular or solid-state bond characteristics, as well as to approximate the electronic transport in the nanosystems. We start from the well known fact that the

electron density is closely related to the many-particle wave function, and for the system with N electrons we have the particle density in the form

$$n(\mathbf{r}_1...\mathbf{r}_N) = N \cdot |\Psi_N(\mathbf{r}_1...\mathbf{r}_N)|^2, \tag{20}$$

where $\Psi_N(\mathbf{r}_1...\mathbf{r}_N)$ is the N-particle wave function. The expression for the electron density in the second quantization formulation is obtained by integration over all the electron configurations and yields Eq. (A16), the calculation is detailed in Appendix A.2. In Fig. 20ab we can see the electron density profiles of the chosen atomic configurations. The profiles are obtained for the configurations in the ground state and at the optimal interatomic distance. The interesting fact is the densities are heavily dependent on the correlation functions $\langle\Phi_N|a_i^+ a_j|\Phi_N\rangle$, which provide the significant contribution to the overall electron density. In the *Hartree-Fock* theory, for example, it takes the form

$$n_{HF}(\mathbf{r}) = \sum_i |w_i(\mathbf{r})|^2, \tag{21}$$

where $\{w_i(\mathbf{r})\}$ are the *Wannier* functions centered respectively on $\{i \equiv \mathbf{R}_i\}$. We present in Fig. 21ab the relative error of the *Hartree-Fock* theory. One should note the difference is nonnegligible and its value is up to 80% depending on the region in space.

Obviously, the EDABI approach, as well as the *Hartree-Fock* treatment, utilize the optimized *Wannier* basis when determining the electron density. However, only the EDABI approach incorporates the average occupation factor of the basis states and the correlation functions in the many-particle state.

4.5 The *Wannier* basis

We determine the *Wannier* functions by applying the relation (B1) to the $1s$ atomic orbitals (11). The variational parameter α is taken to minimize the ground state energy of the many-particle state. The following figure shows one of such functions for the H_6 configuration. Obviously, the remaining

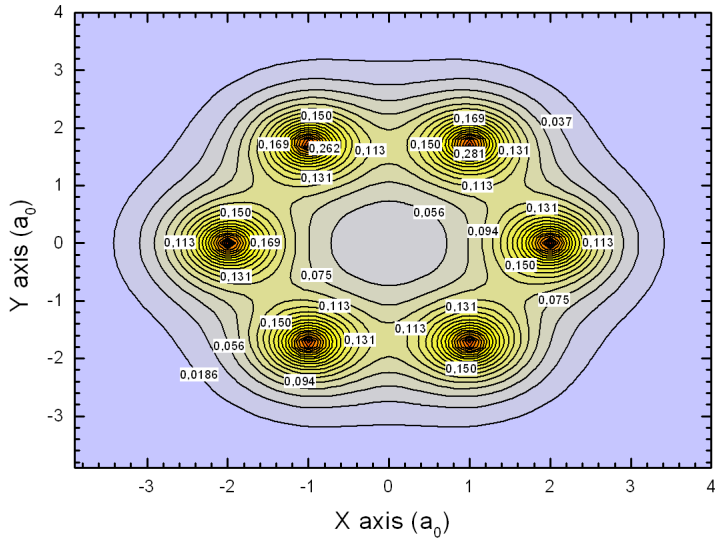

(a)

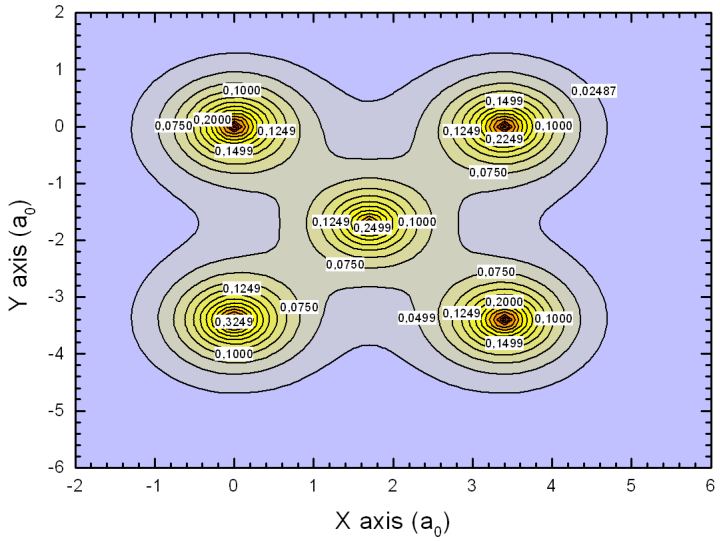

(b)

Figure 20: The profiles of the electron density of in units a_0^{-3} for the H_6 (a) and the *Fcs* (b) configurations for the ground state and at the optimal interatomic distance.

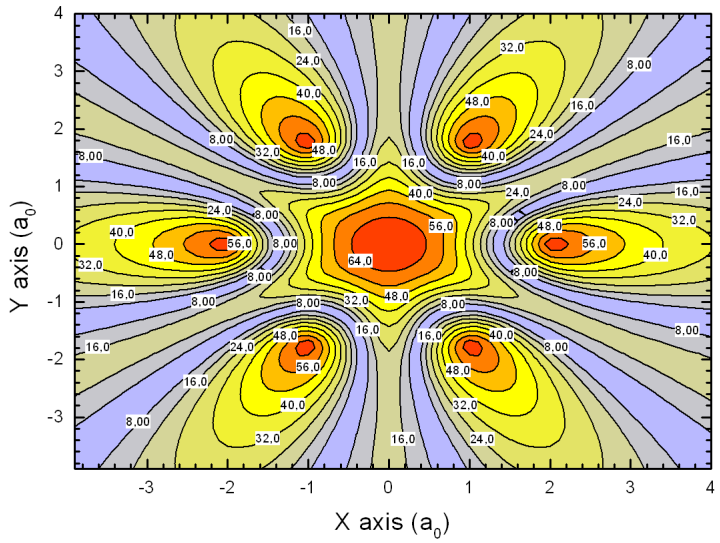

(a)

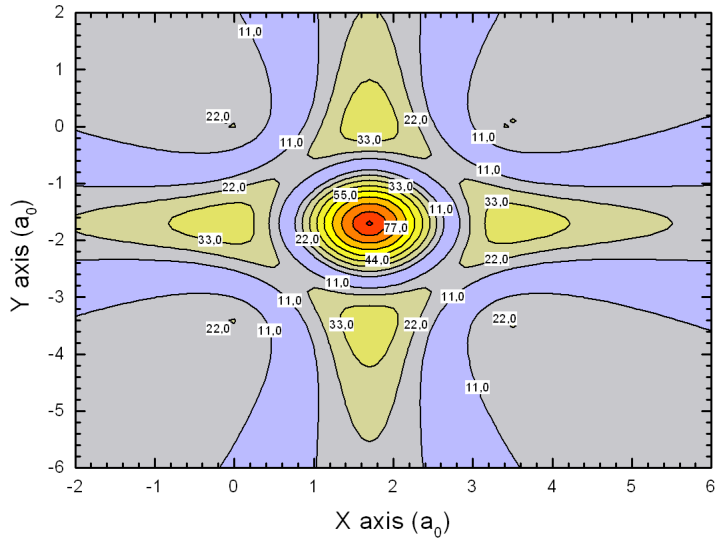

(b)

Figure 21: The relative error (%) in the electron density of the *Hartree-Fock* theory for the H_6 (a) and the *Fcs* (b) configurations for the ground state and at the optimal interatomic distance.

single-particle wave functions are of the same shape, since the system is rotationally invariant.

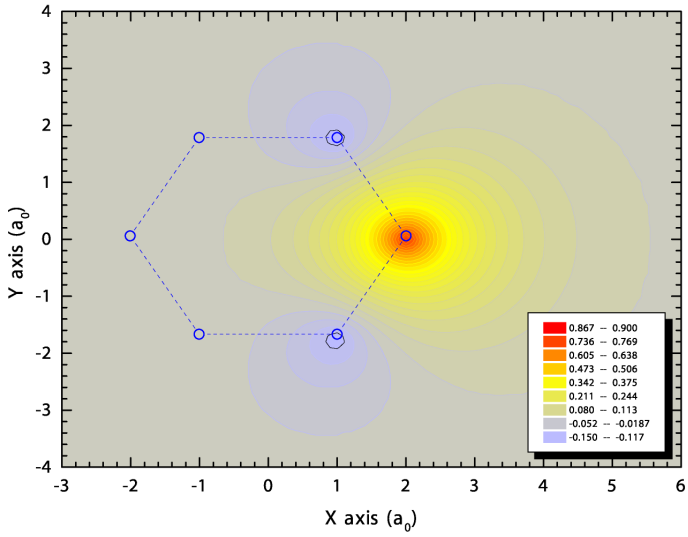

Figure 22: Single *Wannier* function for the H_6 configuration for the ground state and at the optimal interatomic distance. Note the negative values at the nearest neighboring sites.

The system with two different *Wannier* function shapes is the *Fcs* configuration, we can see these functions in Fig. 23ab. The function localized on the central atom (Fig. 23b) is more compact, since it is influenced by the surrounding electrons. All the figures also show that our method of determining the *Wannier* functions (cf. Appendix B.1) always makes them localized on the individual atoms. Such localization features are crucial to make the renormalization *ansatz* (cf. Appendix B.2) work better.

4.6 The excited states

Apart from the ground states of the nanosystems, we determine the excited states as well. The EDABI approach allows us to obtain all the eigenenergies and the eigenstates of the Hamiltonian for each of the studied systems.

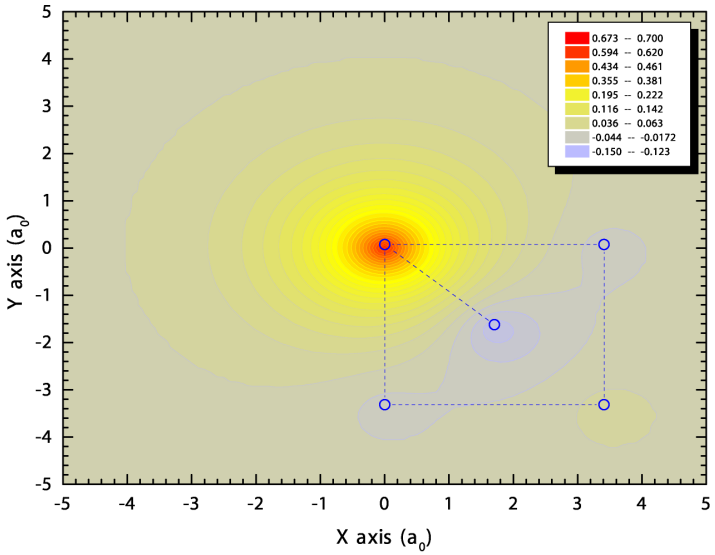

(a)

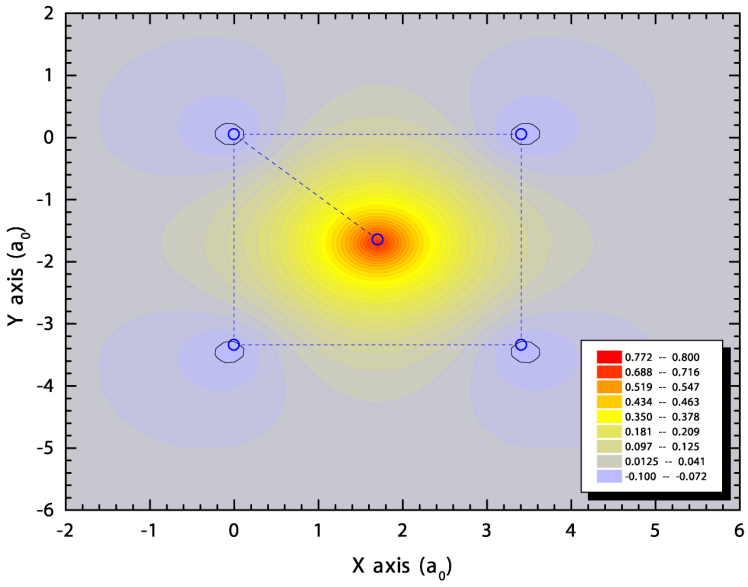

(b)

Figure 23: *Wannier* functions for the *Fcs* configuration for the ground state and at the optimal interatomic distance. (a) The function is centered on the border atom. (b) The same, but on the central atom.

Moreover, we can classify the many-particle states of the systems into the classes with the constant number of double occupancies. Each of the classes is expected to be characterized by the energies significantly different from the others by the single-site *Hubbard* interaction U, which is the major contribution to the system energy. As we can see in Fig. 24, the excited states, in general, follow the pattern of the double-occupancy classes and each of the classes represents the particular subband of the electronic structure in the nanosystem. The results suggest that the subbands are thin and separated by the *Hubbard* gap for a larger interatomic distance, which collapses as the interatomic distance decreases.

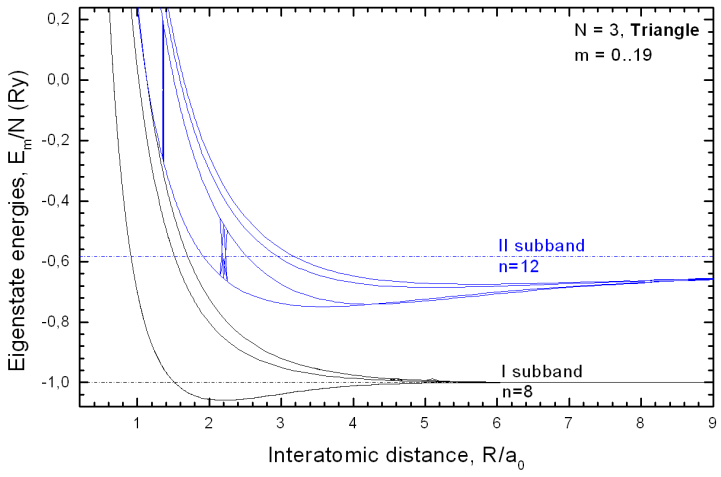

Figure 24: The energy spectrum (per atom, including both the electron and the lattice contributions) for the *Triangle* configuration. The double-occupancy classes are seen at larger R values.

The maximal gap width in the limit of large interatomic distance can be easily calculated, since the *Wannier* functions tend to the atomic functions and the variational parameter α tends to unity then. Hence, the single-site *Hubbard* interaction U determines the gap width and, according to Eq. (C22), in the $R \to \infty$ limit the width is equal to 1.25 Ry. We mark such maximal gap values with dashed horizontal lines (cf. Fig. 24, 25ab).

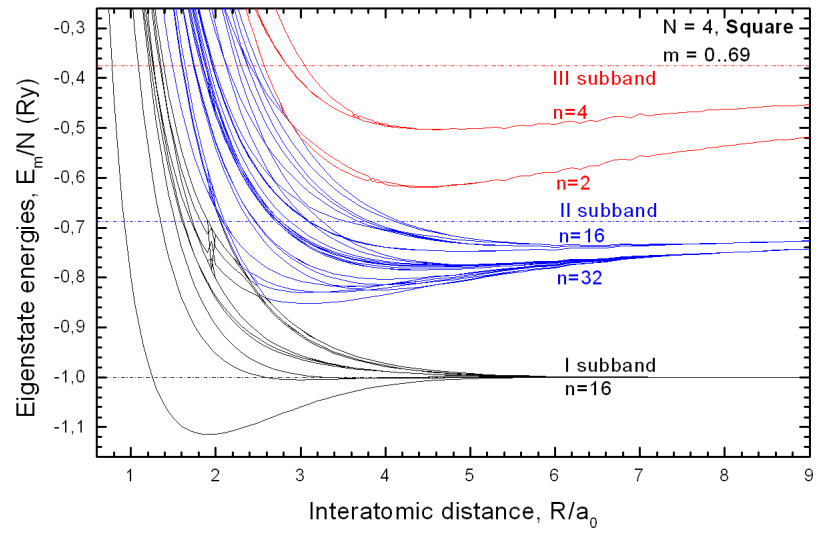

(a)

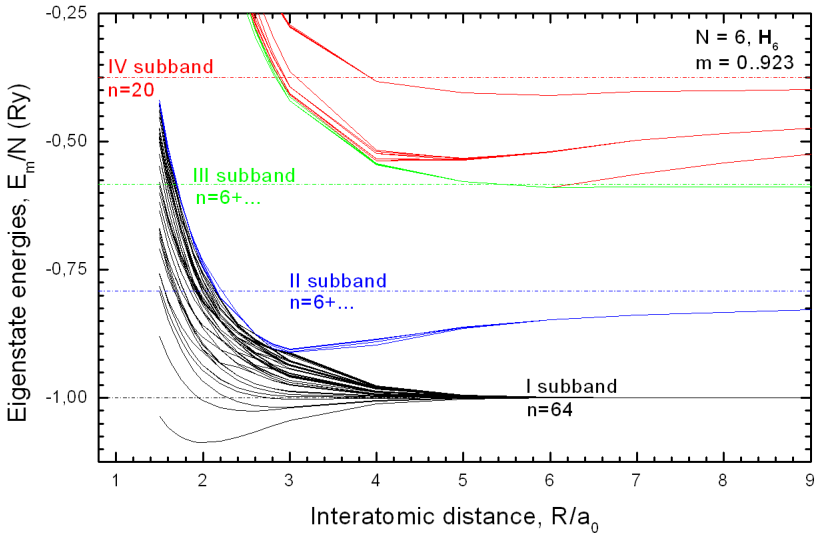

(b)

Figure 25: The energy spectrum (per atom, including both the electron and the lattice contributions) for the *Square* (a) and the H_6 (b) configurations. The subbands appear clearly when R increases.

Table 7: The approximate interatomic distance R/a_0, at which the *Hubbard* gaps collapse.

Configuration	1st gap	2nd gap	3rd gap
Triangle	1.14	-	-
Square	2.6	3.0	-
H_6	3.0	?	6.0

An interesting feature of the nanosystems is that they can have more than two distinct *Hubbard* subbands (Fig. 25ab). The well known lower and the upper *Hubbard* subbands seem to be just the lowest two in this model. Thus, the complete band structure of any of the systems consists of the *Hubbard* subbands in the large R limit, and all the *Hubbard* gaps collapse as the interatomic distance decreases. The gap values at the optimal interatomic distance determine whether the system is quasimetallic, semiconducting, or insulating. Hence, the ability to determine them provides a valuable insight into the system transport properties. This feature of the EDABI approach is of the particular interest, for it provides characterization in terms of the interatomic distance, at which the collapse occurs, and not in terms of the interaction magnitude, as is usually the case. In the Table 7 we list the approximate interatomic distances, at which the gaps collapse. One should note that all the gaps collapse at the distances comparable to the optimal ones (cf. Table 5). This can indirectly explain why the solids appear in many different states from the elastic transport point of view.

4.7 The absolute stability

The nanosystems with non-unitary filling of the orbitals can also be studied with the EDABI approach. The most interesting and widely considered [28, 29, 30] is the H_3^+ ion. This ion plays an important role in many different fields, such as chemistry, plasma physics, and astronomy. It was discovered in the diffuse interstellar medium and characterizes the Jupiter atmosphere. It is also the dominant positively charged ion in the molecular hydrogen plasma. What is more important, it has been found both the ion is stable and lacks

a stable excited state, as well as a permanent electric dipole moment. These features make electronic and rotational spectroscopy inapplicable here, and the only excited states that can be detected in the case of this ion belong to the low-energy rotation-vibration infrared spectrum. Recently, there have been discovered the quasi-bound predissociative states in the high-energy region also.

In Fig. 26a we can see the energy spectrum of the H_3^+ ion. The results are obtained by considering the atomic configuration identical to the *Triangle* configuration and the *Fock* space spanned with the many-particle states having two electrons instead of three. The H_3^+ ion ground state and two pairs of its (degenerate) excited states are found to have a global minimum with respect to the interatomic distance. However, this does not mean they are stable yet, we analyze the dissociation patterns of the H_3^+ ion to determine that.

Table 8: The optimal interatomic distance, the orbital size, and the separation energy for the systems relevant to the H_3^+ ion study.

Configuration	R/a_0	a (a_0)	$E_{sep.}$ (eV)	$E_{sep.}/N$ (eV)
H_3^+	1.69	0.72	8.09	2.70
H_2	1.45	0.84	4.02	2.01
H_2^+	2.0	0.81	2.35	1.18
Triangle	2.2	0.93	2.38	0.79

The possible patterns of dissociation, e.g. initiated by a photon, can be expressed with the following chemical equations

$$H_3^+ + h\nu_1 \rightarrow H + H + H^+,$$

$$H_3^+ + h\nu_2 \rightarrow H_2 + H^+,$$

and

$$H_3^+ + h\nu_3 \rightarrow H_2^+ + H.$$

The first dissociation pattern (I) is clearly an endothermic process, what can be seen in Fig. 26a. The dissociation leads to the separation of all the ion

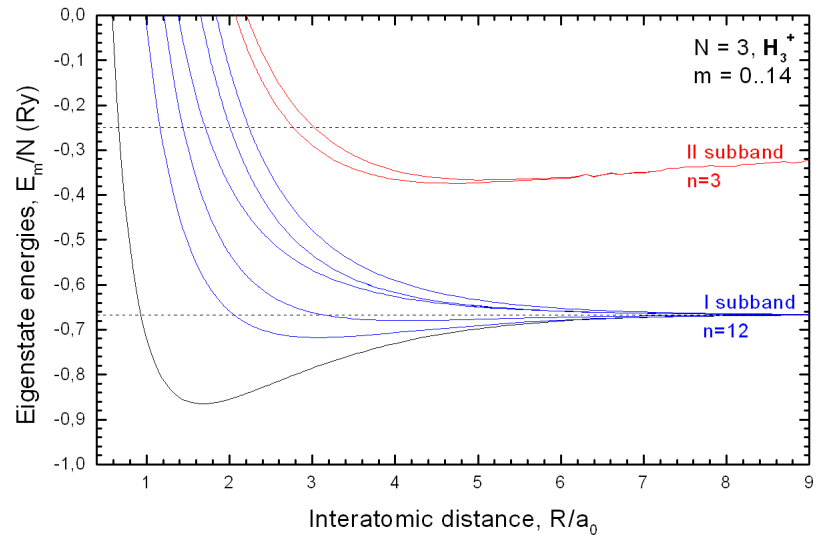

(a)

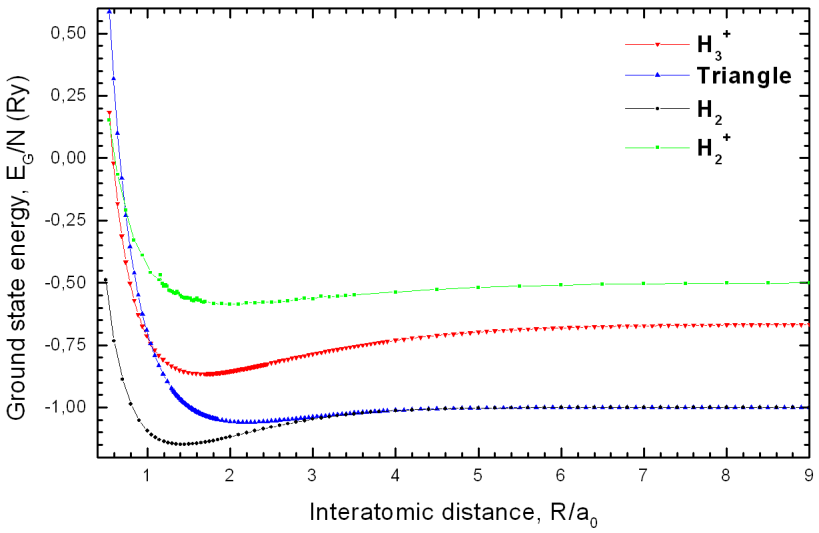

(b)

Figure 26: (a) Excited-state energy spectrum (per atom, including both the electron and the lattice contributions) for the H_3^+ ion. (b) Comparison of the ground-state energy dependencies for the systems relevant to the H_3^+ ion study.

components, what is equivalent to setting $R \to \infty$. Thus, the required energy can be easily calculated ($h\nu_1 = 8.09$ eV). The two remaining dissociation patterns (III and II) are also endothermic, and the required energies are lessened then with the separation energies of the H_2 molecule and the H_2^+ ion ($h\nu_2 = 4.07$ eV and $h\nu_3 = 5.74$ eV). The above results are obtained by analyzing Table 8 and the following diagram (Fig. 27) presents the energy levels for all the configurations taking part in the dissociation. As we can see, the H_3^+ ion has the lowest energy, and hence is an absolutely stable configuration.

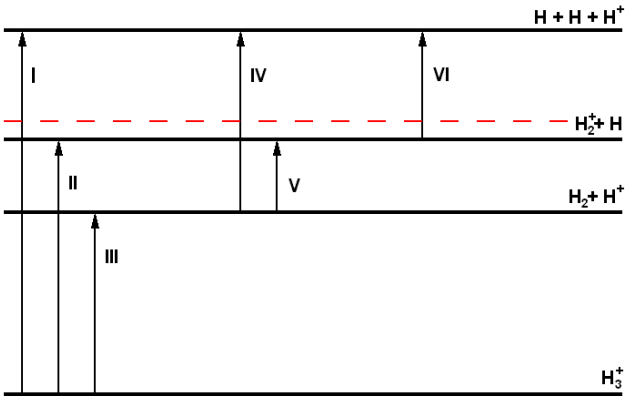

Figure 27: The energy levels of the configurations relevant to the H_3^+ ion study. The red, dashed line represents the lowest excited state of the H_3^+ ion.

The excited states of the H_3^+ ion, on the other hand, are unstable since the energy of the lowest of them lies above the energy of the dissociated ion (Fig. 27). As we can see, this result is compatible with the experimental data. Here, the transitions (IV and VI) represent the dissociations of the H_2 molecule and the H_2^+ ion, and are irrelevant in our study. Also, the transition (V) indicates instability of the H_2^+ ion since the following dissociation direction is preferred

$$H_2^+ + H \to H_2 + H^+ + h\nu_4,$$

where $h\nu_4 = 1.67$ eV. Apart from the H_3^+ ion stability, the major source of

its destruction is recombination with an electron or a neutral molecule. The common destruction mechanisms can be expressed with the equations

$$H_3^+ + e^- \rightarrow Triangle \rightarrow H_2 + H + h\nu_5,$$

and

$$H_3^+ + X \rightarrow XH^+ + H_2.$$

The second equation indicates that the H_3^+ ion is an efficient donor of positive charge to neutral molecules (X), yet this is out of the scope of this Thesis. The recombination with an electron, on the other hand, provides energy gain that can be easily calculated (Fig. 26b). Thus, such processes probably are accompanied with the photon emissions ($h\nu_5 = 9.54$ eV), and yet it is not clear whether the *Triangle* configuration appears as an intermediate metastable configuration in these processes.

4.8 The computational limitations

The EDABI approach, in its current form, presents serious computational limitations when considering the larger systems ($N > 12$). Hence, it is applicable only to either dealing with the smallest nanosystems or considering just the few essential orbitals. The main reason for this limitation is computational intractability of the Hamiltonian diagonalization for the larger number of sites in the system. To address the problem we can do one of the following:

1. apply symmetry criterions which reduce the size of the *Fock* space,
2. use one of the QMC-class methods instead of the *Lanczos* algorithm,
3. reduce the size of the *Fock* space by neglecting the vectors with minor contribution to the final ground state of the system.

The third solution to the problem seems to be the next step of development of the EDABI approach. However, there are questions if such vectors can be accounted for and how to identify them. Obviously, each of the vectors

in the *Fock* space contributes to the ground state with different amplitude. The probability of detection of the particular electronic configuration is

$$p_{i_1 \ldots i_N} = |\langle i_1 \ldots i_N | \Phi_N \rangle|^2 , \tag{22}$$

where $|\Phi_N\rangle$ is the N-particle ground state and $|i_1 \ldots i_N\rangle$ represents the particular electronic configuration. Therefore, the effective number of vectors in the ground state, according to *Shannon* expression for the number of configurations, can be determined with the following relation

$$L^{eff} \equiv 2^{-\sum_{i_1 \ldots i_N} p_{i_1 \ldots i_N} \log_2 p_{i_1 \ldots i_N}} = \prod_{i_1 \ldots i_N} (p_{i_1 \ldots i_N})^{-p_{i_1 \ldots i_N}} . \tag{23}$$

In this manner we examine the effective size of the *Fock* space for the ground state of the system under study.

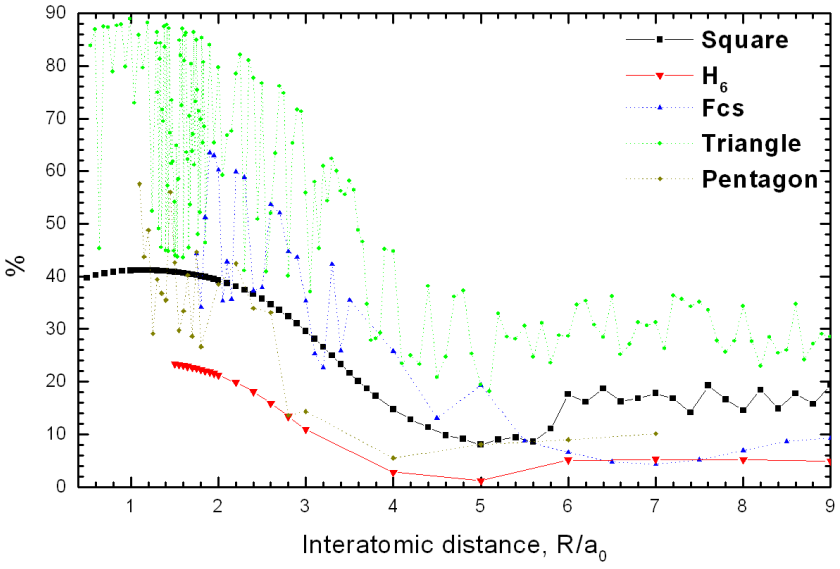

Figure 28: Effective number of basis vectors in the *Fock* space contributing to the ground state of several nanosystems. The number is taken as relative to the size of the *Fock*-space dimension for given model.

One should note that the effective size vs. R/a_0, presented in Fig. 28, is regular for the *Square* and the H_6 configurations, and more or less chaotic for the other. All the configurations show the increase in the effective size for the lower interatomic distances as well as its decrease with the increasing number of sites in the system. This corresponds to the precursory effects connected with formation of the effective symmetry-broken state with $N \to \infty$.

The last feature provides rationale behind the reducing the size of the *Fock* space for the larger systems. However, the aim of this Thesis is not to provide an algorithm of discarding some vectors in the *Fock* space, but to present that it is possible. This, was achieved by showing that the effective size can be much less than the size of the model *Fock* space even in the case of the nanosystems we study.

5 Electron tunneling

In this Chapter we present an approach to determining the electron tunneling current through nanosystems. At the present, the most frequently utilized approach is the *Landauer-Büttiker* formalism [5, 31, 32, 33]. According to this approach (cf. Appendix A.3), the *Landauer* equation (A22) determines the current flow through the system, and depends basically on the chemical potentials of the leads, the excitation spectrum of the system, and on the system transmittance (it is equal to unity in the ballistic transport). Thus, most methods differ in by the manner they provide the excited states or the transmittance of the nanosystems. The common preconditions for all the approaches have been detailed in Appendix A.3. One should note that none of them applies to the systems with the $1s$ atomic orbitals and for small number of sites.

5.1 The analytical approach

The approach of determining electronic current through the system should not be limited to the *Landauer-Büttiker* theory. The preferred by us method is to utilize the second-quantization formulation, where many-particle current-density operator can be derived from the single particle momentum operator, namely

$$\widehat{j} \equiv \widehat{\Psi}^{+}(\mathbf{r}) \left(-\frac{e}{m}\widehat{p}\right) \widehat{\Psi}(\mathbf{r}) = \frac{ie\hbar}{m} \widehat{\Psi}^{+}(\mathbf{r}) \nabla \widehat{\Psi}(\mathbf{r}), \tag{24}$$

where $\widehat{\Psi}(\mathbf{r})$ and $\widehat{\Psi}^{+}(\mathbf{r})$ are the field operators, and by taking the real part of the above expression we obtain a well known equation for the current density

$$\widehat{j} = \frac{ie\hbar}{2m} \left(\widehat{\Psi}^{+}(\mathbf{r}) \left(\nabla \widehat{\Psi}(\mathbf{r})\right) - \left(\nabla \widehat{\Psi}^{+}(\mathbf{r})\right) \widehat{\Psi}(\mathbf{r})\right), \tag{25}$$

and, by the use of Eq. (3), we have

$$\widehat{j} = \frac{ie\hbar}{2m} \sum_{ij\sigma} a_{i\sigma}^{+} a_{j\sigma} \left(w_i^{*}(\mathbf{r}) \nabla w_j(\mathbf{r}) - \nabla w_i^{*}(\mathbf{r}) w_j(\mathbf{r})\right) = \sum_{ij\sigma} a_{i\sigma}^{+} a_{j\sigma} \cdot \mathbf{j}_{ij}(\mathbf{r}), \tag{26}$$

and

$$\mathbf{j}_{ij}\left(\mathbf{r}\right)=\frac{ie\hbar}{2m}\left(w_{i}^{*}(\mathbf{r})\nabla w_{j}(\mathbf{r})-\nabla w_{i}^{*}(\mathbf{r})w_{j}(\mathbf{r})\right), \tag{27}$$

where $\{w_i(\mathbf{r})\}$ are the *Wannier* functions.

The above result is much more general than the *Landauer-Büttiker* formalism [15] which, in fact, can be obtained by taking a particular limit of the above quantum mechanical formulation. We can easily prove this fact by applying a different expansion relation of the field operators

$$\widehat{\Psi}\left(\mathbf{r}\right)=\sum_{k\sigma}\chi_{\sigma}\psi_{k}\left(\mathbf{r}\right)a_{k\sigma}, \tag{28}$$

what transforms the operator of current density to the form

$$\widehat{j}=\frac{ie\hbar}{2m}\sum_{k_{1}k_{2}\sigma}a_{k_{1}\sigma}^{+}a_{k_{2}\sigma}\left(\psi_{k_{1}}^{*}\left(\mathbf{r}\right)\nabla\psi_{k_{2}}\left(\mathbf{r}\right)-\nabla\psi_{k_{1}}^{*}\left(\mathbf{r}\right)\psi_{k_{2}}\left(\mathbf{r}\right)\right), \tag{29}$$

where $\{\psi_k(\mathbf{r})\}$ are the *Bloch* functions. The proof requires us make basically two assumptions, the first concerning single-particle states $\nabla\psi_k(\mathbf{r})\approx i\mathbf{k}\psi_k(\mathbf{r})$, what is obviously true, strictly speaking, only for plain waves, and the second one concerning multi-particle states $\langle\Phi_N|a_{k_1\sigma}^{+}a_{k_2\sigma}|\Phi_N\rangle\approx\delta_{k_1k_2}\langle\Phi_N|n_{k_1\sigma}|\Phi_N\rangle$. Under these conditions, the current-density operator simplifies to the form

$$\widehat{j}=\frac{ie\hbar}{2m}\sum_{k\sigma}n_{k\sigma}|\psi_{k}\left(\mathbf{r}\right)|^{2}\left(-2i\mathbf{k}\right)=\sum_{k\sigma}n_{k\sigma}\cdot\mathbf{j}_{k}\left(\mathbf{r}\right), \tag{30}$$

where

$$\mathbf{j}_{k}\left(\mathbf{r}\right)=-e|\psi_{k}\left(\mathbf{r}\right)|^{2}\frac{\hbar\mathbf{k}}{m}. \tag{31}$$

Obviously, the above formula is essentially equivalent to the *Landauer* formula (A22) when we additionally assume the dense homogeneous momentum space, the energy dependent occupation distribution function, and the constant single-particle density. As we can see, the *ab initio* quantum mechanical treatment of current density is the proper one to describe nanoscopic multi-particle systems, as they violate each of the assumptions necessary for the *Landauer-Büttiker* approach to become valid.

5.2 The complementary descriptions

The expression (26) for the current density can be used to determine the average current density in the ground state of the nanosystem. The detailed calculations have been carried out in Appendix A.3. The final expression (C47) for the current through the system depends only on the correlation function, and not on the particle occupations, as in the *Landauer-Büttiker* approach.

These two approaches represent two complementary descriptions of the current flow. The quantum mechanical approach derives the current from the correlation between single-particle states in the ground state of the system, and the *Landauer-Büttiker* approach derives it from the occupation of the single-particle states, which have a self-current accompanied with. We show the two descriptions originate from Eq. (26) when we take the *Wannier* functions of the form

$$w_i(\mathbf{r}) = \Omega_i(\mathbf{r})\, e^{i\omega_i(\mathbf{r})}, \tag{32}$$

where Ω_i and ω_i are real functions. The expression for the current amplitude $\mathbf{j}_{ij}(\mathbf{r})$ then has the following form

$$\mathbf{j}_{ii}(\mathbf{r}) = -\frac{e\hbar}{m} |w_i(\mathbf{r})|^2 \nabla\omega_i(\mathbf{r}), \tag{33}$$

in the case of the particle-occupation contribution, and

$$\begin{aligned} \mathbf{j}_{i\neq j}(\mathbf{r}) &= -\frac{e\hbar}{m} w_i^*(\mathbf{r})\, w_j(\mathbf{r})\, \frac{\nabla\omega_i(\mathbf{r}) + \nabla\omega_j(\mathbf{r})}{2} \\ &- \frac{e\hbar}{m} \left[\Omega_i(\mathbf{r})\nabla\Omega_j(\mathbf{r}) - \nabla\Omega_i(\mathbf{r})\,\Omega_j(\mathbf{r})\right] \frac{e^{i\omega_j(\mathbf{r}) - i\omega_i(\mathbf{r})}}{2i}, \end{aligned} \tag{34}$$

in the case of the correlation-function contribution. One should note we can distinguish between two different origins of the above contributions to the total current. The first originates from the self-current carried by particles occupying individual single-particle states and depends on the momentum-like character of the single-particle basis. The *Landauer-Büttiker* approach

operates within this context

$$\mathbf{j}^{\mathbf{occ}}(\mathbf{r}) = -\frac{e\hbar}{m}\sum_{ij\sigma}\left\langle a_{i\sigma}^{+}a_{j\sigma}\right\rangle w_i^{*}(\mathbf{r})\, w_j(\mathbf{r})\,\frac{\nabla\omega_i(\mathbf{r})+\nabla\omega_j(\mathbf{r})}{2}. \tag{35}$$

The second contribution to the current originates from the correlation between the single-particle states and is the only one that provides results in the case of the single-particle basis built of the hydrogen-like $1s$ orbitals (11). It does not appear in the *Landauer-Büttiker* theory, and yet it is essential for the systems we study

$$\begin{aligned}\mathbf{j}^{\mathbf{cor}}(\mathbf{r}) &= -\frac{e\hbar}{m}\sum_{i<j\sigma}\left[\Omega_i(\mathbf{r})\,\nabla\Omega_j(\mathbf{r})-\nabla\Omega_i(\mathbf{r})\,\Omega_j(\mathbf{r})\right]\\ &\times\ Im\left\{\left\langle a_{i\sigma}^{+}a_{j\sigma}\right\rangle e^{i\omega_j(\mathbf{r})-i\omega_i(\mathbf{r})}\right\}.\end{aligned} \tag{36}$$

We can see, studying the electronic transport through the nanosystems requires implementation yet another approach that is missing in the studies of the mesoscopic systems or any *Landauer*-derivative approach, i.e. the *Keldysh* formalism. The approach is especially useful in the fields, where the *Landauer-Büttiker* theory is inapplicable, i.e. few-atom nanowires.

5.3 The transport analysis

The electronic transport through the system made of few hydrogenic-like atoms can be determined with the use of Eq. (C47). The overall current is obtained as a sum of the components representing current flow between the sites of the system on the pair-like basis. The component of each individual pair of sites depends on the imaginary part of the effective hopping operator (C36) in the ground state as well as the transport amplitude (C46).

It can be clearly seen, there is a maximum in the transport amplitude (Fig. 29) for the specific interatomic distance

$$R_{max} = \frac{1+\sqrt{5}}{2}\cdot\frac{1}{\alpha} = \frac{1+\sqrt{5}}{2}\cdot a, \tag{37}$$

where a is the effective size of the atomic orbitals and the multiplication factor

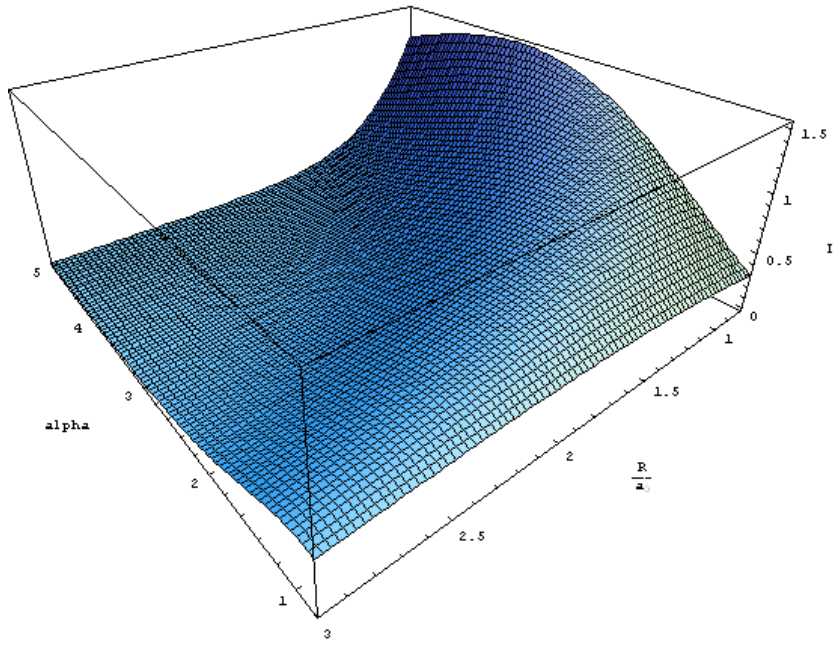

Figure 29: The electronic-transport amplitude (I) profile for the single pair of sites ($i'j'$) as a function of both the interatomic distance R/a_0 and the variational parameter α.

is the "golden section" factor. The amplitude diminishes gradually as either interatomic distance increases or the atomic wave-function size decreases for given R/a_0.

The provided approach formulated here can be implemented in a direct manner to more realistic situation with the starting ns-like orbitals and for $n > 1$. However, this would require the extension of our numerical code to those cases. Also, the consideration of the so-called *Coulomb* blockade phenomenon requires an introduction of external leads not included as yet. This should be a starting point in the future.

6 A brief summary

In this Thesis we have applied the EDABI method to small clusters, as well as to calculations of the tunneling current across a nanoscopic system. In both situations the $1s$-like atomic wave functions were taken from the start as composing the *Wannier* (orthogonalized-atomic) orbitals.

In the case of small clusters, the systems containing up to $N = 6$ atoms were discussed in both two- and three-dimensional configurations. The ground- and the excited-state configurations were explicitly singled out and the existence of the *Hubbard*-like subband structure has been demonstrated. Also, the renormalized single-particle wave function has been determined explicitly. Some of the configurations are metastable and their dissociation routes have been discussed. The translationally invariant electron density has been defined and the microscopic parameters have been tabulated as a function of the interatomic distance. The numerical results are based on the approximation that the three- and four-site contributions to the expressions for the microscopic parameters in the atomic representation can be calculated from the conditions that their counterparts in the *Wannier* representation vanish.

In the final part of the Thesis we have sketched the method of calculating the intrinsic tunneling conductivity of the system by disregarding the influence of the (semi) macroscopic leads. Obviously, the conductivity of such a nanoscopic system will always be non-zero, as it is represented by a quantum tunneling of electrons through a barrier of both the finite width and height. That Chapter should be elaborated much further to explain e.g. the *Coulomb* blockade phenomenon observed in quantum wires.

The Appendices contain a detailed analysis of various formal aspects of the problems constituting the Thesis, as well as provide some particulars of reasoning when deriving various formulas.

Appendices

A Quantum characteristics of nanosystems

In this Appendix we present general aspects, as well as some of the formal expressions for the calculated properties of the system at hand, once the EDABI approach has been implemented.

A.1 Relation to MCI method

The MCI method proved to be very useful in quantum chemistry, yet computationally very expensive. The vast number of electron configurations for any but the smallest systems makes the variational energy optimization a difficult task. Thus, in most applications of the MCI method, we consider only a small subset of the total number of electron configurations or the LCAO coefficients are taken for granted. This is because the first-quantization representation MCI makes the representation of different configurations clumsy.

The EDABI approach, on the other hand, allows us to take into account all electron configurations and diagonalize rigorously the Hamiltonian within the finite *Hilbert* subspace of single-particle states relevant to the system. This is because the occupation-number representation of the N-particle state is just a combination of unity and zero in different columns of the basis vector. The equivalence of both methods can be established by considering the relation between the N-particle state $|\Phi_N\rangle$ in the *Fock* space and N-particle wave function $\Psi_N(\mathbf{r}_1...\mathbf{r}_N)$ in the *Hilbert* space. The field operator $\widehat{\Psi}(\mathbf{r})$ for electron is defined in terms of the sum over a complete set of the *Wannier* functions $\{w_i(\mathbf{r})\}$:

$$\widehat{\Psi}(\mathbf{r}) = \sum_i w_i(\mathbf{r}) a_i, \tag{A1}$$

where the spin-index is ignored for the sake of simplicity (it can be incorporated into the set of quantum numbers $\{i\}$). The N-particle state $|\Phi_N\rangle$ in the *Fock* space can be expressed through the field operators in the following manner (cf. e.g. [34])

$$|\Phi_N\rangle = \frac{1}{\sqrt{N!}} \int d^3\mathbf{r}_1 ... d^3\mathbf{r}_N \Psi_N(\mathbf{r}_1 ... \mathbf{r}_N) \hat{\Psi}^+(\mathbf{r}_1) ... \hat{\Psi}^+(\mathbf{r}_N)|0\rangle. \tag{A2}$$

Conversely, the N-particle wave function $\Psi_N(\mathbf{r}_1 ... \mathbf{r}_N)$ can be expressed in terms of the field operators and $|\Phi_N\rangle$ as follows

$$\Psi_N(\mathbf{r}_1 ... \mathbf{r}_N) = \frac{1}{\sqrt{N!}} \langle 0|\hat{\Psi}(\mathbf{r}_1) ... \hat{\Psi}(\mathbf{r}_N)|\Phi_N\rangle, \tag{A3}$$

where $|0\rangle$ is the vacuum state in the *Fock* space. Substituting Eq. (A1) to Eq. (A3) we obtain

$$\Psi_N(\mathbf{r}_1 ... \mathbf{r}_N) = \frac{1}{\sqrt{N!}} \sum_{i_1 ... i_N} \langle 0|a_{i_1} ... a_{i_N}|\Phi_N\rangle w_{i_1}(\mathbf{r}_1) ... w_{i_N}(\mathbf{r}_N). \tag{A4}$$

Recognizing that within the *Fock* space we have that

$$|\Phi_N\rangle = \frac{1}{\sqrt{N!}} \sum_{i_1 ... i_N} C_{i_1 ... i_N} \cdot a^+_{i_1} ... a^+_{i_N}|0\rangle, \tag{A5}$$

where $C_{i_1 ... i_N}$ are the so-called configuration interaction (CI) coefficients. Substituting then Eq. (A5) to Eq. (A4) we finally obtain

$$\begin{aligned} \Psi_N(\mathbf{r}_1 ... \mathbf{r}_N) &= \frac{1}{N!} \sum_{i_1 ... i_N} \sum_{j_1 ... j_N} C_{i_1 ... i_N} \cdot w_{j_1}(\mathbf{r}_1) ... w_{j_N}(\mathbf{r}_N) \\ &\times \langle 0|a_{j_1} ... a_{j_N} a^+_{i_1} ... a^+_{i_N}|0\rangle. \end{aligned} \tag{A6}$$

The expression $\langle 0|...|0\rangle$ provides $N!$ non-zero terms, each equal to $(-1)^P$, where P represents the number of permutations of quantum numbers $(j_1 ... j_N)$ with respect to $(i_1 ... i_N)$. In other words, we can rewrite the above relation to

$$\Psi_N(\mathbf{r}_1 ... \mathbf{r}_N) = \frac{1}{\sqrt{N!}} \sum_{i_1 ... i_N} C_{i_1 ... i_N} \cdot (A, S) \left[w_{i_1}(\mathbf{r}_1) ... w_{i_N}(\mathbf{r}_N) \right]. \tag{A7}$$

This is the MCI starting expression for the N-particle wave function. The symbols A and S represent, respectively, the antisymmetrization for fermions and the symmetrization for bosons. Essential is that we have the same expansion coefficients $C_{i_1...i_N}$ for both the representation of the state $|\Phi_N\rangle$ in the *Fock* space and the wave function $\Psi_N(\mathbf{r}_1...\mathbf{r}_N)$ in the *Hilbert* space. Therefore, the expressions (A5) and (A7) represent equivalent approaches. Thus, whether we variationally determine the wave function in the *Hilbert* space or minimize energy of the state in the *Fock* space we have got the same CI coefficients.

A.2 Particle density profile in the second-quantization scheme

Single-particle density is an attribute of the system most naturally representing its stationary state. Evaluation of the particle density supplies the clear real-space picture of the electronic structure of the system. Let us consider the definition of the probability density for a single particle, which can be defined as

$$\rho(\mathbf{r}_N) = \int d^3\mathbf{r}_1...d^3\mathbf{r}_{N-1}|\Psi_N(\mathbf{r}_1...\mathbf{r}_N)|^2, \tag{A8}$$

where $\Psi_N(\mathbf{r}_1...\mathbf{r}_N)$ is the N-particle wave function and from Eq. (A3) we have

$$|\Psi_N(\mathbf{r}_1...\mathbf{r}_N)|^2 = \frac{1}{N!}\langle\Phi_N|\widehat{\Psi}^+(\mathbf{r}_N)...\widehat{\Psi}^+(\mathbf{r}_1)|0\rangle\langle 0|\widehat{\Psi}(\mathbf{r}_1)...\widehat{\Psi}(\mathbf{r}_N)|\Phi_N\rangle. \tag{A9}$$

The state $|\Phi_N\rangle$ represents the constant number (N) of particles and hence we can rewrite the above expression as follows

$$|\Psi_N(\mathbf{r}_1...\mathbf{r}_N)|^2 = \frac{1}{N!}\langle\Phi_N|\widehat{\Psi}^+(\mathbf{r}_N)...\widehat{\Psi}^+(\mathbf{r}_1)\widehat{\Psi}(\mathbf{r}_1)...\widehat{\Psi}(\mathbf{r}_N)|\Phi_N\rangle. \tag{A10}$$

We can derive the final result by applying the expression (A1) for the field operator $\widehat{\Psi}(\mathbf{r})$, defined with the help of the orthonormal basis $\{w_i(\mathbf{r})\}$, what leads to the relation

$$\widehat{\Psi}^+(\mathbf{r})\widehat{\Psi}(\mathbf{r}) = \sum_{i_1 i_2} w^*_{i_1}(\mathbf{r}) w_{i_2}(\mathbf{r}) a^+_{i_1} a_{i_2}, \tag{A11}$$

and by regrouping the probability density (A8) in the following way

$$\rho(\mathbf{r}_N) = \int d^3\mathbf{r}_2 ... d^3\mathbf{r}_{N-1} \left(\int d^3\mathbf{r}_1 |\Psi_N(\mathbf{r}_1 ... \mathbf{r}_N)|^2 \right), \tag{A12}$$

where

$$\begin{aligned} \int d^3\mathbf{r}_1 |\Psi_N(\mathbf{r}_1 ... \mathbf{r}_N)|^2 &= \qquad\qquad (A13) \\ &= \frac{1}{N!} \int d^3\mathbf{r}_1 \langle \widehat{\Psi}^+(\mathbf{r}_N) ... \widehat{\Psi}^+(\mathbf{r}_1) \widehat{\Psi}(\mathbf{r}_1) ... \widehat{\Psi}(\mathbf{r}_N) \rangle \\ &= \frac{1}{N!} \sum_{i_1 i_2} \int d^3\mathbf{r}_1 w^*_{i_1}(\mathbf{r}_1) w_{i_2}(\mathbf{r}_1) \\ &\times \langle \widehat{\Psi}^+(\mathbf{r}_N) ... a^+_{i_1} a_{i_2} ... \widehat{\Psi}(\mathbf{r}_N) \rangle \\ &= \frac{1}{N!} \langle \widehat{\Psi}^+(\mathbf{r}_N) ... \widehat{\Psi}^+(\mathbf{r}_2) \sum_i n_i \widehat{\Psi}(\mathbf{r}_2) ... \widehat{\Psi}(\mathbf{r}_N) \rangle. \end{aligned}$$

The expectation value of the particle-number operator $\sum_i n_i$ is unity for the many-particle state $\widehat{\Psi}(\mathbf{r}_2) ... \widehat{\Psi}(\mathbf{r}_N)|\Phi_N\rangle \sim |\Phi_1\rangle$. Obviously, the procedure applied subsequently $N-2$ times leads to the result

$$\rho(\mathbf{r}_N) = \frac{1}{N} \langle \widehat{\Psi}^+(\mathbf{r}_N) \widehat{\Psi}(\mathbf{r}_N) \rangle. \tag{A14}$$

This result can be understood by means of the particle-density operator $\widehat{n}(\mathbf{r}) \equiv \widehat{\Psi}^+(\mathbf{r})\widehat{\Psi}(\mathbf{r})$, and thus the particle density is

$$n(\mathbf{r}) \equiv N \cdot \rho(\mathbf{r}) = \langle \widehat{\Psi}^+(\mathbf{r}) \widehat{\Psi}(\mathbf{r}) \rangle. \tag{A15}$$

Finally, we obtain the explicit expression for the density of particles by applying Eq. (A11):

$$n(\mathbf{r}) = \sum_i |w_i(\mathbf{r})|^2 \cdot \langle n_i \rangle + \sum_{i_1 \neq i_2} w^*_{i_1}(\mathbf{r}) w_{i_2}(\mathbf{r}) \cdot \langle a^+_{i_1} a_{i_2} \rangle, \qquad \text{(A16)}$$

where averages $\langle ... \rangle$ are taken with the N-particle state $|\Phi_N\rangle$.

The first of the two terms represents contribution of the particle-number operator to the total density of particles. The other term can provide a significant contribution in the case of highly correlated systems, yet what is more important the term is missing in the *Hartree-Fock* theory and can substantially improve estimations of the density of particles.

A.3 *Landauer-Büttiker* transport

A common approach to describe electronic transport in mesoscopic systems is to utilize the semiclassical *Landauer-Büttiker* formalism [15]. Some authors [14, 31, 32, 33] apply it to the nanoscopic systems as well, even though their single-particle states are discrete, what contradicts the assumptions of the theory.

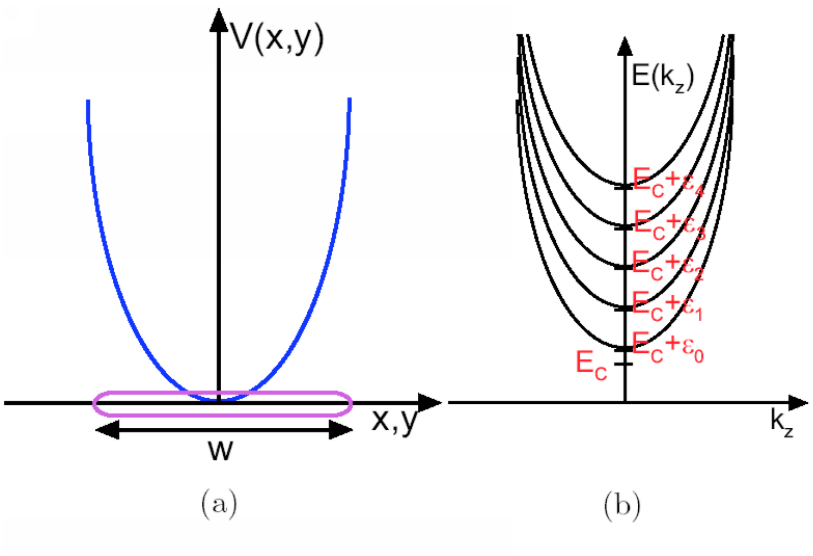

Figure A1: (a) Lateral potential confining the electrons within the width of the conductor. (b) Schematic dispersion relations for the transverse modes. ([35])

Let us consider two metallic contacts connected to a narrow conductor strip. The contacts are reflectionless, i.e. electrons inside the conductor can exit into wide contacts with a negligible probability of reflection. The transport inside the conductor is ballistic meaning that the transmission probability of electrons is close to unity. The electron dynamics in the effective mass-approximation inside the conductor is described by the *Schrödinger* equation

$$\left[E_C + \frac{\widehat{p}^2}{2m^*} + V(x,y)\right]\psi(x,y,z) = E\psi(x,y,z), \tag{A17}$$

where E_C is the conduction band edge and $V(x,y)$ is a confining potential (Fig. A1a). Since the conductor is translationally invariant in the z direction we can postulate the solution of the form

$$\psi_{nk_z}(x,y,z) = \chi_n(x,y)e^{ik_z z}, \tag{A18}$$

$$E_n(k_z) = E_C + \epsilon_n + \frac{\hbar^2 k_z^2}{2m^*}. \tag{A19}$$

The $\chi_n(x,y)$ states are called transverse modes, and electrons entering the conductor must have the energy equal to an unoccupied transverse mode (Fig. A1b). The effective current comes from difference in the occupation of $+k_z$ states, originated in one contact, and $-k_z$ states, originated in the other. Each state carries the current

$$I_{nk_z} = -en_n \cdot v_{k_z} = -\frac{e}{L} \cdot \frac{1}{\hbar}\frac{\partial E_n(k_z)}{\partial k_z}, \tag{A20}$$

where n_n is the linear electron density for an electron inside a conductor of length L and v_{k_z} is the electron velocity. Thus, the effective current can be expressed with the relation

$$I = \sum_n \sum_{k_z\sigma} I_{nk_z}\left[f\left(nk_z,\mu_1\right) - f\left(nk_z,\mu_2\right)\right], \tag{A21}$$

where $f\left(nk_z,\mu\right)$ is the distribution function of electrons in the contacting electrodes. The k_z state spectrum is dense in the case of long conductors, and therefore we can write that

$$\begin{aligned} I &= -\frac{e}{L}\cdot\frac{1}{\hbar}\sum_n 2\times\frac{L}{2\pi}\int_0^\infty dk_z\frac{\partial E_n(k_z)}{\partial k_z}\left[f\left(nk_z,\mu_1\right)-f\left(nk_z,\mu_2\right)\right] \\ &= -\frac{2e}{h}\cdot\sum_n\int_{E_C+\epsilon_n}^\infty dE\left[f\left(E,\mu_1\right)-f\left(E,\mu_2\right)\right] \\ &= -\frac{2e}{h}\cdot\int_{-\infty}^\infty dEM(E)\left[f\left(E,\mu_1\right)-f\left(E,\mu_2\right)\right], \end{aligned} \tag{A22}$$

where

$$M(E)=\sum_n\theta\left(E-\epsilon_n-E_C\right). \tag{A23}$$

In result, we have obtained a well known expression for the electronic tunneling (ballistic) transport. As we can see, the transport reveals a stepwise behavior with the increasing drain-source bias voltage, and the steps become sharper as the temperature decreases. The $2e/h$ quantity is considered to be a quantum of the electronic transport in the spin unpolarized processes.

A.4 Renormalized wave-equation

For the sake of completeness we characterize here the self-adjusted wave equation proposed by *Spałek* (2000)[2]. We start from a formal expression for the system energy $E_G = E_G\{t_{ij}, V_{ijkl}\}$, in which the microscopic parameters t_{ij} and V_{ijkl} depend functionally on the single-particle (*Wannier*) functions $\{w_i(\mathbf{r})\}$. If we use the approach conserving the number of particles, the renormalized wave functions $\{w_i(\mathbf{r})\}$ are determined by the *Euler* variational procedure with the constraint that the functions are normalized, i.e. $\langle w_i|w_j\rangle = \delta_{ij}$. Since E_G contains only $\{w_i(\mathbf{r})\}$ and their gradients $\{\nabla w_i(\mathbf{r})\}$, the self-adjusted and stationary wave equation for single-particle in the *millieu* of all other particles reads

$$\frac{\delta E_G}{\delta w_i^*(\mathbf{r})}-\nabla\cdot\frac{\delta E_G}{\delta\left(\nabla w_i^*(\mathbf{r})\right)}-\sum_{i>j}\lambda_{ij}w_j(\mathbf{r})=0, \tag{A24}$$

[2] cf. for details [24]

where λ_{ij} are the *Lagrange* multipliers. In the case of explicitly orthogonal basis $\lambda_{ij} = 0$ and the above equation reduces to the *Euler* equations for the renormalized basis $\{w_i(\mathbf{r})\}$. In this Thesis we have used the *Ritz* variational version of solving this equation by postulating the form of atomic functions, which compose the final *Wannier* functions.

B Applied algorithms

In this Appendix we present various algorithms providing us with the analytical tools when implementing the EDABI approach.

B.1 The *Wannier* basis determination

An explicit evaluation of the parameters t_{ij} and V_{ijkl} requires the knowledge of the single-particle (*Wannier*) basis $\{w_i(\mathbf{r})\}$. The EDABI approach expresses *Wannier* functions as linear combinations of atomic states. Namely, we start from the decomposition:

$$w_l(\mathbf{r};\alpha) = \sum_{j=1}^{M} \beta_{lj} \Phi_j(\mathbf{r};\alpha), \tag{B1}$$

where $\Phi(\mathbf{r};\alpha)$ is the atomic wave function of an adjustable size. The normalization condition takes then the form

$$\begin{aligned} \langle w_l(\mathbf{r};\alpha)|w_{l'}(\mathbf{r};\alpha)\rangle &= \sum_{jk} \beta^*_{lj}\beta_{l'k}\langle \Phi_j(\mathbf{r};\alpha)|\Phi_k(\mathbf{r};\alpha)\rangle \\ &= \sum_{jk} \beta^*_{lj}\beta_{l'k} S_{kj} \\ &\equiv \delta_{l'l}, \end{aligned} \tag{B2}$$

where $S_{kj} = \langle \Phi_j(\mathbf{r};\alpha)|\Phi_k(\mathbf{r};\alpha)\rangle$ is an overlap between the atomic functions $\Phi_j(\mathbf{r};\alpha)$ and $\Phi_k(\mathbf{r};\alpha)$.

In the matrix language, the formalism we use for subsequent calculations, the above condition can be written as

$$\beta S \beta^+ = 1, \tag{B3}$$

or, equivalently

$$\beta^+ \beta = S^{-1}, \tag{B4}$$

where S is the overlap matrix and β – the matrix of coefficients.

The β matrix can be left-multiplied with a unitary matrix and still satisfies the condition. The ambiguity reflects the basic fact that rotations of the

basis do not influence the results. Therefore, we can arbitrarily choose the β matrix in the form $\beta = \beta^{+}$. In effect, such choice leads to the relation:

$$\beta = S^{-1/2}. \tag{B5}$$

The above method is known as the *Löwdin* method of determining the orthonormal basis and, in general, needs to be supplemented with series expansion. Namely, we make use of the fact that the overlap integral matrix tends to the unit matrix as elements of the system are separated from each other. Thus, the β matrix can be written down as the following series expansion:

$$\beta = 1 + \sum_{n=1}^{\infty} \frac{(-1)^n \triangle^n}{2^n n!} \prod_{k=1}^{n} (2k-1) = 1 + \sum_{n=1}^{\infty} \triangle^n \prod_{k=1}^{n} (\frac{1}{2k} - 1), \tag{B6}$$

where the small parameter has been selected as $\triangle \equiv S - 1$. The above series, however, does not converge in the case of tight binding systems, for which the overlap matrix is far from unity. Therefore, we alter the *Löwdin* relation (B5) slightly by redefining the expansion coefficient according to the prescription

$$\beta = (1+C)^{-1/2} (\frac{S}{1+C})^{-1/2}, \tag{B7}$$

and hence, we have

$$\beta = (1+C)^{-1/2} [1 + \sum_{n=1}^{\infty} \triangle_C^n \prod_{k=1}^{n} (\frac{1}{2k} - 1)], \tag{B8}$$

where $\triangle_C \equiv S/(1+C) - 1$. The C parameter allows us to control the series convergence as the convergence condition is

$$\| \triangle_C \| < 1, \tag{B9}$$

where the metrics $\|\cdot\|$ can be chosen arbitrarily. We take it in the form

$$\|\triangle_C\|_\infty \equiv \max_{ij}\{|\frac{S_{ij}}{1+C} - \delta_{ij}|\} = \max\{\frac{C}{1+C}; \frac{\max_{i\neq j}|S_{ij}|}{1+C}\}. \tag{B10}$$

As we can see, the chosen metrics has a minimum with respect to C and satisfies the convergence condition when the C parameter is taken as

$$C = \max_{i\neq j}|S_{ij}|. \tag{B11}$$

The present method of determining the *Wannier* basis can be applied to the single-band, as well as multiple-band systems. What is most important, the method is effective also in the case of irregular or deformed systems.

B.2 The 3- and 4-site contributions

The systems with the number $N > 2$ of atoms suffer from the difficulties of determining the 3- and 4-site integrals reflecting the electron-electron interaction term. Nonetheless, they are required to determine accurately the parameters of Hamiltonian and the system ground state energy. We can express the relation between the expressions for the interaction parameters in the *Wannier* and the atomic representations (B1) in the following way

$$V_\xi \equiv V_{ijkl} = \sum_{i'j'k'l'} V'_{i'j'k'l'} \cdot \beta^*_{ii'}\beta^*_{jj'}\beta_{ll'}\beta_{kk'} \equiv \sum_{\xi'} V'_{\xi'} \cdot \beta_{\xi\xi'}, \tag{B12}$$

where ξ and ξ' represent respectively sequences of four indices, $ijkl$ and $i'j'k'l'$. A common way of dealing with the difficulties is to neglect the integrals that are difficult to determine. However, a consequence of such assumption is often the inaccurate results. Thus, we choose yet another approach, namely we have found the 3- and 4-site interaction parameters vanish in the optimized *Wannier* representation, but the corresponding 3- and 4-site terms in the atomic representation can be determined by solving a complete set of linear equations determined from that condition. In effect, such a procedure leads to the renormalization of the 1- and 2-site interaction parameters. We call the procedure the renormalization *ansatz*.

Explicitly, to express the renormalization procedure we denote by $\xi_{|3,4}$ the indices with 3 or 4 different sites and likewise, by $\xi_{|1,2}$ the indices with 1 or 2 different sites only. In this notation, the transformation (B12) involving the 3- and 4-site parameters can be written in the following matrix form:

$$\begin{bmatrix} . & . & . & . & | & . \\ . & . & . & . & | & . \\ . & . & \beta_{\xi_{|3,4}\xi'_{|3,4}} & . & | & \beta_{\xi_{|3,4}\xi'_{|1,2}} \\ . & . & . & . & | & . \\ - & - & - & - & + & - \\ . & . & \beta_{\xi_{|1,2}\xi'_{|3,4}} & . & | & \beta_{\xi_{|1,2}\xi'_{|1,2}} \end{bmatrix} \times \begin{bmatrix} . \\ . \\ V'_{\xi'_{|3,4}} \\ . \\ - \\ V'_{\xi'_{|1,2}} \end{bmatrix} = \begin{bmatrix} . \\ . \\ V_{\xi_{|3,4}} \\ . \\ - \\ V_{\xi_{|1,2}} \end{bmatrix}, \tag{B13}$$

or equivalently,

$$\begin{cases} V_{\xi_{|3,4}} = \sum_{\xi'_{|3,4}} \beta_{\xi_{|3,4}\xi'_{|3,4}} V'_{\xi'_{|3,4}} + \sum_{\xi'_{|1,2}} \beta_{\xi_{|3,4}\xi'_{|1,2}} V'_{\xi'_{|1,2}} \\ V_{\xi_{|1,2}} = \sum_{\xi'_{|3,4}} \beta_{\xi_{|1,2}\xi'_{|3,4}} V'_{\xi'_{|3,4}} + \sum_{\xi'_{|1,2}} \beta_{\xi_{|1,2}\xi'_{|1,2}} V'_{\xi'_{|1,2}} \end{cases}. \tag{B14}$$

Now, assuming that $V_{\xi_{|3,4}} = 0$ we obtain

$$\sum_{\xi'_{|3,4}} \beta_{\xi_{|3,4}\xi'_{|3,4}} V'_{\xi'_{|3,4}} = -\left(\sum_{\xi'_{|1,2}} \beta_{\xi_{|3,4}\xi'_{|1,2}} V'_{\xi'_{|1,2}} \right). \tag{B15}$$

The above set of linear algebraic equations provides an explicit expression for the $V'_{\alpha'_{|3,4}}$ integrals via $V'_{\alpha'_{|1,2}}$. These relations can be used further in Eq. (B14) to renormalize the 1- and 2-site interaction parameters. One should note the renormalization procedure is valid for any set of the integrals we cannot determine explicitly as long as we can estimate the same number of interaction parameters.

B.3 The modified *Lanczos* algorithm

A common method of diagonalizing the Hamiltonian is the so-called *Lanczos* method. We can determine the ground as well as the excited eigenstates and eigenenergies of the system with the use of the modified *Lanczos* algorithm.

The modified algorithm is much more transparent and easy to implement, and yet its computational complexity is comparable to the standard algorithm.

The standard *Lanczos* algorithm generates from 50 to 100 orthonormal vectors in the *Fock* space, starting with a randomly chosen vector. The Hamiltonian matrix in their representation has a tridiagonal form, what makes the diagonalization a relatively easy task. However, limited numerical precision prevents us from generating larger vector sets, and the procedure needs to be repeated until the required precision is reached.

In the modified algorithm, similarly to the standard one, we start with a $|\varphi_0\rangle$ vector in the *Fock* space and determine the $|\psi_0\rangle$ vector with the following relation

$$|\psi_n\rangle = \widehat{H}\,|\varphi_n\rangle - a_n\,|\varphi_n\rangle\,, \tag{B16}$$

where

$$a_n = \frac{\langle\varphi_n|\,\widehat{H}\,|\varphi_n\rangle}{\langle\varphi_n|\varphi_n\rangle}, \tag{B17}$$

and

$$\langle\psi_n|\varphi_n\rangle = 0. \tag{B18}$$

In the next step of the algorithm, as distinct from the standard method, we make a linear combination of them that minimizes (or maximizes) the energy of the system. Such a vector is then recursively used to finetune the result. Subsequent steps are determined with the relation

$$|\varphi_{n+1}\rangle = c_n \cdot |\varphi_n\rangle + |\psi_n\rangle\,, \tag{B19}$$

where

$$c_n = \frac{1}{2}\left\{(a_n - a'_n) \mp \sqrt{(a_n - a'_n)^2 + 4b_n}\right\}, \tag{B20}$$

with

$$a'_n = \frac{\langle\psi_n|\,\widehat{H}\,|\psi_n\rangle}{\langle\psi_n|\psi_n\rangle},\ \text{and}\ b_n = \frac{\langle\psi_n|\psi_n\rangle}{\langle\varphi_n|\varphi_n\rangle}. \tag{B21}$$

As we can see, the above method can produce the ground state of the

system as well as the excited states by restricting the *Fock* space to the subspaces orthogonal to the Hamiltonian eigenstates. One should note the a_n and a'_n terms represent mean energy of the system in the $|\varphi_n\rangle$ and $|\psi_n\rangle$ states, respectively. The method convergence can be easily proved in the case energy spectrum of the system is bounded, what is always true for finite systems. The proof can be acomplished through the relation

$$\forall a_n, a'_n, b_n : c_n + a'_n = a_{n+1} \leq a_n, \tag{B22}$$

and the energy gain in each step

$$|a_{n+1} - \min\{a_n; a'_n\}| \approx \frac{b_n}{|a_n - a'_n|}. \tag{B23}$$

Thus, the modified *Lanczos* algorithm we employ is computationally less complex than the standard one and supplies us with a stable diagonalization procedure.

C *Ab-initio* calculations of the microscopic parameters

In this Appendix we carry out the detailed calculations providing us with the starting Hamiltonian parameters for the EDABI approach.

C.1 The 3-center integral

Much of the effort is concentrated on the evaluation of the integrals that express the Hamiltonian parameters. The single-particle term does not cause difficulties when the *Slater*-like functions are applied. Unfortunately, there is a substantial difficulty with the two-particle term, namely only the 1- and 2-site interaction coefficients can be obtained analytically, and even these require 3-center integrals to be evaluated. The 3-center integrals appear in the hopping parameters as well when we take into account sites contributing with their potentials to the hopping and different from the pair involved. The exemplary expression for the 3-center integral is

$$\begin{aligned} I &\equiv \frac{1}{\pi}\alpha^3 \cdot \int d^3r \frac{2}{|\mathbf{r}-\mathbf{r'}|} e^{-\alpha(|\mathbf{r}-\mathbf{R}_i|+|\mathbf{r}-\mathbf{R}_j|)} \\ &= \frac{2}{\pi}\alpha^3 \cdot \int d^3r \frac{1}{|\mathbf{r}-\mathbf{p}|} e^{-\alpha(|\mathbf{r}|+|\mathbf{r}-\mathbf{R}_{ji}|)}, \end{aligned} \tag{C1}$$

where $\mathbf{p} \equiv \mathbf{r'} - \mathbf{R}_i$. The vectors drawn schematically in Fig. C1 we represent in the spheroidal coordinate system. The coordinates (λ, μ, φ) are defined through the relations

$$\begin{cases} \lambda \cdot R_{ji} = |\mathbf{r}| + |\mathbf{r}-\mathbf{R}_{ji}|, \text{ for } 1 < \lambda < \infty \\ \mu \cdot R_{ji} = |\mathbf{r}| - |\mathbf{r}-\mathbf{R}_{ji}|, \text{ for } -1 < \mu < 1 \end{cases}. \tag{C2}$$

Additionally, the integration element can be expressed as follows

$$\int d^3r = \int_1^\infty d\lambda_r \int_{-1}^1 d\mu_r \int_0^{2\pi} d\varphi_r \cdot \left(\frac{R_{ji}}{2}\right)^3 \left(\lambda_r^2 - \mu_r^2\right). \tag{C3}$$

The only term of the integral (C1) that requires special treatment is the *Coulomb*-like potential. Fortunately, we can use the *Neumann* decomposition in the spheroidal coordinates for the term:

$$\begin{aligned}\frac{1}{|\mathbf{r}-\mathbf{p}|} &= \frac{2}{R_{ji}}\sum_{k=0}^{\infty}\sum_{m=-k}^{k}(-1)^m(2k+1)\left[\frac{(k-|m|)!}{(k+|m|)!}\right]^2 e^{im(\varphi_r-\varphi_p)} \\ &\times P_k^{|m|}(\min\{\lambda_r;\lambda_p\})\,Q_k^{|m|}(\max\{\lambda_r;\lambda_p\}) \\ &\times P_k^{|m|}(\mu_r)\,P_k^{|m|}(\mu_p)\,, \end{aligned} \tag{C4}$$

where P and Q are the *Legendre* polynomials of the first and the second order, respectively.

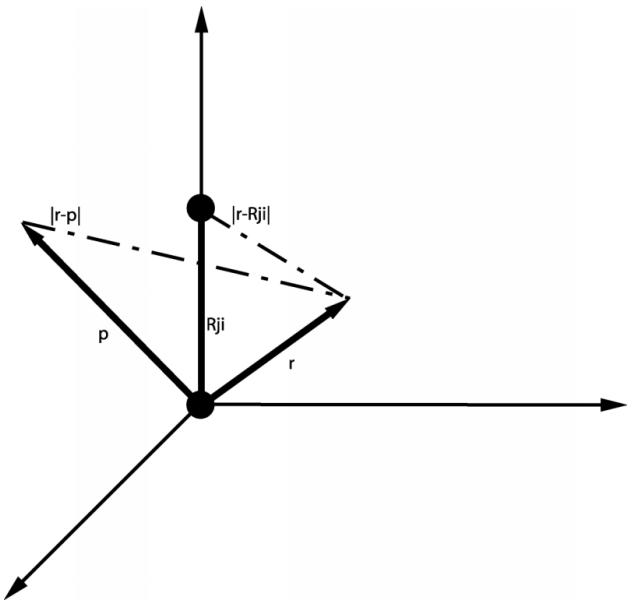

Figure C1: Positions of the **r** and **p** vectors in the coordinate system.

The above decomposition when substituted to Eq. (C1) and after we take the integration over φ_r and utilize the condition

$$\int_0^{2\pi} d\varphi_r \cdot e^{im\varphi_r} = \begin{cases} 2\pi, \text{ if } m=0 \\ 0, \text{ if } m\neq 0 \end{cases}, \tag{C5}$$

leads to the expression

$$\begin{aligned} I &= \frac{2}{\pi}\alpha^3 \cdot \left(\frac{R_{ji}}{2}\right)^3 2\pi \cdot \int_1^\infty d\lambda_r e^{-\alpha R_{ji}\lambda_r} \int_{-1}^1 d\mu_r \left(\lambda_r^2 - \mu_r^2\right) \\ &\times \frac{2}{R_{ji}} \sum_{k=0}^\infty (2k+1) \cdot P_k\left(\min\left\{\lambda_r;\lambda_p\right\}\right) Q_k\left(\max\left\{\lambda_r;\lambda_p\right\}\right) P_k\left(\mu_r\right) P_k\left(\mu_p\right) \\ &= \alpha^3 R_{ji}^2 \cdot \sum_{k=0}^\infty (2k+1) P_k\left(\mu_p\right) \cdot \int_1^\infty d\lambda_r e^{-\alpha R_{ji}\lambda_r} \\ &\times P_k\left(\min\left\{\lambda_r;\lambda_p\right\}\right) Q_k\left(\max\left\{\lambda_r;\lambda_p\right\}\right) \\ &\times \int_{-1}^1 d\mu_r \left(\lambda_r^2 - \mu_r^2\right) P_k\left(\mu_r\right). \end{aligned} \tag{C6}$$

The *Legendre* polynomials are ortogonal and the multiplicative term in the last integration in Eq. (C6) involves only a linear combination of the $P_0\left(\mu_r\right) = 1$ and $P_2\left(\mu_r\right) = \frac{3}{2}\left(\mu_r^2 - \frac{1}{3}\right)$ terms, so only the $k = 0$ and $k = 2$ terms survive and yield

$$\begin{aligned} I &= \alpha^3 R_{ji}^2 \cdot \int_1^\infty d\lambda_r e^{-\alpha R_{ji}\lambda_r} Q_0\left(\max\left\{\lambda_r;\lambda_p\right\}\right) \int_{-1}^1 d\mu_r \left(\lambda_r^2 - \mu_r^2\right) \\ &+ \alpha^3 R_{ji}^2 \cdot 5P_2\left(\mu_p\right) \int_1^\infty d\lambda_r e^{-\alpha R_{ji}\lambda_r} P_2\left(\min\left\{\lambda_r;\lambda_p\right\}\right) \\ &\times Q_2\left(\max\left\{\lambda_r;\lambda_p\right\}\right) \int_{-1}^1 d\mu_r \left(\lambda_r^2 - \mu_r^2\right) P_2\left(\mu_r\right) \\ &= \alpha^3 R_{ji}^2 \cdot \left[\int_1^{\lambda_p} + \int_{\lambda_p}^\infty\right] d\lambda_r e^{-\alpha R_{ji}\lambda_r} Q_0\left(\max\left\{\lambda_r;\lambda_p\right\}\right) 2\left(\lambda_r^2 - \frac{1}{3}\right) \\ &- \alpha^3 R_{ji}^2 \cdot \frac{4}{3} P_2\left(\mu_p\right) \left[\int_1^{\lambda_p} + \int_{\lambda_p}^\infty\right] d\lambda_r e^{-\alpha R_{ji}\lambda_r} P_2\left(\min\left\{\lambda_r;\lambda_p\right\}\right) \\ &\times Q_2\left(\max\left\{\lambda_r;\lambda_p\right\}\right). \end{aligned} \tag{C7}$$

We know the explicit form of the second-order *Legendre* polynomials, which are $Q_0\left(\lambda\right) = \frac{1}{2}\ln\frac{\lambda+1}{\lambda-1}$ and $Q_2\left(\lambda\right) = \frac{3}{4}\left[\left(\lambda^2 - \frac{1}{3}\right)\ln\frac{\lambda+1}{\lambda-1} - 2\lambda\right]$, and therefore the whole term reduces to:

$$I = \alpha^3 R_{ji}^2 \cdot \ln\frac{\lambda_p + 1}{\lambda_p - 1} \cdot \int_1^{\lambda_p} d\lambda_r e^{-\alpha R_{ji}\lambda_r} \left(\lambda_r^2 - \frac{1}{3}\right)$$

$$
\begin{aligned}
&+ \quad \alpha^3 R_{ji}^2 \cdot \int_{\lambda_p}^{\infty} d\lambda_r e^{-\alpha R_{ji}\lambda_r} \ln\frac{\lambda_r+1}{\lambda_r-1}\left(\lambda_r^2-\frac{1}{3}\right) \\
&- \quad \alpha^3 R_{ji}^2 \cdot 2\left(\mu_p^2-\frac{1}{3}\right) Q_2(\lambda_p) \int_1^{\lambda_p} d\lambda_r e^{-\alpha R_{ji}\lambda_r} P_2(\lambda_r) \\
&- \quad \alpha^3 R_{ji}^2 \cdot 2\left(\mu_p^2-\frac{1}{3}\right) P_2(\lambda_p) \int_{\lambda_p}^{\infty} d\lambda_r e^{-\alpha R_{ji}\lambda_r} Q_2(\lambda_r)\,. \qquad \text{(C8)}
\end{aligned}
$$

The integrals appearing in Eq. (C8) can be calculated separately and the entire expression takes the form:

$$
\begin{aligned}
I &= \alpha^3 R_{ji}^2 \cdot \ln\frac{\lambda_p+1}{\lambda_p-1} \cdot I_1 \\
&+ \alpha^3 R_{ji}^2 \cdot I_2 \\
&- \alpha^3 R_{ji}^2 \cdot \frac{9}{4}\left(\mu_p^2-\frac{1}{3}\right)\left[\left(\lambda_p^2-\frac{1}{3}\right)\ln\frac{\lambda_p+1}{\lambda_p-1}-2\lambda_p\right] I_1 \\
&- \alpha^3 R_{ji}^2 \cdot \frac{9}{4}\left(\mu_p^2-\frac{1}{3}\right)\left(\lambda_p^2-\frac{1}{3}\right)(I_2-2I_3)\,, \qquad \text{(C9)}
\end{aligned}
$$

where the integrals are

$$
\begin{aligned}
I_1 &= \int_1^{\lambda_p} d\lambda_r e^{-\alpha R_{ji}\lambda_r}\left(\lambda_r^2-\frac{1}{3}\right) \\
&= \frac{2}{\alpha^3 R_{ji}^3}\cdot e^{-\alpha R_{ji}}\left(1+\alpha R_{ji}+\frac{\alpha^2 R_{ji}^2}{3}\right) \\
&- \frac{2}{\alpha^3 R_{ji}^3}\cdot e^{-\alpha R_{ji}\lambda_p}\left(1+\alpha R_{ji}\lambda_p+\frac{\alpha^2 R_{ji}^2}{2}\left(\lambda_p^2-\frac{1}{3}\right)\right), \qquad \text{(C10)}
\end{aligned}
$$

$$
\begin{aligned}
I_2 &= \int_{\lambda_p}^{\infty} d\lambda_r e^{-\alpha R_{ji}\lambda_r}\ln\frac{\lambda_r+1}{\lambda_r-1}\left(\lambda_r^2-\frac{1}{3}\right) \\
&= 2\cdot\frac{e^{-\alpha R_{ji}\lambda_p}\left(1+\alpha R_{ji}\lambda_p+\frac{\alpha^2 R_{ji}^2}{2}\left(\lambda_p^2-\frac{1}{3}\right)\right)}{\alpha^3 R_{ji}^3}\ln\frac{\lambda_p+1}{\lambda_p-1} \\
&- 4\int_{\lambda_p}^{\infty} d\lambda_r \frac{e^{-\alpha R_{ji}\lambda_r}\left(1+\alpha R_{ji}\lambda_r+\frac{\alpha^2 R_{ji}^2}{2}\left(\lambda_r^2-\frac{1}{3}\right)\right)}{\alpha^3 R_{ji}^3}\cdot\frac{1}{\lambda_r^2-1}
\end{aligned}
$$

$$
\begin{aligned}
&= \frac{2}{\alpha^3 R_{ji}^3} \cdot e^{-\alpha R_{ji}\lambda_p} \left(1 + \alpha R_{ji}\lambda_p + \frac{\alpha^2 R_{ji}^2}{2}\left(\lambda_p^2 - \frac{1}{3}\right)\right) \ln\frac{\lambda_p + 1}{\lambda_p - 1} \\
&- \frac{2}{\alpha^2 R_{ji}^2} \cdot e^{-\alpha R_{ji}\lambda_p} \\
&- \frac{2}{\alpha^3 R_{ji}^3} \cdot e^{\alpha R_{ji}} \left(1 - \alpha R_{ji} + \frac{\alpha^2 R_{ji}^2}{3}\right) Ei\left(-\alpha R_{ji}\left(\lambda_p + 1\right)\right) \\
&+ \frac{2}{\alpha^3 R_{ji}^3} \cdot e^{-\alpha R_{ji}} \left(1 + \alpha R_{ji} + \frac{\alpha^2 R_{ji}^2}{3}\right) Ei\left(-\alpha R_{ji}\left(\lambda_p - 1\right)\right), \quad \text{(C11)}
\end{aligned}
$$

and

$$
I_3 = \int_{\lambda_p}^{\infty} d\lambda_r e^{-\alpha R_{ji}\lambda_r} \cdot \lambda_r = \frac{1}{\alpha^2 R_{ji}^2} \cdot e^{-\alpha R_{ji}\lambda_p}\left(1 + \alpha R_{ji}\lambda_p\right). \quad \text{(C12)}
$$

Now, we combine these partial results together and substitute them into Eq. (C9). We obtain:

$$
\begin{aligned}
I &= \left[\ln\frac{\lambda_p + 1}{\lambda_p - 1}\left(1 - \frac{9}{4}\left(\mu_p^2 - \frac{1}{3}\right)\left(\lambda_p^2 - \frac{1}{3}\right)\right) + \frac{9}{2}\left(\mu_p^2 - \frac{1}{3}\right)\lambda_p\right] \\
&\times \frac{2}{R_{ji}}\left\{S_{ji} - e^{-\alpha R_{ji}\lambda_p}\left(1 + \alpha R_{ji}\lambda_p + \frac{\alpha^2 R_{ji}^2}{2}\left(\lambda_p^2 - \frac{1}{3}\right)\right)\right\} \\
&+ \left[1 - \frac{9}{4}\left(\mu_p^2 - \frac{1}{3}\right)\left(\lambda_p^2 - \frac{1}{3}\right)\right] \\
&\times \left\{\begin{array}{c}
\frac{2}{R_{ji}} \cdot e^{-\alpha R_{ji}\lambda_p}\left(1 + \alpha R_{ji}\lambda_p + \frac{\alpha^2 R_{ji}^2}{2}\left(\lambda_p^2 - \frac{1}{3}\right)\right)\ln\frac{\lambda_p+1}{\lambda_p-1} \\
-2\alpha e^{-\alpha R_{ji}\lambda_p} \\
-\frac{2}{R_{ji}} \cdot \widetilde{S_{ji}} \cdot Ei\left(-\alpha R_{ji}\left(\lambda_p + 1\right)\right) \\
+\frac{2}{R_{ji}} \cdot S_{ji} \cdot Ei\left(-\alpha R_{ji}\left(\lambda_p - 1\right)\right)
\end{array}\right\} \\
&+ \frac{9}{2}\left(\mu_p^2 - \frac{1}{3}\right)\left(\lambda_p^2 - \frac{1}{3}\right) \cdot \alpha e^{-\alpha R_{ji}\lambda_p}\left(1 + \alpha R_{ji}\lambda_p\right). \quad \text{(C13)}
\end{aligned}
$$

By reorganizing the above expression we arrive at the form used in the computations:

$$
I(R_{ji}; \lambda_p; \mu_p) = -2\alpha e^{-\alpha R_{ji}\lambda_p}
$$

$$
\begin{aligned}
&+ \quad \frac{9}{R_{ji}}\left(\mu_p^2-\frac{1}{3}\right)\cdot\left\{\lambda_p S_{ji}-e^{-\alpha R_{ji}\lambda_p}\left(\lambda_p+\frac{\alpha R_{ji}}{3}\right)\right\} \\
&+ \quad \frac{2}{R_{ji}}\left[1-\frac{9}{4}\left(\mu_p^2-\frac{1}{3}\right)\left(\lambda_p^2-\frac{1}{3}\right)\right] \\
&\times \quad \left\{\begin{array}{c} S_{ji}\cdot\ln\frac{\lambda_p+1}{\lambda_p-1} \\ -\widetilde{S_{ji}}\cdot Ei(-\alpha R_{ji}(\lambda_p+1)) \\ +S_{ji}\cdot Ei(-\alpha R_{ji}(\lambda_p-1)) \end{array}\right\},
\end{aligned}
\tag{C14}
$$

where the *Ei* function means the first-order *Euler* integral. The other expressions are

$$
\widetilde{S_{ji}} \equiv \left[-\alpha R_{ji}\left(1-\frac{\alpha R_{ji}}{3}\right)+1\right]e^{\alpha R_{ji}}, \tag{C15}
$$

and the overlap integral

$$
S_{ji} \equiv \left[\alpha R_{ji}\left(1+\frac{\alpha R_{ji}}{3}\right)+1\right]e^{-\alpha R_{ji}}. \tag{C16}
$$

As we can see, the result (C14) has a complex form, as it contains a non-analytical function, and thus, is a major obstacle to calculating the 3- and 4-site interaction coefficients analytically.

C.2 The *Euler* integral

The first-order *Euler* integral is a non-analytical function and in the numerical computations needs to be estimated accurately. The estimation is essential, since the integral appears in the expression for the Hamiltonian parameters. The definition of the integral is as follows:

$$
Ei(-x) \equiv -\int_x^\infty \frac{dt}{t}e^{-t}. \tag{C17}
$$

To estimate the integral we can use either the power series expansion or the asymptotic expansion. The power series has the form

$$
Ei(-x) = \gamma + \ln x + \sum_{n=1}^{\infty}\frac{(-x)^n}{n\cdot n!}, \tag{C18}
$$

where $\gamma \approx 0.5772156649$ is the *Euler* constant. On the other hand, the

asymptotic expansion is of the form

$$Ei(-x) = -\frac{e^{-x}}{x} \sum_{n=0}^{\infty} \frac{n!}{(-x)^n}. \tag{C19}$$

The power series works well for small values of x, whereas the asymptotic expansion is rapidly convergent for large x values. The limit for their use is approximately equal to $|\ln EPS|$, where EPS is the required relative error.

C.3 The microscopic parameters

We now provide the explicit expressions for these microscopic parameters of the Hamiltonian that can be determined analytically. All of the interaction coefficients, except the 3- and 4-site interaction terms, have the analytical form. Obviously, the microscopic parameters depend on the variational parameter α, which is determined by minimizing the system ground state energy once the interaction among particles is included. The expressions for the atomic energy and the hopping parameters in the atomic representation are, respectively

$$t'_{ii} = \alpha^2 + 2\alpha Z \cdot \left[\sum_{R_m \neq R_i} \left(1 + \frac{1}{\alpha R_{mi}}\right) e^{-2\alpha R_{mi}} - 1 \right] - \sum_{R_m \neq R_i} \frac{2Z}{R_{mi}}, \tag{C20}$$

and

$$\begin{aligned} t'_{ij} &= -\alpha^2 \cdot S_{ji} + 2\alpha\,(\alpha - Z)\,[1 + \alpha R_{ji}]\, e^{-\alpha R_{ji}} \\ &- Z \cdot \sum_{R_m \neq R_i} I\left(R_{ji}; \frac{R_{mi} + R_{mj}}{R_{ji}}; \frac{R_{mi} - R_{mj}}{R_{ji}}\right), \end{aligned} \tag{C21}$$

where $I(R_{ji}; \lambda; \mu)$ represents the 3-center contributions (C14) to the hopping parameter. The *Slater* (1963) integrals define the two-particle interaction parameters, namely the single-site (intraatomic) *Hubbard* term, the two-site (interatomic) *Coulomb* term, the *Heisenberg* exchange integral, and the so-called *correlated hopping* term, which have the respective forms:

$$U'_i \equiv V'_{iiii} = \frac{5}{4}\alpha, \tag{C22}$$

$$K'_{ij} \equiv V'_{ijij} = \frac{2}{R_{ji}} - \alpha e^{-2\alpha R_{ji}} \left[\frac{2}{\alpha R_{ji}} + \frac{11}{4} + \frac{3}{2}\alpha R_{ji} + \frac{1}{3}\alpha^2 R_{ji}^2 \right], \tag{C23}$$

$$\begin{aligned} J'_{ij} \equiv V'_{ijji} &= \frac{12}{5R_{ji}} \left\{ \begin{array}{c} S_{ji}^2 \cdot (\lambda + \ln \alpha R_{ji}) \\ -2S_{ji}\widetilde{S_{ji}} \cdot Ei(-2\alpha R_{ji}) \\ +\widetilde{S_{ji}}^2 \cdot Ei(-4\alpha R_{ji}) \end{array} \right\} \\ &+ \alpha e^{-2\alpha R_{ji}} \left[\frac{5}{4} - \frac{23}{10}\alpha R_{ji} - \frac{6}{5}\alpha^2 R_{ji}^2 - \frac{2}{15}\alpha^3 R_{ji}^3 \right], \end{aligned} \tag{C24}$$

and

$$V'_{ij} \equiv V'_{jiii} = \alpha \left\{ \begin{array}{c} e^{-\alpha R_{ji}} \left[2\alpha R_{ji} + \frac{1}{4} + \frac{5}{8\alpha R_{ji}} \right] \\ -\frac{1}{4} e^{-3\alpha R_{ji}} \left[1 + \frac{5}{2\alpha R_{ji}} \right] \end{array} \right\}. \tag{C25}$$

The above microscopic parameters are the only appearing for the H_2 molecule (two sites). For $N \geq 3$ atoms, the 3-site and for $N \geq 4$ atoms, the additional 4-site terms appear. Although they cannot be calculated analytically we still can include them using an *ansatz* explained in detail in Appendix B.2.

C.4 The transport amplitude

In order to determine electronic transport through nanosystems we need an efficient method of calculating the electron current in the second quantization language. The definition of the current density operator $\widehat{j}$, expressed with the use of the field operators, can be written down as follows

$$\widehat{j} = \widehat{\Psi}^{+}(\mathbf{p}) \left(-\frac{e}{m}\widehat{p} \right) \widehat{\Psi}(\mathbf{p}), \tag{C26}$$

where $\widehat{p}$ is the single-particle momentum operator, $\widehat{\Psi}(\mathbf{p})$ and $\widehat{\Psi}^{+}(\mathbf{p})$ are the field operators expressed as functions of the momentum space, not the real

space as is usually the case. The choice of the momentum-space representation of the field operators simplifies significantly the calculations, since the single-particle momentum operator is of the straightforward form $\widehat{p} \equiv \mathbf{p}$. The field operators, similarly to Eq. (3), can be described within this complete single-particle basis as follows

$$\widehat{\Psi}(\mathbf{p}) \equiv \sum_{i\sigma} w_i(\mathbf{p}) \chi_\sigma \cdot a_{i\sigma}, \tag{C27}$$

where $\{w_i(\mathbf{p})\}$ is the orthonormal basis that is the representation of the *Wannier* basis in the momentum space. Its relation to the real-space *Wannier* basis representation is defined with the equation

$$\int d^3 r w_i(\mathbf{r}) |\mathbf{r}\rangle = |w_i\rangle = \int d^3 p w_i(\mathbf{p}) |\mathbf{p}\rangle . \tag{C28}$$

The real-space representation $\{w_i(\mathbf{r})\}$, according to Eq. (B1), yields

$$\begin{aligned} \int d^3 r w_i(\mathbf{r}) |\mathbf{r}\rangle &= \int d^3 r \sum_j \beta_{ij} \Phi_j(\mathbf{r}) |\mathbf{r}\rangle = \sum_j \beta_{ij} |\Phi_j\rangle \\ &= \sum_j \beta_{ij} \int d^3 p \Phi_j(\mathbf{p}) |\mathbf{p}\rangle , \end{aligned} \tag{C29}$$

and hence

$$w_i(\mathbf{p}) = \sum_j \beta_{ij} \Phi_j(\mathbf{p}) . \tag{C30}$$

One should note that the β coefficients are the same for both the representations. The momentum-space representation of the atomic wave functions can be obtained through the relation

$$\Phi_j(\mathbf{p}) = \langle \mathbf{p}|\Phi_j\rangle = \int d^3 r \Phi_j(\mathbf{r}) \langle \mathbf{p}|\mathbf{r}\rangle = \left(\frac{1}{2\pi\hbar}\right)^{3/2} \int d^3 r \Phi_j(\mathbf{r}) e^{-\frac{i}{\hbar}\mathbf{p}\cdot\mathbf{r}}, \tag{C31}$$

where $\Phi_j(\mathbf{r}) \equiv \Phi(\mathbf{r} - \mathbf{R}_j)$ is the real-space atomic wave function (11). As we can see, calculation of the momentum-space representation of the atomic wave functions is the starting point in the electronic transport determination.

The result is obtained by applying Eq. (11) to the relation (C31), what yields

$$\begin{aligned}\Phi_j(\mathbf{p}) &= \left(\frac{1}{2\pi\hbar}\right)^{3/2}\sqrt{\frac{\alpha^3}{\pi}}\int d^3r e^{-\alpha|\mathbf{r}-\mathbf{R}_j|-\frac{i}{\hbar}\mathbf{p}\cdot\mathbf{r}} \\ &= \left(\frac{1}{2\pi\hbar}\right)^{3/2}\sqrt{\frac{\alpha^3}{\pi}}e^{-\frac{i}{\hbar}\mathbf{p}\cdot\mathbf{R}_j}\int d^3r e^{-\alpha|\mathbf{r}|-\frac{i}{\hbar}\mathbf{p}\cdot\mathbf{r}} \\ &= \left(\frac{1}{2\pi\hbar}\right)^{3/2}\sqrt{\frac{\alpha^3}{\pi}}e^{-\frac{i}{\hbar}\mathbf{p}\cdot\mathbf{R}_j}\frac{4\pi\hbar}{p}\int_0^\infty dr r e^{-\alpha r}\sin\left(\frac{pr}{\hbar}\right) \\ &= \left(\frac{1}{2\pi\hbar}\right)^{3/2}\sqrt{\frac{\alpha^3}{\pi}}e^{-\frac{i}{\hbar}\mathbf{p}\cdot\mathbf{R}_j}\frac{8\pi\alpha}{\left(\alpha^2+(p/\hbar)^2\right)^2}, \end{aligned} \tag{C32}$$

and finally the result is

$$\Phi_j(\mathbf{p}) = \left(\frac{2\alpha}{\hbar}\right)^{3/2}\frac{\alpha}{\pi}\frac{1}{\left(\alpha^2+(p/\hbar)^2\right)^2}e^{-\frac{i}{\hbar}\mathbf{p}\cdot\mathbf{R}_j}. \tag{C33}$$

The current density operator can be obtained then with the use of the above result. The expression is

$$\hat{j} = -\frac{e}{m}\sum_{ij\sigma} a^+_{i\sigma}a_{j\sigma}\cdot w^*_i(\mathbf{p})\,\mathbf{p}w_j(\mathbf{p}). \tag{C34}$$

Substituting Eq. (C30), we have

$$\hat{j} = -\frac{e}{m}\sum_{i'j'}\sum_{ij\sigma} a^+_{i\sigma}a_{j\sigma}\beta^*_{ii'}\beta_{jj'}\cdot\Phi^*_{i'}(\mathbf{p})\,\mathbf{p}\Phi_{j'}(\mathbf{p}). \tag{C35}$$

To simplify the above expression, we introduce the effective hopping operator $\widehat{C^{eff}}_{i'j'}$ and the current density amplitude $\mathbf{j}_{i'j'}(\mathbf{p})$ as follows

$$\widehat{C^{eff}}_{i'j'} \equiv \sum_{ij\sigma} a^+_{i\sigma}a_{j\sigma}\beta^*_{ii'}\beta_{jj'}, \tag{C36}$$

and

$$\mathbf{j}_{i'j'}(\mathbf{p}) \equiv -\frac{e}{m}\Phi^*_{i'}(\mathbf{p})\,\mathbf{p}\Phi_{j'}(\mathbf{p}). \tag{C37}$$

Then, finally

$$\widehat{j} = \sum_{i'j'} \widehat{C^{eff}}_{i'j'} \cdot \mathbf{j}_{i'j'}(\mathbf{p}) . \tag{C38}$$

One should note that the current carried by the system can be obtained by integrating over momenta and averaging the result in the ground state of the system. The ground state is determined from the EDABI approach on a regular basis. The average current through the system is then

$$\mathbf{I} = \sum_{i'j'} \left\langle \widehat{C^{eff}}_{i'j'} \right\rangle \cdot \int d^3p \mathbf{j}_{i'j'}(\mathbf{p}) , \tag{C39}$$

and it is obvious that

$$\int d^3p \mathbf{j}_{i'i'}(\mathbf{p}) \equiv 0. \tag{C40}$$

On the other hand, both the effective hopping operator and the current density amplitude are hermitian with respect to their indices i' and j'. Therefore, the overall current is

$$\begin{aligned} \mathbf{I} &= 2 \sum_{i'<j'} Re \left\{ \left\langle \widehat{C^{eff}}_{i'j'} \right\rangle \cdot \int d^3p \mathbf{j}_{i'j'}(\mathbf{p}) \right\} \\ &= 2 \sum_{i'<j'} Re \left\langle \widehat{C^{eff}}_{i'j'} \right\rangle \cdot Re \int d^3p \mathbf{j}_{i'j'}(\mathbf{p}) \\ &- 2 \sum_{i'<j'} Im \left\langle \widehat{C^{eff}}_{i'j'} \right\rangle \cdot Im \int d^3p \mathbf{j}_{i'j'}(\mathbf{p}) , \end{aligned} \tag{C41}$$

and obviously, we have

$$Re \int d^3p \mathbf{j}_{i'j'}(\mathbf{p}) \equiv 0. \tag{C42}$$

The above allows us to write the simplified form of the expression for electronic transport

$$\mathbf{I} = -2 \sum_{i'<j'} Im \left\langle \widehat{C^{eff}}_{i'j'} \right\rangle \cdot \int d^3p Im \{\mathbf{j}_{i'j'}(\mathbf{p})\}$$

$$= \frac{2e}{m}\left(\frac{2\alpha}{\hbar}\right)^3\left(\frac{\alpha}{\pi}\right)^2 \sum_{i'<j'} Im\left\langle \widehat{C^{eff}}_{i'j'}\right\rangle$$
$$\times \int d^3p \frac{\mathbf{p}}{\left(\alpha^2+(p/\hbar)^2\right)^4}\sin\left(\frac{\mathbf{p}\cdot\mathbf{R}_{i'j'}}{\hbar}\right). \quad \text{(C43)}$$

From, the above expression for the current follows that the vector $\mathbf{I}$ has to be parallel to the vector $\mathbf{R}_{i'j'}$. This simplifies the calculations even further, since we can determine just the scalar value of the current. The momentum vector $\mathbf{p}$ can now be represented by its components $\mathbf{p}_\parallel$ and $\mathbf{p}_\top$. Thus, the last integral can be rewritten as follows

$$\int ... \equiv \int dp_\parallel p_\parallel \sin\left(\frac{p_\parallel\cdot R_{i'j'}}{\hbar}\right)\int d^2p_\top \frac{1}{\left(\alpha^2+\left(p_\parallel/\hbar\right)^2+\left(p_\top/\hbar\right)^2\right)^4}$$
$$= \int dp_\parallel p_\parallel \sin\left(\frac{p_\parallel\cdot R_{i'j'}}{\hbar}\right)\frac{\hbar^8\pi}{3\left(\alpha^2\hbar^2+p_\parallel^2\right)^3}$$
$$= \frac{\hbar^4\pi^2R_{i'j'}^2}{24\alpha^2}\left(1+\frac{1}{\alpha R_{i'j'}}\right)e^{-\alpha R_{i'j'}}, \quad \text{(C44)}$$

and hence, the current is

$$I = \frac{2e}{m}\left(\frac{2\alpha}{\hbar}\right)^3\left(\frac{\alpha}{\pi}\right)^2 \sum_{i'<j'} Im\left\langle \widehat{C^{eff}}_{i'j'}\right\rangle$$
$$\times \frac{\hbar^4\pi^2R_{i'j'}^2}{24\alpha^2}\left(1+\frac{1}{\alpha R_{i'j'}}\right)e^{-\alpha R_{i'j'}}$$
$$= \sum_{i'<j'} Im\left\langle \widehat{C^{eff}}_{i'j'}\right\rangle\cdot\frac{2e\hbar}{3m}\alpha^2R_{i'j'}\left(1+\alpha R_{i'j'}\right)e^{-\alpha R_{i'j'}}. \quad \text{(C45)}$$

The last term in the above expression represents contribution of the individual pair of sites to the overall current through the system. Therefore, by defining

$$I_{i'j'} \equiv \frac{2e\hbar}{3m}\alpha^2R_{i'j'}\left(1+\alpha R_{i'j'}\right)e^{-\alpha R_{i'j'}}, \quad \text{(C46)}$$

we can finally write down the expression for the electronic current in the form

$$I = \sum_{i'<j'} Im \left\langle \widehat{C^{eff}}_{i'j'} \right\rangle I_{i'j'}. \tag{C47}$$

As we can see, the expression for the current for the nanosystems described with the EDABI approach, is an analytical function and depends on both the interatomic distance $R_{i'j'}$ and the variational parameter α. Another interesting feature of the result is that it depends on the imaginary part of the average value of the effective hopping operator only. This indicates that the current is zero for the systems with the Hamiltonian lacking any imaginary parameters.

Bibliography

[1] A. Yazdani, D. M. Eigler, and N. D. Lang. Off-resonance conduction through atomic wires. *Science* ***272***, 1996. 1

[2] A. F. Morpurgo, J. Kong, C. M. Marcus, and H. Dai. Gate-controlled superconducting proximity effect in carbon nanotubes. *Science* ***286****, p.263*, 1999. 1

[3] J. L. Costa-Krämer, N. Garcia, P. Garcia-Mochales, P. A. Serena, M. I. Marqués, and A. Correia. Conductance quantization in nanowires formed between micro and macroscopic metallic electrodes. *Phys. Rev. B* ***55****, 8 p.5416*, 1997. 1, 2

[4] J. L. Costa-Krämer and N. Garcia. Conductance quantization histograms of gold nanowires at 4 K. *Phys. Rev. B* ***55****, 19 p.12910*, 1997. 2, 4

[5] K. Takayanagi, Y. Kondo, and H. Ohnishi. Suspended gold nanowires: ballistic transport of electrons. *Japan Soc. Appl. Phys. International* ***3*** *p.3*, 2001. 2, 4, 57

[6] Z. Yao, C. Dekker, and P. Avouris. Electrical transport through single-wall carbon nanotubes. *Topics Appl. Phys.* ***80*** *p.147*, 2001. 2

[7] D. H. Cobden, M. Bockrath, P. L. McEuen, A. G. Rinzler, and R. E. Smalley. Spin splitting and even-odd effects in carbon nanotubes. *Phys. Rev. Lett.* ***81****, 681*, 1998. 2

[8] S. J. Tans, M. H. Devoret, R. J. A. Groeneveld, and C. Dekker. Electron-electron correlations in carbon nanotubes. *Nature* ***394***, 1998. 3

[9] A. I. Yanson, G. R. Bollingery, H. E. Brom, N. Agraït, and J. M. Ruitenbeek. Formation and manipulation of a metallic wire of single gold atoms. *Nature* ***395***, 1998. 3

[10] C. J. Muller, J. M. Krans, T. N. Todorov, and M. A. Reed. Quantization effects in the conductance of metallic contacts at room temperature. *Phys. Rev. B* ***53****, 1022*, 1996. 4

[11] U. Landman, J. I. Pascual, J. Mendez, J. Gomez-Herrero, A. M. Baro, N. Garcia, W. D. Luedtke, E. N. Bogachek, and H. P. Cheng. Properties of metallic nanowires: from conductance quantization to localization. *Science* ***267*** *p.1783*, 1995. 5

[12] E. H. Lieb and F. Y. Wu. Absence of Mott transition in an exact solution of the short-range one-band model in one dimension. *Phys. Rev. Lett.* ***20*** *p.1445*, 1968. 5

[13] M. Di Ventra, S. T. Pantelides, and N. D. Lang. First-principles calculation of transport properties of a molecular device. *Phys. Rev. Lett.* ***84****, 5 p.979*, 2000. 5

[14] P. Havu, T. Torsti, M. J. Puska, and R. M. Nieminen. Conductance oscillations in metallic nanocontacts. *Phys. Rev. B* ***66*** *p.075401*, 2002. 5, 6, 67

[15] S. Datta. *Electronic Transport in Mesoscopic Systems*. Cambridge University Press, 1995. 6, 58, 67

[16] J. A. Pople. *Energy, structure and reactivity*, pages 51–61. Wiley, New York, 1973. 7

[17] B. O. Roos. *Ab Initio Methods in Quantum Chemistry II*, pages 399–445. Wiley, New York, 1987. 7

[18] J. Simons and J. Nichols. *Quantum Mechanics in Chemistry*. Oxford University Press, 1996. 7, 28

[19] H. Dorsett and A. White. Overview of molecular modelling and *Ab initio* molecular orbital methods suitable for use with energetic materials. Technical report, Weapons Systems Division, Aeronautical and Maritime Research Laboratory, Australia, 2000. 7, 28

[20] H. J. Jacobus van Dam. *Calculations on correlation effects in molecules: convergence and size-consistency of multi-reference methods*. PhD thesis, Utrecht University, The Netherlands, 1997. 9, 28, 33

[21] J. A. Pople, J. S. Binkley, and R. Seeger. Theoretical models incorporating electron correlation. *Int. J. Quantum Chemistry* ***10****, 1*, 1976. 9, 32, 36

[22] R. J. Bartlett. Many-body perturbation theory and coupled cluster theory for electron correlation in molecules. *Ann. Rev. Phys. Chem.* ***32*** *p.359*, 1981. 10, 32, 36

[23] A. Rycerz. *Physical properties and quantum phase transitions in strongly correlated electron systems from a combined exact diagonalization ab initio approach*. PhD thesis, Jagiellonian University, Poland, 2003. 10, 11

[24] E. M. Görlich. *Properties of molecules and nanoscopic systems from a combined exact diagonalization* - ab initio *approach*. PhD thesis, Jagiellonian University, Poland, 2004. 10, 14, 69

[25] E. M. Görlich, R. Zahorbeński, and J. Spałek. Correlated states for atoms and atomic clusters: a combined exact diagonalization - *ab initio* approach. *Acta Phys. Polon. B* ***34****, 2 p.645*, 2003. 11

[26] J. Spałek, A. Rycerz, E. M. Görlich, and R. Zahorbeński. *"Electron correlations at nanoscale", in: Highlights in Condensed Matter Physics*, pages 291–303. Melville, New York, 2003. 11

[27] S. Jacobi and R. Baer. The well-tempered auxiliary-field Monte-Carlo. *J. Chem. Phys.* ***120****(1) p.43*, 2004. 18

[28] J. Tennyson, M. A. Kostin, H. Y. Mussa, O. L. Polyansky, and R. Prosmiti. H_3^+ near dissociation: theoretical progress. *Phil. Trans. Roy. Soc. A* ***358*** *p. 2419*, 2000. 50

[29] E. Herbst. The astrochemistry of H_3^+. *Phil. Trans. Roy. Soc. A* ***358*** *p. 2523*, 2000. 50

[30] B. J. McCall and T. Oka. H_3^+ – an ion with many talents. *Science* ***287*** *p. 1941*, 2000. 50

[31] J. J. Palacios, A. J. Pérez-Jiménez, E. Louis, J. A. Vergés, and E. San-Fabián. Molecular electronics and first-principles methods. *Summer School Nicolas Cabrera*, 2002. 57, 67

[32] J. J. Palacios, A. J. Pérez-Jiménez, E. Louis, E. SanFabián, and J. A. Vergés. A first-principles approach to electrical transport in atomic-scale nanostructures. *Phys. Rev. B* ***66*** *p.035322*, 2002. 57, 67

[33] B. K. Nikolić and P. B. Allen. Quantum transport in ballistic conductors: evolution from conductance quantization to resonant tunnelling. *J. Phys.: Condensed Matter* ***12*** *p.9629-9636*, 2000. 57, 67

[34] B. Robertson. Introduction to field operators in quantum mechanics. *Am. J. Phys.* ***41*** *p.678*, 1973. 63

[35] F. Elsholz. Landauer-Büttiker formalism. Seminar talk, 2002. 67